Development of semi-classical and quantum tools for the high-frequency simulation of nanoscale electron devices

by
Abdelilah BENALI

Submitted to the
Departament d'Enginyeria Electrònica
in partial fulfillment of the requirements for the degree of
PhD in Electronic Engineering
at the
Universitat Autònoma de Barcelona

Thesis supervisor: Xavier Oriols Pladevall

Date of defense: November 2013

Summary

Electronics surrounds many aspects of our everyday life. The progress of our actual society is somehow ultimately linked to the progress of electronics. Such progress demands smaller and faster devices. Therefore, the simulations tools needed to be able, to understand the behavior of emerging electron devices and to improve them, have to be reinvented for each new generation of devices.

The International Technology Roadmap for Semiconductors predicts that, in ten years, electron devices will have less than 10 nanometers of channel length and they will work at THz frequencies. The scientific community has done an important effort to provide reliable simulations tools for studying the DC behavior of state-of-the-art nanoscale devices. Some of the common classical and quantum simulation techniques are mentioned in the **first chapter**. However, a similar effort for the the quantum simulation of the AC performance of such nano metric and THz devices is still missing.

For nanoscale devices, at high frequency, the main difficulties that have to be taken into account are the role of the displacement current (which imply a proper approximation for the many-body problem) and the assumption that the total quantum current needs to be continuously measured. This thesis provides an approximate solution to these problems through the use of quantum (Bohmian) trajectories. As seen in the **second chapter**, such Bohmian trajectories have advantages, from the computational point of view when we deal with the many body problem or the continuous measurement.

In **chapter three**, the practical computation of the particle and displacement currents are discussed using the so called Ramo-Shockley-Pellegrini theorem. We have presented a quantum extension of the theorem using Bohmian (trajectories). We also discuss in detail the implementation of the theorem in the *BITLLES (Bohmian Interacting Transport for non- equiLibrium eLEctronic Structures)* simulator discussed in the appendix C. The expressions of the total current can be used either for classical Monte Carlo solutions of the Botzmann equation with classical trajectories or for the many-particle Schrödinger equation with Bohmian trajectories.

Finally, using the tools developed in the previous chapters of this thesis, in **chapter four**, we have studied the dependence of the current and the noise on the geometry and the electrostatic boundary conditions of nanotransistors. In addition, we have presented and original strategy to improve the cut off frequency of emerging multi-gate ballistic devices. These numerical studies have been carried out by means of the *BITLLES* simulator for classical and quantum scenarios.

This thesis is a step in the direction of providing a reliable dynamic quantum simulator to the industry and the scientific community.

Esta tesis esta dedicada a mis padres Zohra y Mohamed,
mis hermanos , mis hermanas, mis sobrinos , mis sobrinas y toda mi familia.

Acknowledgements

En primer lugar y de forma especial, quiero expresar mi reconocimiento al Dr. Xavier Oriols Pladevall , director de este tesis doctoral, cuyas inestimables orientaciones y sugerencias, y cuyo continuo apoyo y estmulo, han contribuido decisivamente a la realización del presente estudio.

Quiero agradecer a mis compañeros de Universidad Autònoma de Barcelona Guillem, Alfonso, Fabio, Miguel D., Jordi Selga, Marta, Ferran , Eloy, Gabriel, Miguel L., Carlos, Marti, Joli, Albert Cr., Ferran P., Vanesa, Gerard, Nuria, Paris, José, Gerard Za. Albin, Jordi Ag., Marcus , Moises, Vicas y todos los demas compañeros del Departamento.

También quiero dar las gracias a los amigos de la Universidad Autònoma de Barcelona, Hamza B., Taoufiq Aj., Hicham El B. , Rachid Z., Imade H., Mostafa L., Abdelilah E., Yousef Elk., El Ghali Am., Mohamed Ak., Omar Ay., Ihab S., Fadi, Ahmed S. , Bilal Pak, Mouhcine, Ahmed R., Soufiane ElH. , Essame , Rida Tn., Rym Tn., Nawal, Chahrazad N., Imane, Silvia, Mhamed, Mohamed Ab.; de la Universidad de Barcelona : Said A., Mohamed As.; de la Universidad Politécnica de Cataluña: Mohamed Esst., Mohamed Essl., Iqbal, Karima, Mohamed K., Ayoub Z., Hamza N., Mohamed An; de la Universidad Pompeu Fabra: Yousef ElA. y todos los demas amigos dentro y fuera de la universidad.

Finalmente, quiero agradecer profundamente a mi madre, mi padre, mis hermanos y mis hermanas. Me brindaron su apoyo, me comprendieron, tuvieron tolerancia e infinita paciencia y cedieron su tiempo para permitir así que yo haya podido llevar adelante satisfactoriamente el enorme trabajo que representa una tesis doctoral.

Abdelilah BENALI

Septiembre del 2013

Contents

List of Figures

Chapter 1

Small dimensions and high frequencies

1.1 Introduction: The role of electronics in our life

Electronics technology is changing our life broadly. For example, microprocessors and electrical sensors make cars, ships, trains and planes more practical, environmental friendly and secure. Paying bills electronically saves our time. Everyone agrees that the domain of electronics has revolutionized the world during the past century. Only about 30 years ago, the thought of being surrounded by computers, microprocessors and cell or smart phones was unheard of. The use of new technologies gives unimaginable possibilities. Flat screens with network connections replace clumsy TVs. All this revolutionary improvements are due to the evolution of the electronic devices, in general, and the transistor, in particular. The transistor is the *catalyst* of this revolution. The improvement of the transistors is carried out firstly by scaling down the electronic devices or/and secondly by looking for a new materials with high electron mobility to increase their speed and to decrease their power consumption. Doing these steps up requires a hard theoretical and experimental study to understand each new generation of state-of-the art electronic devices. This thesis provides a theoretical effort in the simulation and understanding of the capabilities of these new devices with small dimensions and high frequencies.

This introductory chapter will be organized as follows. Firstly we present a brief historical developments of electronics. After, we discuss the predictions of International Technology Roadmap for Semiconductors (ITRS)[1] toward to nanometirc dimensions and TeraHertz (THz) working frequencies. Finally , we present different theoretical models used in the literature to characterize and study of the classical and quantum electron devices.

1.2 Short historical development of electronics

Electronics began with the invention of the vacuum tube in the first decade of last century. The simplest kind of vacuum tube is the diode, which was invented by John Ambrose Fleming in 1904. A more versatile type of vacuum tube is the triode, or three-terminal tube, invented by Lee Deforest in 1906. Initially, the first vacuum tube was not an amplifier but it soon developed into a device with many functions, including amplifying very small electrical signals. Although the triode was very success, it was a fragile device and it consumed a

lot of power. For these reasons, in the mid-1920s, Julius Edgar Lilienfeld set out to find a solid-state replacement for the thermionic triode. Lilienfeld patented applications to Canada in 1925 and to the United States in 1926. He said explaining his invention [2]:

> *"The invention relates to a method of and apparatus for controlling the flow of an electric current between two terminals of an electrically conducting solid by establishing a third potential between said terminals; and is particularly adaptable to the amplification of oscillating currents such as prevail, for example, in radio communication. Heretofore, thermionic tubes or valves have been generally employed for this purpose...."*

Due to the importance of Lilienfeld's invention, he was acknowledged as pioneer in developing a solid-state-transistor by, for example, John Bardeen. He said in this regard:

> *"Lilienfeld had the basic concept of controlling the flow of current in a semiconductor to make an amplifying device. It took many years of theory development and material technology to make his dream a reality ."*

It appears that Lilienfeld's ideas embody the principles of the modern-day, and he set the cornerstone of field-effect-transistor theory. However, unfortunately, his invention was unsuccessful due to practical problems in the fabrication at that time and a bad selection of materials. The first solid-state transistor successfully fabricated was done, at Bell laboratory, by the team of William Schockley, John Bardeen and Walter Brattain, 50 years after the invention of the vacuum tube [3].

Figure 1.1: John Bardeen, William Shockley, and Walter Brattain [3]).

This team was awarded the Nobel Prize for their work in 1956. Many consider the transistor to be one of the most important inventions in 20th century. Certainly, it is the man-made object more abundant in the world. In this historical development, it is also important to mention the electronic revolution carried on by inventing the integrated circuit by Jack Kilby. The latter proposed a revolutionary concept of creating more than one transistor on a single semiconductor piece. Then he successfully implemented his idea in 1958, realizing a phase shift oscillator on a small piece of germanium, it was the first electronics integrated circuit in Texas Instruments. Jack Kilby received the Noble Prize in

Physics in 2000 for his part in the invention of the integrated circuit. It was a simple device and it has one transistor, a capacitor and resistor all together on a piece of silicon [3]. The next step in the developments electronics was at Fairchild, where Jean Hoerni developed the planar process for transistors. Today the integrated circuit has evolved to have millions of transistors on a single chip and most of all modern computers include microprocessor chip. The microprocessor was introduced as a commercial product by Intel Corporation in 1971.

1.3 Toward nanoscale and THz frequencies

In the near future, the development of electronics is expected to follow the Moore's law [1]. The increase in the number of transistors in a chip, offers more functions per chip with much lower cost per function, which gives as a result smaller electron devices, higher performance and greater energy efficiency. The ITRS points to the improvement of the FET transistor as the best strategy to be followed in the following years. Nonetheless, the scientific community is looking for completely different alternatives to the FET transistors because of the mid-term scaling required by Moore's law (6.5 nm channel length transistors predicted for 2025 [1]) will be technologically and economically unattainable with the present FET technology.

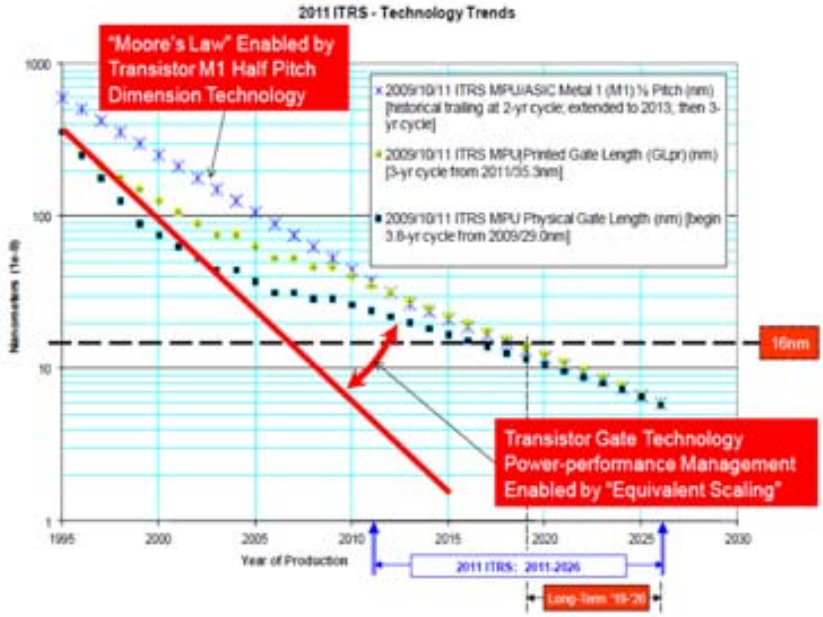

Figure 1.2: MPU (Microprocessor Circuit)/High performance ASIC (Application Specific Integrated Circuit) Half Pitch and Gate Length Trends [1].

It is, however, still not clear which proposals will replace the present transistors in the mid-term future. Some works suggest that a revolution (similar to the substitution of vacuum tubes by solid state transistor in the 50´ s) is awaiting for the electronic industry. Others affirm that such revolution will not take place, but we will see just an evolution of present

[1] "The number of transistors that can be implemented in a chip doubles approximately every 2 years"

FET transistors into smaller structures. In any case, what is unquestionable is that the dimensions of the new commercial electron devices will attain few nanometers, the evolution of physical gate length and other parameters versus years is shown in Fig. 1.2.

Therefore, we are now leaving the microelectronic era to enter into the new nanoelectronic era. The electron transit time, defined as the device length divided by the mean velocity is reaching few picoseconds. Thus, these new electron devices tend to work at THz frequencies, see the table below 4.1 .

Year of production	2011	2012	2013	2014	2015	2016	2017	2018
Extended Planar Bulk	347	396	445	512	578	669	756	-
UTB FD	-	-	477	545	614	704	790	889
Multigate	-	-	-	-	620	710	795	890

Table 1.1: Cutoff frequency (GHz) for different technology evolution according to ITRS 2011.

In this regard, the ITRS suggests to change the generic designation of the present RF (Radio Frequency) devices to HF (High Frequency) devices in order to reflect the much wider spectrum that is expected for nanoscale devices [1].

Since electron devices are entering into the nanoelectronic era, the wave nature of electrons have to be taken into account in the understanding of the behavior of these novel devices. Therefore, theoretical approaches to treat quantum electron devices constitute today a necessary tool to guide the continuous breakthroughs of the electronic industry. However, the separation between classical and quantum transport is somehow artificial. The transition is not clearly defined and the classical theory is a just limit of quantum mechanics when the wave nature of electrons is not relevant. For these reasons, we prefer to split our understanding of electron devices and the transport models used for such understanding between three types: those where the particle-like nature of electrons is relevant, those where the wave-like nature becomes relevant and those where both, the wave and the particle, become relevant.

1.4 Electron transport models in semiconductor devices

A lot of studies have been done and many models have been developed for studying the DC behavior of micro and nano scale devices with quantum and classical tools. A bit less was carried out for the micro scale semiclassical devices at THz frequencies. The poorest studies have been done for nanoscale, at very high frequency (THz), in particular at AC regime. In this work we throw light on characterizing those nanoscale devices at THz frequencies.

The modeling of electron transport in semiconductor devices has become a very important topic. This modeling is important for characterizing these devices before fabrication, and also to anticipate the viability of electron devices. In this section, we present different models following the previous division between those emphasizing the particle-like nature of electrons and those emphasizing the wave-like nature. Then, in the next chapter, we will discuss the Bohmian explanation that can be adequate for electron devices where either the wave or the

particle nature of electrons become relevant. In the first set, we start out by Boltzmann's transport equation which can be obtained , for instance, from Vlasov's equation (Liouville's equation) [4–6]. From the Boltzmann's equation, the kinetic models for electronic devices are using hydrodynamic and drift diffusion models. We present then the transport models where the wave-like nature of electrons become relevant. Such models include the simple Landauer approach, the quantum Wigner-Boltzmann transport equation, then, the Non-equilibrium Green's functions (NEGF) approach, and finally density functional theories.

We will take special attention to discern whether the transport model allows an understanding of the high-frequency behavior of devices or not. In principle, those with a time-dependence in the equations allow such studies, independently of whether they are classical or quantum models. Those with time-independent equations can only be used for transport beyond DC assuming a quasi-static approximation in the AC and transient results. At this point, let us emphasize that most of the quantum models are time-independent and devoted mainly to understand the DC behavior of emerging devices. A quantum treatment beyond the DC transport is mandatory [7] to convoy the electronic evolution.

1.4.1 Electron transport models where the particle-like nature is relevant

Let us start by describing those transport models where the wave-nature of electrons is neglected. We start by the Boltzmann's transport equation.

1.4.1.1 Boltzmann's transport equation

In the semiconductors devices with micrometric dimensions, there are a lot of scattering mechanisms such us ionized impurities, optic and acoustic phonon , electron-electron etc [8, 9]. These mechanisms have a direct effect on the operative characteristics of the electronic devices , thus it is important to include these effects. They can be taken by means of *Boltzmann's transport equation* through the collision integral. The Boltzmann's transport equation was derived , the first time, by Boltzmann in 1872 to describe the gaz behavior.
However, to completely specify electron transport, we should know the state of each carrier within the device. In particular, if the carriers behave as classical particles, we should know each carrier position and momentum as a function of time. Alternatively, we can ask also what is the probability of finding a carrier distribution with momentums centered at $(\vec{p}_1, ..., \vec{p}_N, t)$, locations centered at $(\vec{r}_1, ..., \vec{r}_N, t)$, and time t. The answer is the *many-particle distribution function*:

$$f\left(\vec{r}_1, ..., \vec{r}_N, \vec{p}_1, ..., \vec{p}_N, t\right) d\Omega, \tag{1.1}$$

where $d\Omega$ is an infinitesimal element of the phase space spanned by the coordinates and momenta of all carriers. For most of the systems of interest, the many-particle distribution function, $f(\vec{r}_1, ..., \vec{r}_N, \vec{p}_1, ..., \vec{p}_N, t)$, is too difficult to be determined since it contains all possible *correlations* among particles, i.e. how each particle motion depends on the other particles. The many-particle distribution function fits the following Boltzmann's equation [10–13]

$$\frac{\partial f\left(\vec{r},\vec{p},t\right)}{\partial t}+\frac{\vec{p}}{m}\cdot\vec{\nabla}_{r}f\left(\vec{r},\vec{p},t\right)+\vec{F}\cdot\vec{\nabla}_{p}f\left(\vec{r},\vec{p},t\right)=\left(\frac{\partial f\left(\vec{r},\vec{p},t\right)}{\partial t}\right)_{coll}, \tag{1.2}$$

where $\vec{F}$ is an external force and $\left(\frac{\partial f(\vec{r},\vec{p},t)}{\partial t}\right)_{coll}$ is the so called collision integral, which contains the description of interaction processes. In most of practical cases, the collision integral is approached by Fermi golden rule. Due to the difficulties to solve Boltzmann's equation the *relaxation time approximation* is likely used to solve this equations [9]. Alternatively, there is a direct approach to study this system using Newton equations taking into account random scattering force [11], it is the Monte Carlo solution of the Boltzmann equation. For some example of studying electronic devices via the Boltzmann transport equation with the Monte Carlo method we mention DAMOCLES and synopsys simulators [14, 15]. Although the Boltzmann transport equation accounts for far from equilibrium conditions, its fundamental limitation comes from its single particle formulation and it describes a many particle system of carriers in terms of a *single particle* distribution function.

It is important to emphasize that the Monte Carlo solution of the Boltzmann equation has been successfully used to study high-frequency behavior of micrometric devices. In fact, for such nanometric devices, where the wave nature of electron is not relevant, the Monte carlo solution of the Boltzmann equation can be successfully applied. In this regard, the BITLLES simulator explained in Appendix C includes (i) Monte Carlo solutions of the Boltzmann equation and (ii) Monte Carlo solutions of the many-particle Schrödinger equation. Since both types of simulations describe electrons as (classical or quantum) trajectories, 70 per cent of the software of BITLLES (such as those routines related to the Poisson equation, injection rates, electron dynamics,etc.) are identical. The main difference is that the electron velocity in the classical trajectory is computed from the electric field, while it is related to the many-particle wave function in Bohmian trajectories.

1.4.1.2 Moment methods of Boltzmann's equation: Drift-diffusion and hydrodynamic approaches

The carrier density continuity equation, momentum conservation equation and the energy conservation equation are derived from Boltzmann's equation. Stratton was the first to introduce the general conservation or momentum-energy balance approach to investigate hot electron transport in semiconductors. The analysis is performed by Stratton utilizing a spherical harmonic expansion with the relaxation time approximation [8, 16]. Blotekjaer extended this theory to retain all terms of moments i.e. without any approximation [8, 17]. The conservation equations are obtained through the three first moments of Boltzmann's equation. We have recalled these equations because there are used to derive the kinetics models such us drift-diffusion and hydrodynamic models. Assuming the relaxation time approximation for the collision terms and neglecting generation-recombination processes, the hydrodynamic carrier density continuity , the hydrodynamic momentum conservation , and the hydrodynamic energy conservation equations, respectively read as follows,

$$\frac{\partial n}{\partial t}+\vec{\nabla}\left(n\vec{v}\right)=0, \tag{1.3}$$

$$\frac{\partial \vec{v}}{\partial t} + \left(\vec{v}\vec{\nabla}\right)\vec{v} + \frac{\vec{F}}{m} + \frac{1}{mn}\vec{\nabla}\left(nK_B T_e\right) = -\frac{\vec{v}}{\tau_n\left(\varepsilon\right)}, \tag{1.4}$$

$$\frac{\partial \varepsilon}{\partial t} + \vec{v}\vec{\nabla}\varepsilon + \vec{v}\vec{F} + \frac{1}{n}\vec{\nabla}\left(n\vec{v}K_B T_e\right) = -\frac{\varepsilon - \varepsilon_0}{\tau_e\left(\varepsilon\right)}, \tag{1.5}$$

where n, $\vec{v}$ and ε are the average carrier density, velocity and energy of the electrons respectively, m is the effective mass, K_B and T_e are the Boltzmann constant and the temperature of the carriers, and τ_n and τ_e are the momentum and energy relaxation times respectively. Needless to say that such a simplification of the BTE, besides other additional limitations, still suffers from the same limitations as the BTE, this is from being a *single-particle* approach.

Departing again from the first three moments of the Boltzmann transport equation, but now assuming that the gradient of the carrier's temperature is negligible, that the carriers are always in equilibrium with the crystal, that the term $\left(\vec{v}\vec{\nabla}\right)\vec{v}$ is small enough in comparison with the other terms, and finally assuming a quasi-stationary regime, the equations to be solved are reduced to the drift-diffusion carrier density continuity equation and the drift-diffusion momentum conservation equation, i.e.

$$\frac{\partial n}{\partial t} = \frac{1}{e}\vec{\nabla}\vec{J} + \left(\frac{\partial n}{\partial t}\right)_{coll}, \tag{1.6}$$

$$\vec{J} = n\mu\vec{F} + eD\vec{\nabla}n, \tag{1.7}$$

and the mean-field Poisson equation. In (1.7) D is the diffusion coefficient defined through the Einstein relation $D = \frac{K_B T \mu}{e}$, $\mu = \frac{e\tau_n}{m}$ is the electron mobility, and $\vec{J} = e \cdot \vec{v}$.

Besides still suffering from a *single-particle* treatment of electron dynamics, the drift-diffusion equations assume thermal equilibrium between the crystal and the conducting electrons, which constitutes a strong approximation that forces the system to remain under *near-equilibrium* conditions.

The most popular method to solve the equations of these models is the self-iterative method which is the first time developed by Gummel [18–20]. These models can be found in commercial simulator like SILVACO [21]. They are time-dependant methods which are valid for high frequency behaviors of semiclassical micrometric devices. They are however not valid for quantum transport.

1.4.2 Electron transport models where the wave-like nature is relevant

We present here the models where the wave-nature of electrons is emphasized. They are generally named quantum models. Nowadays modeling and characterizing the quantum electron devices is increasing , thus tending to study this type of components is crucial. For this reason we tackle the quantum simulation tools , we start with Landauer approach, then quantum Wigner-Boltzmann transport equation , after non-equilibrium Green's functions (NEGF) approach and finally density functional theories.

1.4.2.1 Landauer approach

The Landauer approach probably constitutes the simplest quantum description of electron transport. Nonetheless, its ingenious and intuitive formulation has make it possible to understand several quantum transport phenomena. It supposes that the current through a conductor is only expressed in terms of the transmission probability of carriers injected from the external contacts.
The conductance of a large macroscopic sample obeys a simple ohmic law: $G = \sigma W/L$. However, as devices with smaller dimensions are considered, two corrections to this law are needed. In one hand , there is an interface resistance independent of the length L of the sample. In other hand the conductance does not decrease linearly with W. Instead it depends on the number of transverse modes in the conductor and does down in discrete steps [22].

The Landauer formula including both features mentioned before reads [22],

$$G = \frac{2e^2}{h} MT, \tag{1.8}$$

where $G_0 = \frac{2e^2}{h}(12.9k\Omega)^{-1}$ is known as the quantum conductance unit. The factor T represents the average probability that an electron injected at one end of the conductor will transmit to the other end , M is the number of modes. The formula (1.8) relates the macroscopic conductance G with the factor T of the electron device, and provides a conceptual framework of thinking about conductance. More details about the Landauer formula derivation is developed in the book [22].

In Landauer approach, in order to model the I-V characteristics, we consider a one-dimensional structure under an applied source-drain bias, V_{sd}, for various gate bias (that determines the barrier height) conditions. For a finite temperature the Landauer formula [23] is:

$$I_{V_{sd}} = \frac{2q}{h} \int_0^\infty dE \sum_{n,m=1}^{\infty} T_{n,m}(E) \left[f(E) - f(E + qV_{sd}) \right], \tag{1.9}$$

where q is the electron charge, h is the Planck's constant, $f(E)$ and $f(E + qV_{sd})$ are the Fermi-Dirac distributions of source and drain reservoir respectively, and $T_{n,m}(E)$ is the transmission coefficient that depends on the detailed shape that define the potential. Also, $T_{n,m}(E)$ depends on the electron conduction channels that can be defined through the use of the indexes, n and m, that accounts for the electron energy confinement in the two lateral dimensions.

The original formulation of the Landauer approach is a single-particle model and it neglects electron-electron interaction, i.e. it assumes that the systems behave as a Fermi liquid [24]. The popularity and the main virtues of the Landauer approach are due to its simplicity, the relatively low computational requirements and its rather intuitive picture of quantum electron transport. However, since continuous particles (scattering states) are assumed throughout the system, transient simulations are difficult or impossible to implement using the Landauer approach, i.e. it is a *steady-state formalism*. This approach can, by definition, only capture mean field properties of the electron dynamics [25].

1.4.2.2 Quantum Wigner-Boltzmann transport equation

We shall consider a quantum transport based on Wigner function which was introduced by Eugene Wigner in 1932 as a quantum equivalent of classical particle distribution functions [4]. Szilard and Wigner shows that the expressions of the density matrix of quantum dynamics can be transformed in a form directly comparable with its classical analog [26]. Wigner functions were closely scrutinized by theoretical physicists but only recently their value for semiconductor simulation was discovered. The goal was to link the wave function that appears in the Schrödinger equation to a probability distribution in phase space.

It was firstly introduced by Wigner as,

$$f_w\left(\vec{r}_1,...,\vec{r}_N,\vec{k}_1,...,\vec{k}_N,t\right) \propto \sum_j \int_{-\infty}^{+\infty} \Psi_j\left(\vec{r}_1+\vec{y}_1,...,\vec{r}_N+\vec{y}_N,t\right) \tag{1.10}$$

$$\cdot\Psi_j^*\left(\vec{r}_1-\vec{y}_1,...,\vec{r}_N-\vec{y}_N,t\right)\cdot\prod_{k=2}^{N} d\vec{y}_k e^{2i\vec{k}_i\vec{y}_i}. \tag{1.11}$$

Nonetheless, the Wigner function is today understood as the *one-reduced Wigner pseudo-distribution*. Analogously to the deduction of the *one-particle distribution function* $f\left(\vec{r},\vec{p},t\right)$ from the classical *many-particle distribution function* $f\left(\vec{r}_1,...,\vec{r}_N(t),\vec{p}_1,...,\vec{p}_N(t),t\right)$, from the *density matrix*

$$\rho\left(\vec{r}_1,...,\vec{r}_N,t\right)=\sum_j p_j\left|\Psi_j\left(\vec{r}_1,...,\vec{r}_N,t\right)\right\rangle\left\langle\Psi_j\left(\vec{r}_1,...,\vec{r}_N,t\right)\right|, \tag{1.12}$$

we can obtain a *reduced density matrix* as follows

$$\rho\left(\vec{r},\vec{r}',t\right)\propto\sum_j\int\Psi_j\left(\vec{r},\vec{r}_2,...,\vec{r}_N,t\right)\Psi_j^*\left(\vec{r}',\vec{r}_2,...,\vec{r}_N,t\right)\prod_{i=2}^{N}d\vec{r}_i. \tag{1.13}$$

The *Wigner function*, can be then calculated from the *reduced density matrix* as

$$f_w\left(\vec{r},\vec{k},t\right)\propto\int_{-\infty}^{+\infty}\rho\left(\vec{r}+\vec{y},\vec{r}-\vec{y},t\right)d\vec{y}e^{2i\vec{k}\vec{y}}. \tag{1.14}$$

The Wigner equation reads,

$$\frac{\partial f_w\left(\vec{r},\vec{k},t\right)}{\partial t}+\frac{\hbar\vec{k}}{m}\vec{\nabla}_r f_w\left(\vec{r},\vec{k},t\right)+$$
$$\frac{1}{2\pi\hbar}\int d\vec{k}V_w\left(\vec{r},\vec{k}-\vec{k}'\right)f_w\left(\vec{r},\vec{k}',t\right)=0, \tag{1.15}$$

where the Wigner potential V_w is defined as

$$V_w\left(\vec{r},\vec{k}\right)=\frac{1}{i\hbar\left(2\pi\right)^3}\int\left(V\left(\vec{r}-\vec{y}\right)-V\left(\vec{r}+\vec{y}\right)\right)\exp\left(-i\vec{k}\vec{y}\right)d\vec{y}. \tag{1.16}$$

Taking into account Boltzmann scattering , the equation (1.15) becomes [23, 25, 27, 28],

$$\frac{\partial f_w\left(\vec{r},\vec{k},t\right)}{\partial t}+\frac{\hbar\vec{k}}{m}\vec{\nabla}_r f_w\left(\vec{r},\vec{k},t\right)+\frac{1}{2\pi\hbar}\int d\vec{k}V_w\left(\vec{r},\vec{k}-\vec{k}'\right)f_w\left(\vec{r},\vec{k}',t\right) = \left(\frac{\partial f_w\left(\vec{r},\vec{k},t\right)}{\partial t}\right)_{coll}, \tag{1.17}$$

In this regard, the Wigner-Boltzmann formalism is based on solving the Wigner-Boltzmann transport equation in the same way as the Boltzmann transport equation does for classical systems.

The Wigner formalism has several virtues. It constitutes a time-dependent approach to electrical transport accounting for far from equilibrium conditions in a rather natural way. However, the limitations of the Wigner function method are very similar to those of the BTE. In the same way as the collision integral in the BTE, the Wigner's one can account, in principle, for all the many-body interactions. Unfortunately, obtaining analytical expressions for the collision integral is a very complicate job, and in practice, interactions are included just at a two-particle level. In this sense, the Wigner function constitutes in practice a *mean-field* approach to quantum electron transport.

1.4.2.3 Non-Equilibrium Green's Functions (NEGF) approach

Non-Equilibrium Green's Functions (NEGF) is a many-body technique, also referred as *Keldysh formalism*, it was developed by Kadanoff , Baym and Keldysh and it has gained increasing attention in the analysis of transport phenomena in nanometric semiconductors systems [22, 24, 29]. This approach allows us, at least in principle, to solve exactly the time-dependent Schrödinger equation for an interacting many-body system, from which it can compute , in principle, the time-dependent current. This is carried out by solving equations of motion for specific time-dependent single-particle Green's functions, from which the physical properties of interest, can be obtained [30]. The concept of Green's functions appears in many physical context including electrostatics and electromagnetics [31].

We briefly review the basic principles of this approach [22, 24]. To do this goal, we consider the following differential equation,

$$D_{op}R = S \tag{1.18}$$

where the response R is related to the excitation S by a differential operator D_{op} through the equation (1.18). We can define a Green's function and express the response in the form,

$$R = D_{op}^{-1}S = GS \tag{1.19}$$

where $G = D_{op}^{-1}$. Concerning the many-body problem we can write,

$$[E - H_{op}]\psi = S \tag{1.20}$$

where ψ is the wave function and S is an equivalent excitation term due to a wave incident from one of the leads. The corresponding Green's function can be written,

$$G = [E - H_{op}]^{-1} \tag{1.21}$$

where H_{op} is the Hamiltonian operator. The Green's function is like the impulse response of a system. There are different techniques to find out the Green's functions, see the references [22, 24]. There are some simulators to study the electronic transport based on the Green formalism. The most recognized one is the NEMO simulator [32].

Despite the powerful and rigorous character of non-equilibrium Green's functions, they are in general accompanied by a rather nonintuitive and hard mathematical formulation. Even more, although electron-electron interactions beyond the mean-field approximation can be introduced throughout the self-energies, using them, except for simple model systems, it is a huge computationally demanding task, and most of the time outright impossible.

1.4.2.4 Density functional theories

The Density Functional Theory technique (DFT) was originally proposed by P. Hohenberg and W. Kohn [33] to calculate equilibrium ground states (i.e. minimum energy). The description of electronic structure , by the DFT method, focuses on the electron density rather than the wavefunction. In 1964 P. Hohenberg and W. Kohn showed the remarkable theorem which states that ground state energy of an N-electron system is functional of one electron density ρ [33]. Starting from an N-electron Hamiltonian

$$\hat{H}\left(\vec{r}_1, ..., \vec{r}_N, \vec{p}_1, ..., \vec{p}_N\right) = \hat{T} + \hat{W} + \hat{V}, \tag{1.22}$$

where $\hat{T}$ is the kinetic energy operator and $\hat{W}$ is the electron-electron interaction operator. Defining the density operator n evaluated at $\vec{r}' = \vec{r}$,

$$n\left(\vec{r}\right) = N \int \left|\Psi\left(\vec{r}, \vec{r}_2, ..., \vec{r}_N, t\right)\right|^2 \prod_{i=2}^{N} d\vec{r}_i, \tag{1.23}$$

and satisfying

$$\int n\left(\vec{r}\right) d\vec{r} = N, \tag{1.24}$$

then, the operator $\hat{V}$, describing a local static potential (like the electron-ion potential), can be written as

$$\hat{V} = \int d\vec{r} V\left(\vec{r}\right) n\left(\vec{r}\right). \tag{1.25}$$

If it is assumed now that for a given $V(\vec{r})$ we have found a density $n(\vec{r})$, satisfying (1.24), which corresponds to the *ground state* of the Hamiltonian (1.22), then the Hohemberg-Kohn theorem states that two external potentials, which differ by more than a constant, cannot

give the same ground-state density. This establishes a one-to-one correspondence between the external potential and the ground-state density [13, 33, 34]

Inspired on the above theorem, Kohn and Sham deduced in 1965 their famous equations [35],

$$\left[-\frac{\hbar^2}{2m}\vec{\nabla}^2 + V_H\left(\vec{r}\right) + V_{xc}\left(\vec{r}\right) + V\left(\vec{r}\right)\right]\phi_k^{KS}\left(\vec{r}\right) = \varepsilon_k\phi_k^{KS}\left(\vec{r}\right), \tag{1.26}$$

corresponding to the solution of the time-independent Schrödinger equation of auxiliary non-interacting electrons in the presence of the potential $V_{KS}\left(\vec{r}\right) = V_H\left(\vec{r}\right) + V_{xc}\left(\vec{r}\right) + V\left(\vec{r}\right)$, where

$$V_H\left(\vec{r}\right) = e^2\int d\vec{r}'\frac{n\left(\vec{r}'\right)}{\left|\vec{r}-\vec{r}'\right|}, \tag{1.27}$$

is the Hartree potential, and $V_{xc}\left(\vec{r}\right)$ is the *unknown exchange-correlation* potential including all the many-body correlation effects.

Solving the above equations yields the wavefunctions $\phi_k^{KS}\left(\vec{r}\right)$, from which the ground-state density is

$$n\left(\vec{r}\right) = \sum_{k=1}^{N}\left|\phi_k^{KS}\left(\vec{r}\right)\right|. \tag{1.28}$$

All properties of the ground-state system can be then extracted from (1.28). Unfortunately, since the exchange-correlation potential is unknown, some kind of educated guess must be formulated.

The main limitation of the ground-state density functional theory in order to describe electron transport, is precisely its ground-state nature. In other words, such a theory assumes that the system under study occupies a *time-independent equilibrium state*. This seems to be not a good starting point in order to describe electron transport. However, there exists some generalizations of the above theory.

In 1984, Runge and Gross generalized DFT to its time-dependent version [13]. Time-dependent density functional theory (TDDFT) includes time in the previous results in a very natural way, and more importantly, it is capable of describing *non-equilibrium* scenarios.

Including a time-dependence into the Kohn-Sham potential, i.e. $V_{KS}\left(\vec{r},t\right) = V_H\left(\vec{r},t\right) + V_{xc}\left(\vec{r},t\right) + V\left(\vec{r},t\right)$, the time-dependent version of the Kohn-Sham equations becomes

$$\left[i\hbar\frac{\partial}{\partial t} + \frac{\hbar^2}{2m}\vec{\nabla}^2 - V_H\left(\vec{r},t\right) - V_{xc}\left(\vec{r},t\right) - V\left(\vec{r},t\right)\right]\phi_k^{KS}\left(\vec{r},t\right) = 0. \tag{1.29}$$

And the charge density is then

$$n\left(\vec{r},t\right) = \sum_{k=1}^{N}\left|\phi_k^{KS}\left(\vec{r},t\right)\right|. \tag{1.30}$$

TDDFT is in principle capable of accounting for both, far from equilibrium conditions and many-body phenomena. Unfortunately, although such theorems constitute a formal

demonstration of the validity of dynamical density-functional theories on predicting the macroscopic electrical current, the true is that we do not know the exact functionals, and some *mean-field* approximations must be used.There are others ways to study the quantum transport such us Monte-Carlo method which is used to solve the many-particle Schrödinger equation, see reference for more details [23]. On the other hand, there are several simulators developed to study the electronic devices based on the methods DFT such us SIESTA [36], TRANSIESTA [37], and for TDDFT see the Octopus [38] simulators.

1.5 summary

Depending on which aspect of the electrons are relevant in each electron device, the wave or the particle, different electron transport models are presented. In general, for large (micrometric) dimensions, those models that emphasize the particle-like nature of electrons are the appropriate ones. On the contrary, for studying electron devices with small (nanometric) dimensions, those models emphasizing the wave-like nature of electrons are preferred. However, there are devices (such those where Coulomb blockade effects are relevant) or phenomena to be studied (such the noise in quantum devices) where a electron transport model using, both, the wave-like and the particle-like nature of electrons are very welcome. The Bohmian model explained in next chapter will be an example.

Finally, let us emphasize that the development of quantum electron transport models for electron devices are quite recent. Most simulators are developed for modeling/ understanding DC transport and there are still many gaps to fill. Among them, quantum simulators able to study AC transport, transients behaviors and fluctuations of the current (noise). This thesis is a step in the direction of proving to the industry and the scientific community such dynamic quantum simulators. In this regard , this thesis is part of the recent developement of the BITLLES simulator see the Appendix C.

Chapter 2

Introduction to Bohmian Mechanics

2.1 Introduction

As mentioned in the introductory chapter, the modeling of classical and quantum electron transport, merged the wave and the particle nature of electrons. In general, quantum transport formalism deals with the wave nature of electrons by using orthodox quantum mechanics tools. In this thesis, we will model quantum electron transport by using , simultaneously, waves and particles. The theoretical backgrounds of this modeling is based on Bohmian mechanics, which will be briefly introduced in this chapter.

We start out by a brief historical development of quantum mechanics showing different interpretations/formulations. Then a preliminary discussion of Bohmian mechanics and a simple way to derive Bohmian velocity are presented to introduce the readers to this topic. Besides that, single and many particle Bohmian velocities are derived by means of Schrödinger and quantum Hamilton-Jacobi equations. The computation of Bohmian velocity and the quantum equilibrium hypothesis , which are the main basic postulates in Bohmian mechanics, are illustrated. Finally, we answer the question on why we are interested in studying Bohmian mechanics for nanoelectronics, showing their advantages solving the many body problem via using the so called conditional wave function and doing the measurement process without passing by the so called wave collapse.

2.2 Historical development of quantum mechanics

The origins of quantum mechanics started with the beginning of the twenty century. In classical physics quantities such us energy were always assumed to be a continuous variables. In 1900 Max Planck noticed that the measured spectrum of electromagnetic radiation produced by hot objects could be explained only if a discrete quanta electromagnetic energy was considered. In another way, he suggested that the black bodies emit or absorb electromagnetic radiation in discrete energies $h\nu$, where ν is the frequency of the emitted or absorbed radiation and h is a constant, named Planck constant [39]. Planck applied Wien displacement law to find out an expression for the energy radiation. The black body radiation problem was already stated by Gustav Kirchhoff in 1859. Planck won the 1918 Nobel Prize on physics for this work. Based on Planck quantum hypothesis, in 1905 Albert Einstein postulated that

light consists of individual *quanta*. By means of this discovery he explained the photoelectric effect suggesting that the energy transfer between light and matter was done by light quanta. The later came to be called *photon* till 1926. The photoelectric effect is the release of electrons from certain metals or semiconductors by the action of light. Einstein received the 1922 Nobel Prize for physics for his photoelectric effect discovering. From Einstein's and Planck's postulations, strong debate was born, theorizing and testing how to go beyond classical mechanics.

In 1913, based on Rutherford model of hydrogen atom, Niels Bohr developed an atomic hydrogen model [40] , avoiding Rutherford model instability which was developed two years before. Bohr stated two different postulates , the first one accounted for the stability of atom and it stated that an atomic system cannot exist in all mechanically possible states, forming a continuum, but in series of discrete stationary states. The second postulate accounted for line spectra, it claimed that the difference in energy in a transition from one state to another was emitted or absorbed as a light quantum $h\nu$. During the First war world in 1914, Arnold Sommerfeld extended the circular orbits of Bohr to elliptic orbits.

Carrying on this historical quantum development, Werner Heisenberg suggested a new and more general formalism of quantum mechanics that became known a *matrix mechanics*, in 1925 [41–43]. This theory was developed with Max Born and Pascual Jordan helps. Two years later, Heisenberg stated his uncertainty principle. The later states that the process of measuring the position x of a particle disturbs the particle momentum p, so that $\Delta x \Delta p \geq \hbar = \frac{h}{2\pi}$, where Δx is the uncertainty of the position, Δp is the uncertainty of the momentum and $\hbar$ is the reduced Planck constant.

During PhD studies of Luis de Broglie, he was focused on the idea that if light can behave as a particle , then particles should be able to behave as waves. Then, and based on the work of Einstein and Planck, he proposed the theory, namely the particle-wave duality, that the matter has the properties of both particles and waves, this it was in 1923. In particular, starting with Einstein equation $E = mc^2$, de Broglie was able to substrate the key components of the equation and create his own formula $h/p = \lambda$, where E, m and p are respectively energy, mass and momentum of particle. c is a speed of light and λ is a wavelength length associated with particle [44].

In 1926, inspiring from de Broglie work (wave-particle duality), Erwin Schrödinger [45] soon realized that the matter could be described by means of a wave picture and then he searched for the general equation governing such wave. Finally, he proposed a fundamental equation for atomic and molecular structure and its dynamical behavior, it is known as *time dependent Schrödinger equation*. Schrödinger interpretation of the *wave function* ψ , at first, was as the density distribution of the electron charge but then Max Born figured out the statistical meaning of $|\psi|^2$ as the probability density of finding the electron in a particular position $\vec{r}$ at time t. Born suggested that unlike the electromagnetic field , the Schrödinger wave function ψ has no direct physical reality. It is only useful to compute $|\psi|^2$, which was interpreted as a real probability [46]. At that time, the equivalence between a matrix explanation of quantum mechanics, created by Werner Heisenberg, Max Born, and Pascual

Jordan, and the wave function created by Schrödinger (Carl Eckart) in March (September) 1926 [47, 48]. The generalization of matrix mechanics was done by Paul Dirac [47].

In general, the history of quantum mechanics is explained in textbooks as a history where each step follows the previous one. However, the real history was much more chaotic and several routes were explored simultaneously. Among them for instance, the ideas of Born, Bohr, Heisenberg and others give place to the orthodox or Copenhagen interpretation of quantum mechanics. This interpretation were strongly supported by Max Born, Wolfgang Pauli and many others. There were important opponents to this interpretation such us Albert Einstein, Erwin Schrödinger, Luis de Broglie, David Bohm and others. Next, we discuss another coherent explanation of all quantum phenomena: Bohmian mechanics.

2.3 Preliminary discussion about Bohmian mechanics

Bohmian mechanics, is also called de Broglie-Bohm theory, the pilot-wave model or a causal interpretation of quantum mechanic. It is an explanation of quantum phenomena formulated initially by Louis de Broglie in 1927 and rediscovered by David Bohm in 1952 [49, 50]. P. Holland said, showing how Bohm were inspired by de Broglie's work:

> *"It should be noted that Bohm took issue with de Broglie's conception of light in witch 'photons' are conceived as massive corpuscles moving within the electromagnetic guiding field , and proposed instead that the only 'real' parameters are the field coordinates and their conjugate momenta" [51].*

This approach is based on the simultaneous use of wave and particles when describing non-relativistic particles (like elctrons) . Bohmian mechanics has been successfully used to compute quantum trajectories in order to understand and predict the behavior of many physical processes: diffraction experiments , barrier and dynamical tunneling and currents in molecules and electrons devices [52]. The initial concept of quantum trajectory was proposed by de Broglie even before the Orthodox formulation of quantum mechanics was formulated. However, most of young scientists at that time were strongly influenced by the work of the Copenhagen school (Heisenberg, Pauli, Dirac , Jordan etc.) . In fact, de Broglie himself, who works mainly alone in Paris, give up his own theory partly as a result of certain criticisms made by Pauli . D. Bohm commented this abandonment saying *"all of the objections of de Broglie and Pauli could have been met if only de Broglie had carried his ideas to their logical conclusion"* [49].

A simple way to understand the differences between Bohmian mechanics and the Copenhagen or orthodox interpretation briefly explained in the introduction is looking on how the concepts of waves and particles are merged to explain quantum phenomena. Therefore, two different route can be defined [53]:

1. *Wave or particle?*: It is depending on the experimental situation one can choose between a wave or particle behavior. The electron position is determined by means of the probability density $|\psi|^2$ (Born law), on one hand. On the other hand, the particle

nature of the electron appears when we measure the electron position. In Bohr's words, an object cannot be both a wave and a particle at the same time; it must be either one or the other , depending upon the situation. This approach is called (or it fits) the Copenhagen , or orthodox interpretation of the quantum mechanics.

2. *Wave and particle*: This route represents an explanation of the quantum phenomena were the wave and the particle concepts merge at the atomic scale assuming that a pilot-wave solution of Schrödinger's equation guides the electron trajectory , as the electron is guided by the electromagnetic field. This is what we call Bohmian mechanics. One object cannot be a wave and a particle at the same time, but two can.

In this chapter we develop the ideas inspired by the second route. There are several ways to derive these trajectories, we start with a very simple and intuitive one which is based on obtaining a quantum velocity from a generic wave plane [54].

2.3.1 A simple way to derive Bohmian velocity

For this purpose we consider the following generic plane wave,

$$\psi(\vec{r},t) := e^{i(\vec{k}\vec{r}-\omega t)}, \tag{2.1}$$

where the frequency ω is related with particle energy E through Planck equation by,

$$E = \hbar\omega. \tag{2.2}$$

Considering now de Broglie relation $\vec{p} = \hbar\vec{k}$. We now look for an equation of motion for the particle. To obtain $\vec{k}$ from ψ, we do the spacial derivative of (2.1) and we divide by i and ψ. Thus, from (2.1) and (2.2) we get the following motion equation,

$$m\vec{v} = p = \hbar\vec{k} = \frac{\hbar}{i}\frac{\nabla\psi}{\psi}. \tag{2.3}$$

When we consider, instead of (2.1), a general and arbitrary complex-valued wave function, then we end up with a complex velocity vector. The simplest choice is to take the real part of the expression (2.3). Since the equation (2.3) can be rewritten,

$$m\vec{v} = \frac{\hbar}{i}\{Re(\frac{\nabla\psi}{\psi}) + iIm(\frac{\nabla\psi}{\psi})\}, \tag{2.4}$$

where Im and Re mean respectively, imaginary and real parts of this function. Therefore the Bohm equation or the Bohm field velocity is [54],

$$\vec{v}^{\psi} := \frac{\hbar}{m}Im(\frac{\nabla\psi}{\psi}). \tag{2.5}$$

Similarly, we can derive Schrödinger's equation. Classically , the energy of particle is written like,

$$E = \frac{p^2}{2m} + V. \tag{2.6}$$

where V is the potential energy. Using (2.1), (2.2) and (2.3) we found,

$$E = -\frac{\hbar}{i\psi}\frac{\partial\psi}{\partial t}, \tag{2.7}$$

and

$$p^2 = -\hbar^2\frac{\Delta\psi}{\psi}. \tag{2.8}$$

where Δ is the nabla operator. Then substituting (2.7) and (2.8) into (2.6) , we get,

$$-\frac{\hbar}{i\psi}\frac{\partial\psi}{\partial t} = -\frac{\hbar^2}{2m}\frac{\Delta\psi}{\psi} + V. \tag{2.9}$$

Multiplying the last equation (2.9) by ψ we obtain Schrödinger's equation [54],

$$-\frac{\hbar}{i}\frac{\partial\psi}{\partial t} = \{-\frac{\hbar^2}{2m}\Delta + V\}\psi. \tag{2.10}$$

2.4 Bohmian mechanics for single particle

After the intuitive presentation done in the previous subsection, here, we show how to describe a quantum system associated to only one particle (or one degree of freedom) in terms of trajectories, starting from the Schrödinger's equation. In particular, we look for a more formal and general way of defining a Bohmian velocity from Schrödinger's equation. The general procedure is the following: from Schrödinger's equation we derive a continuity equation for $\rho = |\psi|^2$ which includes a definition of current probability and then, by dividing the current probability by ρ, we get a velocity field [23, 54]. After that an equivalent and additional derivation of the velocity will be obtained from the quantum Hamilton-Jacobi equation [23, 49].

2.4.1 Bomian velocity from Schrödinger equation

For a $1D$ system subjected to a scalar time-dependent potential energy, $V(x,t)$, the single-particle Schrödinger equation can be written,

$$i\hbar\frac{\partial\psi(x,t)}{\partial t} = -\frac{\hbar^2}{2m}\frac{\partial^2\psi(x,t)}{\partial x^2} + V(x,t)\psi(x,t). \tag{2.11}$$

The orthodox interpretation of $\psi(x,t)$ (2.11) does not describe a single experiment, but it characterize an ensemble of identical particle (single-particle) experiments [23].

Let us look for a local continuity equation inside Schrödinger equation (2.11). To do this goal , we use $\psi(x,t)$ and its complex conjugate $\psi^*(x,t)$. Then , we can rewrite Eq. (2.11) as,

$$\psi^*(x,t)i\hbar\frac{\partial\psi(x,t)}{\partial t} = -\psi^*(x,t)\frac{\hbar^2}{2m}\frac{\partial^2\psi(x,t)}{\partial x^2} + \psi^*(x,t)V(x,t)\psi(x,t), \tag{2.12}$$

$$-\psi(x,t)i\hbar\frac{\partial\psi^*(x,t)}{\partial t} = -\psi(x,t)\frac{\hbar^2}{2m}\frac{\partial^2\psi^*(x,t)}{\partial x^2} + \psi(x,t)V(x,t)\psi^*(x,t). \tag{2.13}$$

From the the equations (2.12) and (2.13), we found,

$$\frac{\partial|\psi(x,t)|^2}{\partial t} = i\frac{\hbar}{2m}\frac{\partial}{\partial x}\left(\psi^*(x,t)\frac{\partial\psi(x,t)}{\partial x} - \psi(x,t)\frac{\partial\psi^*(x,t)}{\partial x}\right). \tag{2.14}$$

The equation (2.14) can be considered as the local conservation of particles when $\rho(x,t) = |\psi(x,t)|^2$ and we define the current density , $J(x,t)$, as,

$$J(x,t) = i\frac{\hbar}{2m}\left(\psi(x,t)\frac{\partial\psi^*(x,t)}{\partial x} - \psi^*(x,t)\frac{\partial\psi(x,t)}{\partial x}\right). \tag{2.15}$$

The Schrödinger equation is compatible with a local conservation of particles, unlike most wave function equations. This is due, in part, to the fact that $V(x,t)$ is a real function. It can be interpreted $\rho(x,t) = |\psi(x,t)|^2$ as a spatial distribution of an ensemble of trajectories. Now if we want to find the quantum trajectories supported by the local conservation law (2.14), we have to search for a definition of the particle velocity. Knowing that $|\psi(x,t)|^2$ is the distribution of the ensemble of particles in the configuration space , we can easily show that the particle velocity compatible with the local conservation of particles is [23],

$$v(x,t) = \frac{J(x,t)}{|\psi(x,t)|^2}, \tag{2.16}$$

where $J(x,t)$ is defined from equation (2.15). Due to the continuity equation (2.14) , an ensemble of well defined trajectories whose initial positions are all selected according the distribution $|\psi(x_o,t_o)|^2$ will reproduce $|\psi(x,t)|^2$ at all times if they move according to the quantum velocity (2.16). This last property provides full meaning to the definition of the Bohmian velocity for quantum trajectories.

2.4.2 Bomian velocity from quantum Hamilton-Jacobi equation

Alternatively, we can find the same particle velocity from a quantum Hamilton-Jacobi equation. This was the development done by Bohm in his original work [49]. We write the quantum (complex) wave function , $\psi(x,t) = \psi_r(x,t) + i\psi_i(x,t)$, in a polar form,

$$R^2(x,t) = \psi_r^2(x,t) + \psi_i^2(x,t), \tag{2.17}$$

$$S(x,t) = \hbar\arctan\left(\frac{\psi_i(x,t)}{\psi_r(x,t)}\right). \tag{2.18}$$

The wave function phase $S(x,t)$ is not well defined when $\psi_r(x,t) = \psi_i(x,t) = 0$. However, there we get $R(x,t) = 0$, meaning that no electrons will reach this configuration point ,

so that in general we do not need to compute the velocity there. The quantum Hamilton-Jacobi equation can be derived by introducing the polar form of wave function $\psi(x,t) = R(x,t)\exp(iS(x,t)/\hbar)$ into (2.11). On one hand, one of the resulting equation gives the law conservation law,

$$\frac{\partial R^2(x,t)}{\partial t} + \frac{\partial}{\partial x}\left(\frac{1}{m}\frac{\partial S(x,t)}{\partial x}R^2(x,t)\right) = 0. \tag{2.19}$$

On the other hand, the real one gives a quantum Hamilton-Jacobi equation,

$$\frac{\partial S(x,t)}{\partial t} + \frac{1}{2m}\left(\frac{\partial S(x,t)}{\partial x}\right)^2 + V(x,t) + Q(x,t) = 0. \tag{2.20}$$

The term appeared in quantum Hamilton-Jacobi equation is called *quantum potential* and it is defined [49],

$$Q(x,t) = -\frac{\hbar^2}{2m}\frac{\partial^2 R(x,t)/\partial x^2}{R(x,t)}. \tag{2.21}$$

We conclude that we can interpret the wave function solution of Schrödinger equation as an ensemble of quantum trajectories, with different initial positions and velocities. Then the velocity of each trajectory $x[t]$ is defined [23, 49, 55],

$$v[t] = \left[\frac{1}{m}\frac{\partial S(x,t)}{\partial x}\right]_{x=x[t]}. \tag{2.22}$$

It can be shown that the new expression of quantum velocity is identical to what mentioned in expression (2.16),

$$v(x,t) = \frac{1}{m}\frac{\partial S(x,t)}{\partial x} = \frac{J(x,t)}{|\psi(x,t)|^2}, \tag{2.23}$$

where $J(x,t)$ is defined (2.15). The derivation of the Bohm trajectory from quantum Hamilton-Jacobi equation show that the particles moves under the action of a force which is not entirely derivable from the classical potential , $V(x)$, but which also obtains a contribution from the quantum potential , $Q(x,t) = -\frac{\hbar^2}{2m}\frac{\partial^2 R(x,t)/\partial x^2}{R(x,t)}$.

The time derivative of the Bohmian velocity can be written [25, 49],

$$m\frac{d^2 v(x[t],t)}{dt} = [-\frac{-\partial}{\partial x}(V(x,t) + Q(x,t))]_{x=x[t]} \tag{2.24}$$

The quantum trajectories are not solutions of the classical Newton law with the classical energy , but they are solutions of the quantum Newton law (2.24) where a quantum potential , which take into account all non classical effects, is added to the classical potential.

2.5 Bohmian mechanics trajectories for many-particle systems

From a computational point of view, one of the most complicated problem when studying quantum transport is to deal with many body problems. Historically, there are many attempts to tackle this problem with different quantum techniques. Thus, it is mandatory to see how these Bohmian trajectories are defined in many-particle systems. We will see later that these trajectories, somehow, allow us to avoid dealing with the entire wave function when using the conditional wave-function. Here we briefly derive the many-particle Bohmian velocity from Schrödinger and quantum Hamilton-Jacobi many-particle equations. Their derivations are quite similar to those for single particle.

2.5.1 Bohmian trajectories for many-particles from Schrödinger equation

We consider M spinless particles, the dynamic of this system is obtained from the following Schrödinger equation,

$$i\hbar\frac{\partial\psi(x_1,\ldots,x_M,t)}{\partial t}=\left(\sum_{k=1}^{N}-\frac{\hbar^2}{2m}\frac{\partial^2}{\partial x^2}+U(x_1,\ldots,x_M,t)\right)\psi(x_1,\ldots,x_M,t). \tag{2.25}$$

The solution of this equation is called *many particle wave function*. Similarly to how we found the single particle version (2.14) , we can easily found,

$$\frac{\partial|\psi(\vec{x},t)|^2}{\partial t}+\sum_{k=1}^{M}i\frac{\hbar}{2m}\frac{\partial}{\partial x_k}\left(\psi(\vec{x},t)\frac{\partial\psi^*(\vec{x},t)}{\partial x_k}-\psi^*(\vec{x},t)\frac{\partial\psi(\vec{x},t)}{\partial x_k}\right)=0. \tag{2.26}$$

Then k-th component of the $N-$vector current density can be read,

$$J_k(\vec{x},t)=i\frac{\hbar}{2m}\left(\psi(\vec{x},t)\frac{\partial\psi^*(\vec{x},t)}{\partial x_k}-\psi^*(\vec{x},t)\frac{\partial\psi(\vec{x},t)}{\partial x_k}\right). \tag{2.27}$$

Therefore the equation (2.26) is interpreted as a local conservation of particles and $|\psi(x_1,\ldots,x_N,t)|^2$ as a distribution of an ensemble of N trajectories in configuaration space. Finally, the Bohmian velocity of the k-th trajectory is,

$$v_k(x_1,\ldots,x_M,t)=\frac{J_k(x_1,\ldots,x_M,t)}{|\psi(x_1,\ldots,x_M,t)|^2}. \tag{2.28}$$

2.5.2 Bohmian trajectories for many-particles from quantum Hamilton-Jacobi equation

Introducing the polar form of the many particle wave function $\psi(x_1,\ldots,x_M,t) = R(x_1,\ldots,x_M,t)e^{iS(x_1,\ldots,x_M,t)/\hbar}$ into many particle Schrödinger equation (2.25), one find from the imaginary part,

$$\frac{\partial R^2(x_1,\ldots,x_M,t)}{\partial t} + \sum_{k=1}^{M}\frac{\partial}{\partial x_k}\left(\frac{1}{m}\frac{\partial S(x_1,\ldots,x_M,t)}{\partial x_k}R^2(x_1,\ldots,x_M,t)\right) = 0, \tag{2.29}$$

where we recover the local conservation of particles and the Bohmian velocity of the x_k is defined,

$$v_k(x_1,\ldots,x_M,t) = \frac{1}{m}\frac{\partial S(x_1,\ldots,x_M,t)}{\partial x_k}. \tag{2.30}$$

Similar to the case of single particle, the expressions (2.28) and (2.30) are identical. From the real part of the Schrödinger equation we find,

$$\frac{\partial S(x_1,\ldots,x_M,t)}{\partial t} + \sum_{k=1}^{M}\frac{1}{2m}\frac{\partial^2 S(x_1,\ldots,x_M,t)}{\partial x_k^2} + V(x_1,\ldots,x_M,t) + Q(x_1,\ldots,x_M,t) = 0, \tag{2.31}$$

which is the quantum Hamilton-Jacobi equation for many-particles. The Quantum potential is,

$$Q(x_1,\ldots,x_M,t) = \sum_{k=1}^{M} Q_k(x_1,\ldots,x_M,t), \tag{2.32}$$

with,

$$Q_k(x_1,\ldots,x_M,t) = -\frac{\hbar^2}{2m}\frac{\partial^2 R(x_1,\ldots,x_M,t)/\partial x_k^2}{R(x_1,\ldots,x_M,t)}. \tag{2.33}$$

One important conclusions that we get from these results is that the Bohmian velocity of one particle x_1 depends non-locality on the rest of trajectories. This is a fundamental requirement for any accurate explanation of quantum phenomena.

2.6 Main postulates of Bohmian mechanics

Let us present the basic postulates of Bohmian mechanics. We will present the theory in terms of two main basic postulates [23, 53, 56].

2.6.1 First postulate

To illustrate this postulate, we consider a system M electrons described in the spatial coordinates $\vec{r} = \{\vec{r}_1,.....,\vec{r}_M\}$ by the many-particle wave-function $\psi(\vec{r},t)$ obeying to many-particle Schrödinger equation,

$$i\hbar\frac{\partial\psi(\vec{r},t)}{\partial t} = \Big\{\sum_{a=1}^{M} -\frac{\hbar^2}{2m^*}\nabla_a^2 + U(\vec{r},t)\Big\}\psi(\vec{r},t), \tag{2.34}$$

and for simplicity, we have considered a solid-state system where the lattice-electron interaction is included by means of the electron effective mass, m^*. The term $U(\vec{r},t)$ is the potential energy that , here, defines the Coulomb interaction among electrons.

From equation (2.34) it can be demonstrated that the probability distribution, $|\psi(\vec{r},t)|^2$, obeys to the following continuity equation [57] ,

$$\frac{\partial|\psi(\vec{r},t)|^2}{\partial t}+\sum_{a=1}^{M}\nabla_a\vec{j}_a(\vec{r},t)=0, \tag{2.35}$$

where $\vec{j}_a(\vec{r},t)$ is the $a-$th component of the usual probability current density defined as,

$$\vec{j}_a(\vec{r},t)=\frac{i\hbar}{2m}\big(\psi\vec{\nabla}_a\psi^*-\psi^*\vec{\nabla}_a\psi\big). \tag{2.36}$$

From equation (2.35) the vector field defined as

$$\vec{v}_a(\vec{r},t)=\vec{j}_a(\vec{r},t)/|\psi(\vec{r},t)|^2 \tag{2.37}$$

and it can be interpreted as a *velocity field* for the $a-$particle. This velocity can be used to define trajectories in the configuration space,

$$\vec{r}_a(t)=\vec{r}_a(t_0)+\int_{t_0}^{t}\vec{v}_a(\vec{r}(t'),t')dt', \tag{2.38}$$

with $\vec{r}(t)=\{\vec{r}_1(t),...,\vec{r}_M(t)\}$ and $\vec{r}_a(t_0)$ is the initial position.Thus, the dynamic of a single particle in a quantum system is defined by the trajectory $\vec{r}_a(t)$ that moves continuously under the guidance of the Schrödinger equation.

2.6.2 Second postulate

The initial position and velocity of a particular trajectory cannot be certainly known. When an experiment is repeated many times $j=1,...,N$, the initials positions $\vec{r}_a^{\,j}(t_0)$ of an ensemble of trajectories $\vec{r}_a^{\,j}(t)$, associated with the same $\psi(\vec{r},t)$, have to be generated so that the number of trajectories of the ensemble between $\vec{r}$ and $\vec{r}+d\vec{r}$ at the initial time t_0 would be proportional to $|\psi(\vec{r},t_o)|^2$.

The condition on the initial position can be mathematically written as,

$$|\psi(\vec{r},t_0)|^2=\lim_{N\to\infty}\frac{1}{M}\sum_{j=1}^{N}\prod_{a=1}^{M}\delta(\vec{r}_a-\vec{r}_a^{\,j}(t_0))\ \text{ for } t=t_0, \tag{2.39}$$

where $j=1,...,N$ is the number of different trajectories of the ensemble. If the probability density for the configuration satisfies $R^2(\vec{r},t_o)=|\psi(\vec{r},t_o)|^2$ at t_0, then the probability density at any time t is given by $R^2(\vec{r},t)=|\psi(\vec{r},t)|^2$. This is an extremely important property of any Bohmian mechanics. That condition together with the continuity equation (2.35), which make Bohmian mechanics to predict the same results as orthodox quantum theory. In other word, these assumption which guarantees a total agreement between Bohmian mechanics and quantum mechanics regarding the results of any experiment, and it is called

quantum equilibrium hypothesis [53, 58]. Equations (2.34), (2.35), (2.36), (2.37) and (2.38) constitute a basic set of equations describing Bohmian mechanics [53].

In fact, it is argued that the second postulate about the quantum equilibrium is just a consequence, not a postulate, of the behavior of the universal many-particle wave-function [58, 60]. Additionally, for system of identical particles, a third postulate can be presented to ensure the proper symmetrization of the wave function, it is not discussed in this thesis. Again, it is argued that such symmetrization is not a postulate in Bohmian mechanics, but a consequence of dealing with identical Bohmian trajectories in the configuration space [58, 60]. This topics are certainly far from the scope of the present thesis.

2.7 Measurement in Bohmian mechanics

In general, the orthodox quantum measurement is explained in the configuration space of the system alone. According to the orthodox interpretation, the quantum measurement process causes a random *collapse* of the wave function describing the quantum system. This evolution is different from the one obtained from the Schrödinger equation. We resume here two quite different laws which govern the time evolution of the wave function of the quantum system [23, 25, 56]:

1. *First law*: the dynamical evolution of the system is carried out according to the Schrödinger equation and it is deterministic. The final wave function of the quantum system is perfectly determined when we know the initial wave function and the Hamiltonian of the quantum system. This process happens when the system is not measured.

2. *Second law*: this law is what we previously called the collapse of the wave function. The latter before the measurement is substituted by one of the eigenstates of the particular operator $\hat{A}$ related to measuring apparatus. Contrarily to the first law, the collapse is not deterministic. The final wave function is randomly selected from the list of the operator's eigenstates list. This process happens during the measuring period.

We are interesting into studying Bohmian mechanics for its ability , besides to reproduce all results obtained by orthodox mechanic, to predict measurable results without invoking the wave function collapse. In the Bohmian theory the measurement process is treated just as any other quantum process and the previous measurement difficulties of the orthodox interpretation disappear. The whole quantum system , by means of this theory, is described by a particle plus a wave function , rather than a wave function alone in orthodox mechanics. The wave function and the trajectories are both , associated to the quantum system plus the measurement apparatus. The orthodox quantum theory requires an operator to describe the effect of the measuring apparatus, while such operator is not needed in the Bohmian mechanics [23].

The proper modeling of a Bohmian measurement needs an explicit consideration of the degrees of freedom of the pointer in the many particle wave function and many particle Bohmian trajectories that define the whole system. Besides that, a Hamiltonian with or without the measuring apparatus will provide a different evolution of the wave quantum

system wave function according to measurement type. In the next paragraph , we take into account these additional degrees of freedom of the apparatus to explain the measurement process.

The Bohmian explanation of the quantum measurement is the most attractive feature of the Bohmian explanation of the quantum nature [59]. Although the Bohmian and the orthodox explanations of a measurement produce the same probabilistic predictions [49], the mathematical implementation of the motion of the particles is quite different.
In the standard interpretation of quantum theory, the projective measurement process is defined in a particular quantum region, the system. See figure 2.1(b). The state of the quantum system in this particular region is determined by the wave function $\psi_S(\vec{r},t)$. The process of measuring of a particular magnitude is mathematically defined through an operator , for instance $\hat{G}$, acting on the wave function. The possible outcomes of the measurement process correspond to one of the possible eigenvalues g of this operator that satisfy the equation $\hat{G}\psi_g(\vec{r}) = g\psi_g(\vec{r})$, where $\psi_g(\vec{r})$ is an eigenvector of the operator. The set $\psi_g(\vec{r})$ forms an orthogonal basis of the Hilbert space of the quantum system so that the initial wave function at the initial time can be written as,

$$\psi_S(\vec{r},t) = \sum_g c_g(t)\psi_g(\vec{r}) \tag{2.40}$$

where $c_g(t)$ is a complex value fitting the only following restriction $\sum_g |c_g(t)|^2 = 1$. This condition ensures that the wave function $\psi_S(\vec{r},t)$ is well normalized. When measuring the eigenvalue g_a, the total wave function $\psi_S(\vec{r},t)$ collapses into the eigenvector $\psi_{g_a}(\vec{r})$. The probability of getting the value g_a in the measuring apparatus is then just $P_{g_a} = |c_{g_a}(t)|^2$.

In order to mathematically define the measurement process in the Bohmian formalism, besides that the degrees of freedom $\vec{r}$ of the system , the degrees of freedom of the positions of the pointer $\vec{\xi}$ belonging to the measuring apparatus are required [51, 56, 59]. Thus, we define a total wave function $\Phi(\vec{r},\vec{\xi},t)$ in a large configuration space that include the system plus the measuring region, $\{\vec{r},\vec{\xi}\}$. According to the Bohmian postulates, we select a particular trajectory, $\{\vec{r}^{\alpha}(t),\vec{\xi}^{\alpha}(t)\}$ of this larger configuration space, where $\alpha = 1,2,...,M_\alpha \to \infty$. The subindex α takes into account the uncertainty associated with the initial quantum state according to quantum equilibrium condition defined in the section 2.6.2. Then in order to be able to say that a measuring apparatus is able to correctly determine the eigenvalue g, there are some necessary conditions that the entire system has to satisfy:

First, the pointer positions $\vec{\xi}^{\alpha}(t)$ of such an apparatus have to be restricted to a particular region, $\vec{\xi}^{\alpha}(t) \in S_{g_1}$, every time that the quantum system is in the eigenstate $\psi_{g_1}(\vec{r}_S)$. We define S_g as a restricted set of positions in the space of ammeter position ξ. Let us define $\Phi_{g_1}(\vec{r},\vec{\xi},t)$ as the total wave function that fits the property that any experiment whose quantum system is described by $\psi_{g_1}(\vec{r})$ implies that the pointer points in the particular region $\vec{\xi}^{\alpha}(t) \in S_{g_1}$.

Second, the subspaces S_{g1} and S_{g2} of the whole configurational space must be non overlapping during the measuring, i.e. $S_{g1} \cap S_{g2} = 0$. S_{g2} is defined as the restricted region allowed to the pointer positions associated with second eigenstate, $\psi_{g_2}(\vec{r})$, as $\vec{\xi}^{\alpha}(t) \in S_{g_2}$. This implies that the states $\Phi_{g_1}(\vec{r},\vec{\xi},t)$ and $\Phi_{g_2}(\vec{r},\vec{\xi},t)$ do not overlap in the configuration space during the measurement.

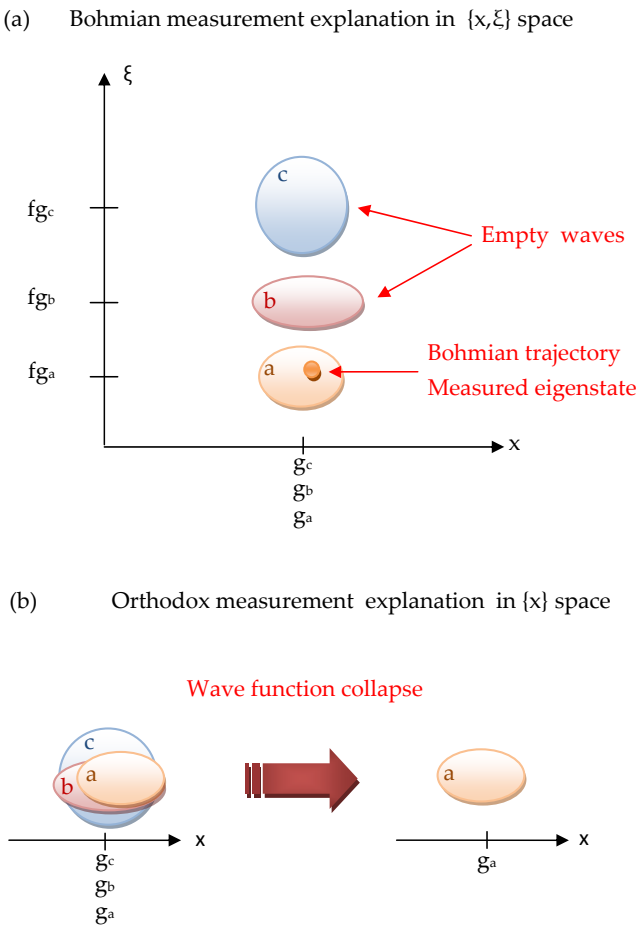

Figure 2.1: (a) Bohmian measurement in the $\{x, \xi\}$ configuration space: from the non overlapping many particle (system+apparatus) wave function, only the g_a part of the wave function where the Bohmian trajectory is present is needed to compute the evolution of the Bohmian system. (b) Orthodox measurement $\{x\}$ space: in this case the system wave function collapses into the eigenvector $\psi_g(\vec{r})$ associated with eigenvalue g_a when the mesurement takes places.

A given good projective measurement apparatus, and a given that the eigenstates $\psi_g(\vec{r})$ form a complete basis, during the measurement, then the only good decomposition for $\Phi_g(\vec{r},\vec{\xi},t)$ is [59],

$$\Phi_g(\vec{r},\vec{\xi},t) = f_g(\vec{\xi},t)\ \psi_g(\vec{r}). \tag{2.41}$$

The $f_g(\vec{\xi},t)$ is a normalized function because $\Phi_g(\vec{r},\vec{\xi},t)$ and $\psi_g(\vec{r})$ are also a normalized functions in their respective space. By construction, $f_{g_1}(\vec{\xi},t) \cap f_{g_2}(\vec{\xi},t) = 0$ during the measuring time. Thus , even if $\psi_{g_1}(\vec{r})$ and $\psi_{g_2}(\vec{r})$ overlap, the states $\Phi_{g_1}(\vec{r},\vec{\xi},t)$ and $\Phi_{g_1}(\vec{r},\vec{\xi},t)$ do not overlap in the larger configuration space. See figure 2.1(a) . We can then ensure that an arbitrary wave function of the quantum system , (2.40), can be rewritten in the whole configuration space associated to a good measuring apparatus as [59],

$$\Phi(\vec{r},\vec{\xi},t) = \sum_g c_g(t)\ \ f_g(\vec{\xi},t)\ \psi_g(\vec{r}) \tag{2.42}$$

In the summary, during the measurement , the only total wave functions that can live in the entire quantum system that includes a good measuring apparatus of the eigenvalues g are the ones written in equation (2.42). An example of such wave functions is depicted in Fig. 2.1(a). It is important to notice that Eq. (2.42) implies no restriction on the wave $\psi_S(\vec{r},t)$ but only on the total wave function $\Phi(\vec{r},\vec{\xi},t)$. If these restrictions are not respected, we can find other types of total wave functions in the configuration space $\{\vec{r},\vec{\xi}\}$, but they would be incompatible with stating that we have an apparatus that is able to measure the eigenvalue g with certainty at time t.

We can now show how the projective measurement is exactly reproduced with the Bohmian mechanics. As we have mentioned, apart from the wave function (2.42), we have to select an initial trajectory $\{\vec{r}^{\alpha}(0),\vec{\xi}^{\alpha}(0)\}$. Such a trajectory will evolve driven by the total wave function , and during the measurement, the particle trajectory $\{\vec{r}^{\alpha}(t),\vec{\xi}^{\alpha}(t)\}$ will be situated in only one of the non overlapping wave packets of (2.42), for example $f_{g_a}(\vec{\xi},t)\psi_{g_a}(\vec{r})$ as depicted in figure 2.1(a).Thus, the pointer positions will be situated in $\vec{\xi}(t) \in S_{g_a}$ and we will conclude with certainty that the eigenvalue of the quantum system is g_a. In addition, the subsequent evolution of this trajectory can be computed from $f_{g_a}(\vec{\xi},t)\psi_{g_a}(\vec{r})$ alone . In other word, we do need the entire wave function (2.42) because the particle velocity can be computed from $f_{g_a}(\vec{\xi},t)\psi_{g_a}(\vec{r})$. The rest of circles of Fig. 2.1(a) are empty waves that do not overlap with $f_{g_a}(\vec{\xi},t)\psi_{g_a}(\vec{r})$ so that they no effect on the velocity of the Bohmian particle.This is how the orthodox collapse is interpreted within Bohmian mechanics.

The Bohmian measurement process explained above implies increasing the number of degrees of freedom that one has to simulate from $\{\vec{r}\}$ to $\{\vec{r},\vec{\xi}\}$. Sometimes , then, the use of the Hermitian operators acting only in the wave function of the quantum system with the ability of providing the outcomes if the measurements process without the explicit simulation of the measuring apparatus is very welcomed. Operators are not needed in Bohmian mechanics but they are very helpful mathematical tricks in practical computations. In the next section we develop the expressions for commutating ensemble results from operators as an infinite sum of Bohmian trajectories

Before finishing this measurement task, we want to mention two technical problems that appear in the numerical simulation of the measurement process done in practical scenarios [56],

1. The first difficulty appears because of the specifying the Hamiltonian determining the system and the apparatus evolution. This difficulty is similar to specifying which is the operator that provides good information about the measuring processus in the orthodox quantum mechanics.

2. The second difficulty is related to the computational limitations coming from solving many particle Schrödinger equation . This problem appears because of adding the pointer which adds degrees of freedom. But this problem disappears when we deal only with the system wave function.

Further discussion of this point can be found in Ref. [56].

2.7.1 The mean value in terms of hermitian operators with Bohmian trajectories

The operators are an indispensable tool in the orthodox formulation of the quantum mechanics to define the measurement process. In contrast, Bohmian mechanics does not require the use Hermitian operators and the wave function collapse as the orthodox mechanics does. Nonetheless , Bohmian mechanics can also express the expectation value of an observable in terms of local observable which are directly deduced from orthodox Hermitian operators. This is a quite usual way of introducing the Bohmian average of measurement.

The exact outcome of a particular quantum experiment described by the pure wave function $\psi(x,t)$ is uncertain. If we repeat a quantum experiment many times with exactly the same wave function $\psi(x,t)$, we obtain a different outcomes. The probabilistic information of the experiment can be treated to obtain the main value.There several equivalent ways for computing the mean value of the magnitude that we are measuring $\hat{A}$. We consider the Hermitian operator $\hat{A}$ and the mean value $\left\langle \hat{A} \right\rangle_{\psi}$ in the position representation.Then the mean value of this operator over the wave function $\psi(x,t)$ is given by,

$$\left\langle \hat{A} \right\rangle_{\psi} = \int_{-\infty}^{\infty} \psi^{*}(x,t) \hat{A} \left(x, -i\hbar \frac{\partial}{\partial x} \right) \psi(x,t) dx. \tag{2.43}$$

Alternatively, the same mean value can be computed from Bohmian mechanics by defining an spatial average of local magnitude $A_B(x)$ weighed by $R^2(x,t)$,

$$\left\langle \hat{A} \right\rangle_{\psi} = \int_{-\infty}^{\infty} R^2(x,t) A_B(x) dx. \tag{2.44}$$

In order to obtain the same value with (2.43) and (2.44), we write $A_B(x)$ as [23, 25],

$$A_B(x) = Real \left(\left[\frac{\psi^{*}(x,t) \hat{A} \left(x, -i\hbar \frac{\partial}{\partial x} \right) \psi(x,t)}{\psi^{*}(x,t)\psi(x,t)} \right]_{\psi(x,t)=R(x,t)e^{i\frac{S(x,t)}{\hbar}}} \right). \tag{2.45}$$

For practical purposes, we will compute the mean value using (Eq. (2.44)) with a large $j = 1, \ldots, M$ number of Bohmian trajectories with different initial positions. The mean value can be written,

$$\left\langle \hat{A} \right\rangle_{\psi} = \lim_{M\to\infty} \frac{1}{M} \sum_{j=1}^{M} A_B(x_j[t]). \tag{2.46}$$

In the limit $M \to \infty$, the value of (2.46) is identical to the value of (2.44). We present now a few exemples of how some common mean values are computed from the orthodox quantum formalism and from Bohmian trajectories. We start computing the mean value of the position,

$$\langle x \rangle_{\psi} = \int_{-\infty}^{\infty} \psi^*(x,t) x \psi(x,t) dx \tag{2.47}$$

with $x_B(x) = x$ so that,

$$\langle x \rangle_{\psi} = \int_{-\infty}^{\infty} R^2(x,t) x dx. \tag{2.48}$$

Identically, the main value of the momentum,

$$\langle p \rangle_{\psi} = \int_{-\infty}^{\infty} \psi^*(x,t) \left(-i\hbar \frac{\partial}{\partial x} \right) \psi(x,t) dx \tag{2.49}$$

with $p_B(x) = \partial S(x,t)/\partial x$,

$$\langle p \rangle_{\psi} = \int_{-\infty}^{\infty} R^2(x,t) \frac{\partial S(x,t)}{\partial x} dx. \tag{2.50}$$

For the classical potential, we have,

$$\langle V \rangle_{\psi} = \int_{-\infty}^{\infty} \psi^*(x,t) V(x,t) \psi(x,t) dx \tag{2.51}$$

with $V_B(x) = V(x,t)$ so that,

$$\langle V \rangle_{\psi} = \int_{-\infty}^{\infty} R^2(x,t) V(x,t) dx. \tag{2.52}$$

We compute now the mean value of the kinetic energy,

$$\langle K \rangle_{\psi} = \int_{-\infty}^{\infty} \psi^*(x,t) \left(-\frac{\hbar^2}{2m} \frac{\partial^2}{\partial x^2} \right) \psi(x,t) dx. \tag{2.53}$$

The local mean value of the kinetic energy takes into account the Bohmian kinetic energy plus the quantum potential. In particular, $K_B(x)$ can be obtained from the expression [23, 25],

$$K_B(x) = Real \left(- \frac{R(x,t) e^{-iS(x,t)/\hbar} \frac{\hbar^2}{2m} \left(\frac{\partial}{\partial x} \right)^2 R(x,t) e^{iS(x,t)/\hbar}}{R^2(x,t)} \right). \tag{2.54}$$

The real part of K_B is [23, 25],

$$K_B = \frac{1}{2m}\left(\frac{\partial S(x,t)}{\partial x}\right)^2 + Q(x,t) \tag{2.55}$$

so that, finally we obtain the Bohmian expression of the mean kinetic energy of the ensemble of trajectories,

$$\langle K\rangle_\psi = \int_{-\infty}^{\infty} R^2(x,t)\left(\frac{1}{2m}\left(\frac{\partial S(x,t)}{\partial x}\right)^2 + Q(x,t)\right)dx. \tag{2.56}$$

In particular, if we want to compute the ensemble (Bohmian) kinetic energy , without the quantum potential $\langle Q\rangle$, using (2.46), it read,

$$\langle K_B\rangle - \langle Q\rangle = \lim_{M_\alpha\to\infty}\frac{1}{M_\alpha}\sum_{\alpha=1}^{M_\alpha}\frac{1}{2}m^* v^2(x^\alpha(t),t). \tag{2.57}$$

Finally, let us notice that the probability density operator can be written as $|x\rangle\langle x|$ and its expected value is $\langle\psi|\, x\rangle\langle x|\,\psi\rangle = |\psi(x,t)|^2$, or it is $\langle\psi|\, x\rangle\langle x|\,\psi\rangle = R^2(x,t)$ in Bohmian language. The hermitian current operator can be written as $\hat{J} = 1/(2m)(|x\rangle\langle x|\,\hat{p}+\hat{p}\,|x\rangle\langle x|)$. It can be demonstrated,

$$\langle J\rangle_\psi = J(x,t) = v(x,t)R^2(x,t) = \lim_{M\to\infty}\frac{1}{M}\sum_{j=1}^{M} v(x_j[t])\delta(x - x_j[t]). \tag{2.58}$$

The average value of the current density depends on the position and it is equal to the average Bohmian velocity multiplied by the square modulus of $R(x,t)$. At a particular position x, this current is just the sum of all particles that reside around the position $x = x_i[t]$ at time t. It is not always possible to know that we have selected a good operator that perfectly describes the system.

2.8 Why Bohmian mechanics for nanoelectronics?

At first sight, it is not at all evident why Bohmian mechanics can help in studying high-frequency quantum transport in nanoelectronic devices. Let us mention that such quantum scenarios need a proper solution of the many-body (Coulomb) to deal with the displacement current and manageable solution of the measurement problem because the AC transport assumes a continuous measurement of the current. There are mainly two reasons why such Bohmian trajectories are useful.

- The use of the (Bohmian) Conditional wave functions to deal with Coulomb interaction
- The use of Bohmian trajectories to deal with the measurement process

In this section, we discuss both.

2.8.1 The Bohmian Conditional Wave Function

One of the reasons of the utility of Bohmian mechanics is its ability to tackle the *many-body* problem discussed before in a different and original way. The active region of an electron device can contain hundreds of electrons. The quantum computation of a wave function with such number of electrons is a very difficult task, in fact, impossible. The many-particle Schrödinger equation can be solved exactly only for very few degrees of freedom, i.e. one, two, three electrons. A standard way to proceed consists then on reducing the complexity of this problem by tracing out some degrees of freedom. For this goal, we discuss in this section how a trajectory-based formulation allows us to tackle this problem with a different way. The concept of *conditional wave function* [58, 60] provides an original tool to deal with open many-body quantum system [56].

To illustrate this point, let consider a bipartite system $A + B$ whose spacial coordinates can be split as $\vec{r} = \{\vec{r}_a, \vec{r}_b\}$. We call each subsystem a A system and its complement a B system or the environment of system A. We define $\vec{r}_a$ as the position of $a-$electron in $\mathbf{R}^3$, while $\vec{r}_b = \{\vec{r}_1, ..., \vec{r}_{a-1}, \vec{r}_{a+1}, ..., \vec{r}_M\}$ are the positions of the rest of electrons in a $\mathbf{R}^{3(M-1)}$ space. The actual particle trajectories are accordingly denoted by $\vec{r}(t) = \{\vec{r}_a(t), \vec{r}_b(t)\}$. Our question now is ,

> *"How one can assign a wave function to each system A and B?"*

In general it is not possible to do that if the two subsystems are entangled, it means that the total wave function cannot be written as product $\psi(\vec{r}) = \psi_a(\vec{r}_a)\psi_b(\vec{r}_b)$. However, asking by another way,

> *"What is the wave function of the system A that provides the exact velocity $\vec{v}_a$ for a given particular position $\vec{r}_b(t)$ in B ?"*

The answer is given by the Bohmian mechanics and it is called *conditional wave function*, this function can be written [56, 58, 60, 61],

$$\psi_a(\vec{r}_a, t) = \psi(\vec{r}_a, \vec{r}_b(t), t), \tag{2.59}$$

which constitutes a multi-dimensional slice of the whole wave function. The expression is considered as a *wave function effective* of the system A [60].

In order to use the conditional wave function to reduce the degrees of freedom of a system we must know how it evolves in time. It can be demonstrated [62] that $\psi_a(\vec{r}_a, t)$ obeys the following wave equation,

$$\begin{aligned} i\hbar\frac{\partial\psi_a(\vec{r}_a,t)}{\partial t} = \Big\{ -\frac{\hbar^2}{2m}\nabla_a^2 + U_a(\vec{r}_a, \vec{r}_b(t), t) \\ +G_a(\vec{r}_a, \vec{r}_b(t), t) + iJ_a(\vec{r}_a, \vec{r}_b(t), t)\Big\}\psi_a(\vec{r}_a, t). \end{aligned} \tag{2.60}$$

The explicit expression of the potential $G_a(\vec{r}_a, \vec{r}_b(t), t)$ and $J_a(\vec{r}_a, \vec{r}_b(t), t)$ that appears in (2.60) can be found in the Ref. [62]. However their values are in principle unknown and

they need some educated guesses. On the other hand, the total electrostatic potential energy among the M electrons that appears in (2.34) , has been divided into two parts,

$$U(\vec{r}_a, \vec{r}_b(t), t) = U_a(\vec{r}_a, \vec{r}_b(t), t) + U_b(\vec{r}_b(t), t), \tag{2.61}$$

The term $U_a(\vec{r}_a, \vec{r}_b(t), t)$ can be any type of many-particle potential defined in the position-representation, in particular it can include short-range and long-range Coulomb interactions [56]. The remaining term $U_b(\vec{r}_b(t), t)$ in (2.61) is contained in the coupling potential G_a in (2.60). From a practical point of view , all quantum trajectories $\vec{r}(t)$ have to be computed simultaneously. In order to gather all the above concepts, let us discuss a practical computation with conditional wave function by detailing a sequential procedure [56]:

1. At the initial time t_0, we fix the initial position of all $a-$particles, $\vec{r}_a(t_0)$, according to (2.39), and their associated single-particle wave function $\psi_a(\vec{r}_a, t_0)$.

2. From all particle positions, we compute the exact value of the potential $U_a(\vec{r}_a, \vec{r}_b(t_0), t)$ for each particle. An approximation for the terms G_a and J_a is required at this point.

3. We then solve each single particle Schrödinger equation , (2.60), from $t = 0$ till $t_0 + dt$.

4. From the knowledge of the single-particle wave function $\psi_a(\vec{r}_a, t_0+dt)$, we can compute the new velocities $\vec{v}_a(t_0 + dt)$ for each $a-$particle.

5. With the previous velocity , we compute the new position of each $a-$particle as $\vec{r}_a(t_0 + dt) = \vec{r}_a(t_0) + \vec{v}_a(t_0 + dt)dt$.

6. Finally, with the set of new positions and wave functions , we repeat the whole procedure (steps (a) till (e)) for another infinitesimal time dt till the total simulation time is finished.

The advantages of the above algorithm using (2.60) instead of (2.34) is that , in order to find an approximate , $\vec{r}_a(t)$, we do not need to evaluate the wave function and potential energies in the whole configuration space , but only over a smaller number of configuration points, $\{\vec{r}_a, \vec{r}_b(t)\}$. The main difficulty in this procedure is how to define the terms G_a and J_a. The simplest solution of the conditional wave-function is just ignoring them as explained in Refs. [56, 59].

2.8.2 A sequential measurement with Bohmian trajectories

Next, we present why Bohmian mechanics can help in dealing with the problem of the measurement of the current. During the measurement, a non-unitary evolution of the system is required. In other words, the global wave function is collapsed (into an eigenstate of the measuring operator) or it suffers a strong perturbation. Here we present an explanation on how Bohmian mechanics explains the unitary and non-unitary evolution of the quantum system.The wave packet in figure 2.2 represent the solution of the (unitary) Schrödinger equation of wave packet incident upon a tunneling barrier, at three different times. The initial wave packet , with normal equal to one, is divided into a transmitted plus a reflected

wave packets. According to Copenhagen explanation , when the system is measured at time t_1, a non unitary evolution appears in the wave function and , randomly, the reflected wave packet disappears. Only the transmitted wave packet describes the electron at time t_1. Then when the system is measured again at t_2, the electron is still represented the transmitted wave packet.

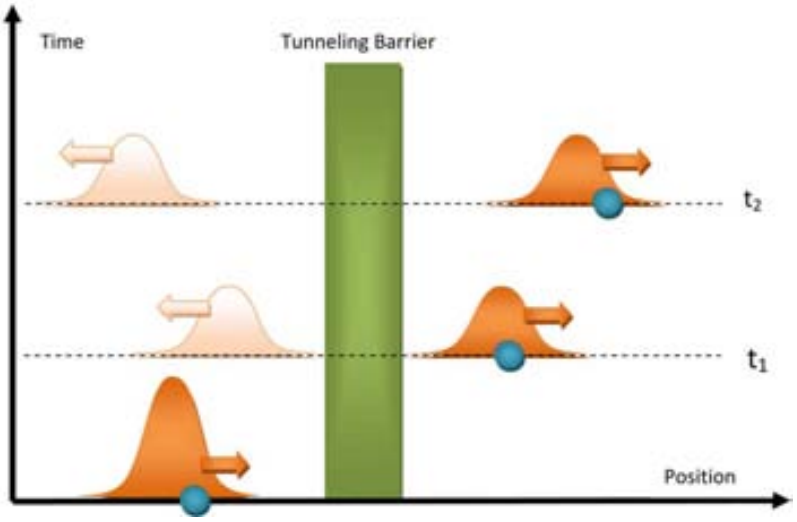

Figure 2.2: Schematic explanation of the ability of Bohmian mechanics to discuss unitary and non-unitary evolution of a wave packet incident upon a tunneling barrier.

Alternatively, the same unitary and non-unitary evolution can be explained with Bohmian mechanics. The initial position of the Bohmian trajectory is selected randomly at the initial time. Then, at times t_1 and t_2 the evolution of the trajectory is only determined by the transmitted wave packet .The reflected wave packet is an empty wave that has no effect on the evolution of the trajectory. In this explanation, we have taken into account an idealized role of the measuring apparatus.

2.9 Summary

The basic tools to characterize a quantum system by means of Bohmian trajectories are presented in this chapter. We have presented the Bohmian trajectory formalism using different methods. We emphasize that all predictions done by orthodox quantum mechanics are exactly reproduced with Bohmian mechanics. We have discussed how the measurement is explained in Bohmian mechanics. Finally, we have discussed why it can be useful, from a computational point of view, to study quantum system, in general, and electron transport, in particular. We emphasize its ability to deal with the measurement problem and to tackle many-body problems in terms of conditional wave-functions. In next chapter, we will use Bohmian trajectories to compute the total current.

Chapter 3

Total current for classical and quantum systems

3.1 Introduction

In this chapter, we discuss the computation of the total current in classical and quantum nanoelectronics devices. We start by showing the important role of the displacement current in the high-frequency behavior of nanometric devices. We present a historical development of the Ramo-Shockley-Pelligrini (RSP) theorem. After that we discuss how the RSP theorem is extended to the quantum world though a proper ensemble. We end this chapter showing the numerical difficulties that appears in the practical implementation of the Ramo-Shockley-Pelligrini expressions used in the BITLLES simulator C.

3.2 The role of displacement current

In the first section we want to discuss the difficulties that appears when trying to correctly model high frequency classical and quantum transport, and the relevance of the displacement current in such scenarios. For DC transport, we generally deal only with the particle current $I_p(t)$ related to the number of electrons crossing a particular surface S_i. Nevertheless, the electric field inside a quantum device is both inhomogeneous and time varying because of its time dependence on the external bias and the movement of electrons. Under such time-dependent scenarios, a displacement current $I_d(t)$, proportional to the time-derivative of the electric field, is always present in electronic devices.

The displacement current has no role when modeling DC because, by definition, the time-average value of $I_d(t)$ is zero. However, $I_d(t)$ has a fundamental role when modeling high-frequency transport. The total current is $I(t) = I_p(t) + I_d(t)$ and it has to satisfy a current conservation law, meaning that $I(t)$ evaluated on a closed surface S must be zero at any time. This is just a consequence of the Maxwell equations [63, 65].

Let us see now the importance of the displacement current, when we want that the simulated and the measured currents to be exactly equal at all time. It is common to compute the electrical current on the (simulated) surface S_D of the active region of figure 3.1, while a real measurement is performed on the (non-simulated) surface S_A in the ammeter. It is then

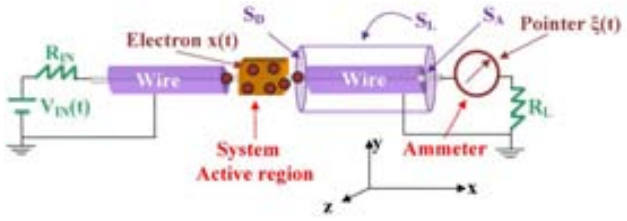

Figure 3.1: Schematic representation of a typical electrical circuit used in this chapter for studying the difference between the computed and the measured current in electrical device. Device simulators compute the current on the surface, S_D, of the active region, while the ammeter measures it on the surface, S_A.

crucial to understand in which extension is the current on S_A equal to that on S_D. In fact, these currents will be only equal if we consider the total current $I(t) = I_p(t) + I_d(t)$, where $I_p(t)$ and $I_d(t)$ are respectively the particle and displacement components. Since the Maxwell equations ensure that the total current density $\vec{J}(\vec{r}_1, t)$ is a vector with a null divergence, then we can write $\int_S \vec{J}(\vec{r}_1, t)d\vec{s} = 0$ for a closed surface $S = \{S_D, S_A, S_L\}$ where S_L is a the surface parallel to the transport direction in the cable as drawn in figure 3.1. In particular, for a cable we can assume $\int_{S_L} \vec{J}(\vec{r}_1, t)d\vec{s} = 0$, so finally we get $\int_{S_D} \vec{J}(\vec{r}_1, t)d\vec{s} = -\int_{S_A} \vec{J}(\vec{r}_1, t)d\vec{s}$. The important point is that we have to simulate the total current (not only the particle current) in S_D if we want to ensure that the simulated result si equal to the measured one at S_A.

Before starting the RSP theorem, let us write the standard expressions of the total time dependent current. The displacement current expression , $I_d(t)$, is,

$$I_d(t) = \int_{S_i} \epsilon(\vec{r}_i) \frac{d\vec{E}(\vec{r}_i, t)}{dt} d\vec{s}, \tag{3.1}$$

where $\epsilon(\vec{r}_i)$ is electric permittivity , $\vec{E}(\vec{r}_i, t)$ is electric field vector at the position $\vec{r}_i$ at the time t and S_i is surface where this current evaluated. Such electric field requires the self-consistent solution of the charge and the electric field. In quantum mechanics, this means working with a many-particle wave function. The particle (conduction) current expression, $I_p(t)$, is,

$$I_p(t) = \int_{S_i} \vec{J}_i(\vec{r}_i, t) \cdot d\vec{s} = \lim_{\Delta t \to 0} \sum_{i=1}^{N_p} \frac{q_i}{\Delta t} sgn(i) \tag{3.2}$$

where $\vec{J}_i(\vec{r}_i, t)$ is the current density vector at the position $\vec{r}_i$ at the time t and the sum N_p is the number of electrons that have crossed the surface S_i during the temporal step dt. The function $sgn(i)$ is equal to 1 when one electron leaves the volume Ω through the surface S_i, while it is $sgn(i) = -1$ when the electron enters.

3.2.1 The total current is a continuous function of time

It is clear that the expression (3.2) id discontinuous when the electron crosses the surface, the same happens for the expression (3.1). However, the total current measured on a particular surface is a continuous function of time. At first sight, this result can seem somehow surprising because we have realized that neither the conduction nor the displacement currents are continuous. Since the continuity of the total current is not explicitly discussed in most textbooks, we provide here a formal demonstration of this property.

First, let us compute the discontinuity of the particle current at the time $t = t_1$ when an electron is just going to cross a particular surface S_i (from left to right). The surface S_i is defined by the points $\vec{r}_s = \{x_s, 0 \leq y_s \leq L_y, 0 \leq z_s \leq L_z\}$. We assume that at time $t = t_1$ the electron is still in the left side of S , while at $t_1 + \Delta t$ it is already on the right. The conduction current at that time $t = t_1$ can be defined as:

$$I_p(t_1) = \lim_{\Delta t \to 0} \frac{q}{\Delta t} \tag{3.3}$$

The particle current is zero every time except during the time interval $[t_1, t_1 + \Delta t$ where it takes the value (3.3), which tends to infinite because $\Delta t \to 0$.
Second, we compute the discontinuity of the displacement current at that time $t = t_1$. The displacement current, written in equation (3.1) can be rewritten here as,

$$I_d(t_1) = \lim_{\Delta t \to 0} \frac{\int_{S_i} \epsilon(\vec{r})\vec{E}(\vec{r}, t_1 + \Delta t)d\vec{s} - \int_{S_i} \epsilon(\vec{r})\vec{E}(\vec{r}, t_1)d\vec{s}}{\Delta t} \tag{3.4}$$

In order to simplify the mathematical burden, we consider that the electron moves only in the $x-$direction with the following $\vec{r}_B[t] = \{x_B[t], 0, 0\}$. The electric field flux on the surface S_i of lateral section $(L_y \cdot L_z)$ situated on a position $x = x_s$ at $[t_1 + \Delta t]$, can be written as,

$$\int_{S_i} \vec{E}(\vec{r}_s, t_1 + \Delta t)d\vec{s} = \int_0^{L_z}\int_0^{L_y} \frac{q}{4\pi\epsilon} \frac{(x_s - x_B[t_1 + \Delta t])dz_s dy_s}{[(x_s - x_B[t + \Delta t])^2 + y_s^2 + z_s^2]^{3/2}} \tag{3.5}$$

If we assume that $x_B[t] \approx x_B[t_1] + v\Delta t$ during the time interval $[t_1, t_1 + \Delta t]$ with v the electron velocity and $(x_s - x_B[t + \Delta t])^2$ much smaller than $y_s^2 + z_s^2$, then expression (3.5) can be rewritten ,

$$\begin{aligned}\int_{S_i} \vec{E}(\vec{r}_s, t_1 + \Delta t)d\vec{s} = &- \int_0^{L_z}\int_0^{L_y} \frac{q}{4\pi\epsilon} \frac{(-x_s + x_B[t])}{[y_s^2 + z_s^2]^{3/2}} dz_s dy_s \\ &+ \int_0^{L_z}\int_0^{L_y} \frac{q}{4\pi\epsilon} \frac{-v\Delta t}{[y_s^2 + z_s^2]^{3/2}} dz_s dy_s\end{aligned} \tag{3.6}$$

The first term of the right hand side of (3.6) can be interpreted as the electric field flux generated by the electron on the surface S_i^* of lateral dimension $(L_y \cdot L_z)$ situated on the position $\vec{r}_s^* = \{2x_B[t] - x_s, 0 \leq y_s \leq L_y, 0 \leq z_s \leq L_z\}$. Let notice that the distance between these two surfaces is $x_s - (2x[t] - x_s) \equiv \Delta x \approx 0$. Finally, we write (3.4) as,

$$I_d(t_1) = \int_0^{L_z}\int_0^{L_y} \frac{q}{4\pi\epsilon}\frac{-v}{[y_s^2+z_s^2]^{3/2}}dz_s dy_s + \lim_{\Delta t\to 0}\frac{-\int_{S_i^*}\epsilon(\vec{r})\vec{E}(\vec{r},t_1)d\vec{s} - \int_{S_i}\epsilon(\vec{r})\vec{E}(\vec{r},t_1)d\vec{s}}{\Delta t} \tag{3.7}$$

We consider the volume V_T which is enclosed by the total surface S_T composed by the surfaces S_i^* and S_i , plus two additional surfaces $L_z\Delta x$ and two $L_y\Delta x$. Since $\Delta x \approx 0$, only the surfaces S_i^* and S_i are relevant. Therefore , we can rewrite (3.7) as,

$$I_d(t_1) = \int_0^{L_z}\int_0^{L_y} \frac{q}{4\pi\epsilon}\frac{-v}{[y_s^2+z_s^2]^{3/2}}dz_s dy_s + \lim_{\Delta t\to 0}\frac{-\int_{S_T}\epsilon(\vec{r})\vec{E}(\vec{r},t_1)d\vec{s}}{\Delta t} \tag{3.8}$$

The first term can be interpreted as the time derivative of the electric field flux for un electron located very close (but not equal) to surface S. From the Gauss law integrated on the closed surface S_T, the second term is equal to the total charge inside the volume V_T, which is in our particular volume at $t = t_1$ is q. Therefore, the displacement current (3.8) can be written,

$$I_d(t_1) = \int_S \frac{d\vec{E}(\vec{r},t_1+\Delta t)}{dt}d\vec{s} - \lim_{\Delta t\to 0}\frac{q}{\Delta t} \tag{3.9}$$

Certainly the value (3.9) gives an infinite negative value because of the limit $\Delta t \to 0$, in the second term of the right hand side. However, summing that current with the particle current (3.3), the infinite values disappear and therefore we obtain a continuous current at any time , even when the electron is traversing the surface S.

At this point, after showing mathematically the continuity of the total current, we can anticipate the numerical difficulties that we will get when trying to achieve such continuity. This preliminary discussions will be enlarged in the last section of this chapter. In Fig. 3.2, we have presented an example where the total current is computed using for a resonant tunneling diode composed of two highly doped drain-source $GaAs$ regions, two $AlGaAs$ barriers with the length of 1.6 nm and height 0.5 eV, and a quantum well with a length of 2.4 nm. It is assumed a constant effective mass $m = 0.067\ m_0$, with m_0 the electron free mass, along the whole $3D$ structure. Transport takes place from source to drain in the $x-$direction. The lateral dimensions of the RTD are 24 nm in the $y-$ and $z-$ directions, limited by an impenetrable material. This simulation is carried out using Bohmian trajectories (but exactly the same difficulties appears for classical ones).

It is clear from figure 3.2 that the current computed by means of the RSP theorem is numerically more efficient than that computed directly from expressions (3.1) and (3.2). The former are free from the spurious discontinuities when the electrons crosses the surface. The difficulties appear because neither Δt nor the spatial grid Δx can be zero numerically. The RSP expressions are not completely free from this difficulties, but we will see later that they combine the particle and displacement currents in such a way they the expressions become more efficient numerically. See more details about this study in Ref. [66].

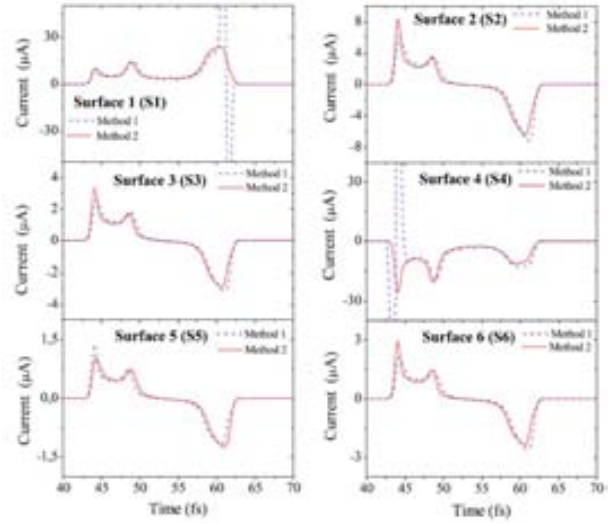

Figure 3.2: *Time-dependent total current computed on the six surfaces that form the volume* Ω *of figure 3.3 . The computation of the current within the first method (3.1) and (3.2) expressions (dashed lines) has spurious effects that are not present when the second method (3.27) and (3.28) expressions (solid line) is used [66].*

3.3 Brief history of the Ramo-Shockley-Pellegrini theorem

The RSP theorem provides an alternative expressions for the computation of the time dependent total current different from the definitions of the displacement current (3.1) and particle current (3.2). The main benefits in using these alternatives expressions is to avoid some numerical problems and to show explicitly the dependence of the current on the spatial geometry, this last property will be used in the next chapter 4. The currents are computed using the 3D integral domain (in general, the 3D active region of the device) instead of only 2D integral domain (the surface where we compute the current). We will see later these advantages in details .

Before presenting a mathematical development of the classical and quantum RSP theorem, we provide an introductory overview of its historic development. We anticipate that this theorem has had a quiet limited success. In our opinion, the numerically viable algorithm to extend the RSP theorem to quantum scenarios using the quantum (Bohmian) trajectories that we present in this thesis, together with the ability of state-of-the-art emerging devices to work at frequencies above the THz regime [67–71], will provide a renewed interest for this theorem.

The original work of Shockley [72] and Ramo [73] in 1938 and 1939, respectively, was devoted to the computation of the total current for the typical electron devices at that time, i.e. the vacuum tube. A vacuum tube can be designed as two infinite metallic plates separated by air. According to figure 3.3, we name S_4 the left plate and S_1 the right plate. For one electron moving from S_4 to S_1 at velocity $v_x(t)$ in the transport direction, the total

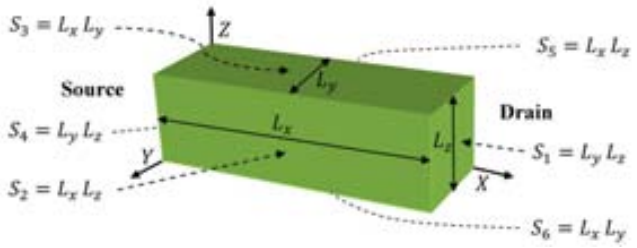

Figure 3.3: *Schematic representation of a two-terminal nanoscale device. We draw an arbitrary parallelepiped of dimensions $L_x \cdot L_y \cdot L_z$, whose volume Ω is limited by the closed surface $S = \{S_1, S_2, ..., S_6\}$.*

current on S_4 can be written as [72, 73],

$$I_4(t) \approx \Gamma_i^q(t) = q\vec{F}_4(\vec{r}) \cdot \vec{v}(t) = -q\frac{v_x(t)}{L_x}. \tag{3.10}$$

The formal demonstration of this expression (3.10) will be done in the next subsection, q is the electron charge without sign. Hereafter, we provide a definition of the $\vec{F}_4(\vec{r})$ function and a preliminary discussion on when the approximation $\vec{F}_4(\vec{r}) = (1/L_x)\vec{x}$ is reasonable. In order to understand such function, we define a set of functions (one set for each particular surface S_i) as the scalar functions $\Phi_i(\vec{r})$ and its vector functions $\vec{F}_i(\vec{r})$, through,

$$\vec{F}_i(\vec{r}) = -\nabla\Phi_i(\vec{r}). \tag{3.11}$$

These functions $\Phi_i(\vec{r})$ and $\vec{F}_i(\vec{r})$ fulfill the equations,

$$\vec{\nabla}(\epsilon(\vec{r}) \cdot \vec{F}_i(\vec{r})) = -\vec{\nabla}(\epsilon(\vec{r}) \cdot \vec{\nabla}\Phi_i(\vec{r})) = 0. \tag{3.12}$$

For the reasons that will be fully evident later, the following particular Dirichlet boundary condition on the definition of $\Phi_i(\vec{r})$ are considered,

$$\Phi_i(\vec{r}) = 1; \vec{r} \in S_i \text{ and } \Phi_i(\vec{r}) = 0; \vec{r} \in S_{h\neq i} \tag{3.13}$$

meaning that $\Phi_i(\vec{r}) = 1$ on the surface S_i and zero on the other surfaces [74]. Let us emphasize that, contrarily to the first set, the functions $\Phi_i(\vec{r})$ and $\vec{F}_i(\vec{r})$ have no direct physical meaning. They are just mathematical arbitrary functions [75].

As indicated, the subindex i means that we have six different possible set of functions, one for each surface S_i. All functions $\Phi_i(\vec{r})$ and $\vec{F}_i(\vec{r})$ share the same defining equations (3.11) and (3.12), but different boundary conditions (3.13).

Going back to our original goal of checking when the approximation $\vec{F}_4(\vec{r}) = (1/L_x)\vec{x}$ is reasonable. In figure 3.4, we have represented $\vec{F}_4(\vec{r})$ (arrows) and $\phi_4(\vec{r})$ (degraded colors) for the solution of equations (3.11) and (3.12) with the particular Dirichlet boundary conditions mentioned in (3.13) in a $2D$ rectangular space [76]. Here, the direction x is the one from $S4$ to $S1$ and the y direction from $S4$ to $S1$. As expected, arrows are almost constant in modulus and direction everywhere inside Ω, except for the negligible surfaces $\{S_2, S_3\}$ on

the top and bottom of the figure 3.4. Because of the geometry, the spatial derivative in the y direction is almost negligible in comparison with that in the x direction. Therefore, the solution of equation (3.12) is basically $\Phi_i(\vec{r}) = 1 - x/L_x$ and $\vec{F}_4(\vec{r}) = (1/L_x)\vec{x}$.

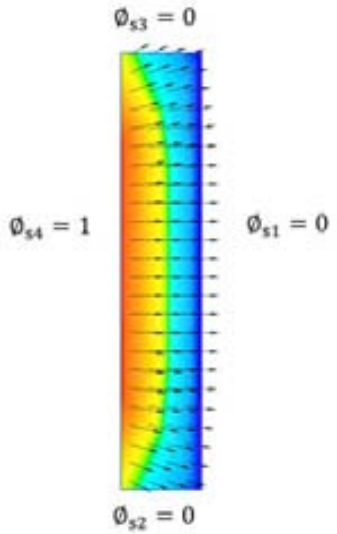

Figure 3.4: *(Color online) the function $\vec{F}(\vec{r})$ (arrows) and $\phi(\vec{r})$ when the longitudinal dimension is smaller than the transversal dimensions. The function $\vec{F}(\vec{r})$ is roughly constant and equal to $1/L_x$ [76].*

Certainly, expression $\vec{F}_4(\vec{r}) = (1/L_x)\vec{x}$ is not general. See, for example, the results in figure 3.5 where the top and bottom surfaces are no longer smaller than the lateral surfaces [76]. Then, $\vec{F}_4(\vec{r})$ is not constant neither in modulus nor direction and we conclude that expression (3.10) is not valid for the geometry depicted in figure 3.5. The geometry of the device has a clear influence on $\vec{F}_4(\vec{r})$ which, in turn, affects the current $I_4(t)$.

After the work of Ramo and Shockley on vacuum tubes, an extension to solid state-state electron devices (with spatial charge density inside Ω) was needed. This effort was carried out by Cavalleri et al. [77] in 1971 for semiconductor detectors. In that work, they assumed that the electrode surfaces S_e completely enclose the volume Ω, i.e. $S = S_e$, with constant potentials on all electrodes. These conditions can be assumed in particle detectors but are certainly not general conditions in most semiconductor devices.

In 1978, the work of Berg et al. [78] provided a complementary demonstration of the theorem including non-electrode surfaces. They defined the surfaces $S_e = S_1, ..., S_N$ of N electrodes, and considered S_o as the remaining surface. They provided some arguments to neglect the current in the surfaces S_o:

> *"All parts of the surface S_0 can be chosen sufficiently far away, so that they are located in field-free regions" [78].*

This explanation can be used to provide simplified expressions that are useful in some particular scenarios, but to neglect non-electrode surface S_o is not always possible. Since S has to be closed surface, there is always a part of the surface S_o that has to be in contact with some electrode surface S_i. Similar approximations are also present in the demonstration

presented by Kim et al. [79] for inhomogeneous media and when the electrodes have a time-varying signal. They used the Green's theorem for their demonstration, but their final expressions ignore what occurs in the non-electrode surfaces because their definition of S is incomplete:

> *"Where V denotes the whole volume of our system except for M electrodes, S is the surface of the M electrodes and $\vec{r}_s$ is the position vector on S " [79].*

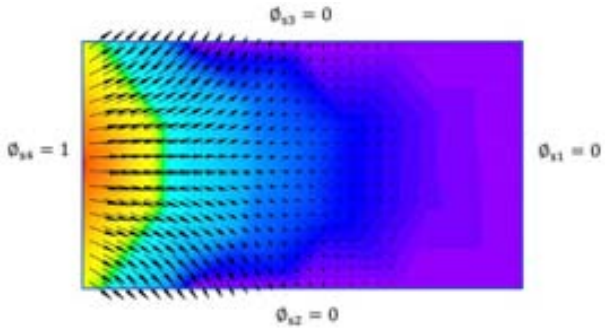

Figure 3.5: *(Color online) the function $\vec{F}(\vec{r})$ (arrows) and $\phi(\vec{r})$ when the longitudinal dimension is larger than the transversal dimensions. The function $\vec{F}(\vec{r})$ (arrows) decreases exponentially from the surface S_4 to the surface S_1 [76].*

To the best of our knowledge, the work of Pellegrini in 1986 provided the first and completely accurate generalization of the Ramo and Shockley theorem for general semiconductor devices [80] where all previous limits and difficulties are totally removed. His theorem is independent of the fact that electrodes have or not a time-dependent voltage or they enclose the whole system completely, or only partially. He also took into account electromagnetic vector potential in his demonstration. In recognition of this achievement, we have called this work Ramo-Shockley-Pellegrini theorem.

We mention also an interesting extension of the RSP theorem done by Yoder et al. [81] in 1996 that can be used in transport models without trajectories. In their demonstration, they assume that the component (of the holes and electrons current densities $J_{n,p}$, the displacement current J_d and the total current J_t) which are normal to the surface S are zero in the non-electrode surface, $J_{n,p,d,t} \cdot \vec{n} = 0$, with $\vec{n}$ is a normal vector to that surface. This condition allows them to relax the boundary conditions mentioned by Pellegrini [80] and used by us in (3.13) when defining $\vec{F}_i(\vec{r})$. However, their extra condition $J_{n,p,d,t} \cdot \vec{n} = 0$ is certainly not general and it can be, in some cases, too restrictive. For example, in a field effect transistor where the interaction between gate and channel electrons is due to the electric field perpendicular to the transport direction, we have $J_{d,t} \cdot \vec{n} \neq 0$ on the gate surface.

The RSP theorem has found a successful application in the Monte Carlo solution of the Boltzmann equation, for AC computations [82–84]. On the other hand, instead of computing the DC current from the number of particles crossing a particular surface, the RSP theorem allows the computation of such DC current from a larger number of particles moving inside a volume that contains the previous surface. The ultimate reason why DC current can be

computed in a volume is because of homogenous value of the DC current (i.e. the DC current can be equivalently computed in a lateral surface located in any position along the transport direction).

Another use of the RSP theorem found in the literature is as a 'justification' for introducing the displacement current without solving/approximating the many-body problem [85, 86]. Roughly speaking, once the velocities or the conduction current inside the active device region are known for non-interacting electrons, the displacement current can be taken into account by means of that theorem. However, the use of the expressions of RSP theorem without such self-consistence can be a reasonable first-order estimation of the time-dependent current, but they are not strictly accurate. In summary, a self-consistent solution of the transport and Gauss equation is needed to compute an accurate value of the total current, with or without the RSP theorem, with classical or with quantum transport formalisms.

The RSP theorem in time-dependent quantum scenarios has been used to discuss some unexpected (Floquet-like) features of time-dependent quantum transport for non-interacting electrons [87]. Finally, an extension of the RSP theorem to quantum system in terms of quantum (Bohmian) trajectories has been proposed by the two authors Alarcón and Oriols [66]. The quantum version of the RSP theorem is effectively accompanied with a computational algorithm for solving Gauss and many-particle Schrodinger equation in terms of trajectories [88].

3.4 Classical demonstration of the RSP theorem

To do this demonstration, we consider an arbitrary parallelepiped of volume $\Omega = L_x \cdot L_y \cdot L_z$ limited by the closed surface S composed of six rectangular surfaces $S = \{S_1, S_2, ..., S_6\}$. The only restriction is that S has to include the surface where the total current $I_i(t)$ is computed. See Fig.3.3.

For our demonstration of the RSP theorem, we consider a second set of scalar function plus the vector function defined as the gradient of the former. In particular, this second set will be the electromagnetic scalar potential $V(\vec{r},t)$ and the vector field $\vec{E}(\vec{r},t)$ related as,

$$\vec{E}(\vec{r},t) = -\vec{\nabla}V(\vec{r},t). \tag{3.14}$$

The reader realizes that we use a quasi-static definition of the electric field. As discussed in Appendix A, the explicit consideration of an electromagnetic vector potential can be neglected in most practical scenarios.

According to the uniqueness theorem for the solution of the Poisson equation [63, 65], both functions, $V(\vec{r},t)$ and $\vec{E}(\vec{r},t)$, are unambiguously defined inside the volume Ω through the well-known Gauss equation:

$$\vec{\nabla}(\epsilon(\vec{r}) \cdot \vec{E}(\vec{r})) = -\vec{\nabla}(\epsilon(\vec{r}) \cdot \vec{\nabla}V(\vec{r})) = q\sum_{k=1}^{N} \delta(\vec{r} - \vec{r}_k[t]), \tag{3.15}$$

plus the appropriate (Dirichlet or Neumann) boundary condition on the whole closed surface S. The right hand side of (3.15) is just the charge density [74] of electrons, q the electron

charge (with sign) and $\delta(\vec{r})$ the 3D delta function. Electrons paths are defined by $\vec{r}_k[t]$ with $k = \{1, 2, ..., N\}$. Here N includes all electrons inside and outside the volume Ω, so that it does not change with time. For simplicity, along this chapter, we will assume a scalar position-dependent permittivity, $\epsilon(\vec{r})$. Although we will not discuss this issue in this work, the device geometry engineering can also include the proper design of $\epsilon(\vec{r})$ to optimize the AC spectrum.

Once we have defined the two sets of (well-behaved [74, 75]) functions, we put them into the following Green's second identity [63–65] evaluated inside the volume Ω and on the limiting closed surface S,

$$\begin{aligned}\int_\Omega [V(\vec{r},t)\cdot\vec{\nabla}\left[\epsilon(\vec{r})\vec{\nabla}\Phi_i(\vec{r})\right] - \Phi_i(\vec{r})\cdot\vec{\nabla}\left[\epsilon(\vec{r})\vec{\nabla}V(\vec{r},t)\right]\cdot dv \\ = \int_S \epsilon(\vec{r})\left[V(\vec{r},t)\vec{\nabla}\Phi_i(\vec{r}) - \Phi_i(\vec{r})\vec{\nabla}V(\vec{r},t)\right]\cdot d\vec{s}\end{aligned} \tag{3.16}$$

with (3.14), (3.15), (3.11) and (3.12), we can rewritten (3.16) as,

$$\begin{aligned}\int_\Omega q\cdot\Phi_i(\vec{r})\cdot\left[\sum_{k=1}^{N}\delta(\vec{r}-\vec{r}_k[t])\right]\cdot dv = \\ -\int_S \epsilon(\vec{r})\left[V(\vec{r},t)\cdot\vec{F}_i(\vec{r}) - \Phi_i(\vec{r})\cdot\vec{E}(\vec{r},t)\right]\cdot d\vec{s}.\end{aligned} \tag{3.17}$$

Finally, taking into account the delta function in the left-hand side and the boundary conditions (3.13) in the last term of the right hand side of (3.17), we obtain,

$$\begin{aligned}\sum_{k=1}^{N} q\cdot\Phi_i(\vec{r}_k[t])\Theta(t-t_k^i)\Theta(t_k^o-t) = \\ -\int_S \epsilon(\vec{r})\cdot\vec{F}_i(\vec{r})\cdot V(\vec{r},t)\cdot d\vec{s} + \int_{S_i}\epsilon(\vec{r})\cdot\vec{E}(\vec{r},t)\cdot d\vec{s},\end{aligned} \tag{3.18}$$

where t_k^i and t_k^o are the times when the electron $\vec{r}_n[t]$ enters and leaves the volume Ω, respectively. The function $\Theta(t)$ is Heaviside function (or unit step function). To relate the delta function in (3.17) and Heaviside function in (3.18), we use,

$$\Theta(t-t_k^i)\Theta(t_k^o-t) = \int_\Omega \delta(\vec{r}-\vec{r}_k[t])\cdot dv \tag{3.19}$$

To avoid unnecessary discussions, those electrons that enter inside Ω several times are considered as different trajectories $\vec{r}_k[t]$ each entering time.

The time derivative of the left-hand side of (3.18) gives,

$$\sum_{k=1}^{N} q \cdot \frac{d}{dt}\left[\Phi_i(\vec{r}_k[t])\Theta(t-t_k^i)\Theta(t_k^o-t)\right] = \sum_{k=1}^{N} q \cdot \vec{F}_i(\vec{r}_k[t]) \cdot \vec{v}_k[t]\Theta(t-t_k^i)\Theta(t_k^o-t)$$
$$\sum_{k=1}^{N} q \cdot \Phi_i(\vec{r}_k[t])\delta(t-t_k^i)\Theta(t_k^o-t) - \sum_{k=1}^{N} q \cdot \Phi_i(\vec{r}_k[t])\Theta(t-t_k^i)\delta(t_k^o-t), \quad (3.20)$$

where we have used $d\Phi_i(\vec{r}_k[t])/dt = -\vec{F}_i(\vec{r}_k[t]) \cdot \vec{v}_k[t]$ with the electron velocity $\vec{v}_k[t] = \frac{d\vec{r}_k[t]}{dt}$. According to (3.19), we can rewrite the first term of the right hand side of (3.20) as,

$$\sum_{k=1}^{N} q \cdot \vec{F}_i(\vec{r}_k[t]) \cdot \vec{v}_k(\vec{r}_k[t])\Theta(t-t_k^i)\Theta(t_k^o-t) = \int_\Omega \vec{F}_i(\vec{r}) \cdot \qquad \vec{J}_c(\vec{r},t) \cdot dv, \quad (3.21)$$

where we define the current density as,

$$\vec{J}_c(\vec{r},t) = \sum_{k=1}^{N} q \cdot \vec{v}_k(\vec{r}_k[t])\delta(\vec{r}-\vec{r}_k[t]). \quad (3.22)$$

The last two terms of the right hand side of expression (3.20) can be rewritten as the number of particles crossing the surface S_i,

$$q\left[\sum_{\vec{r}_k[t_k^i]\in S_i} \delta(t-t_k^i) - \sum_{\vec{r}_k[t_k^o]\in S_i} \delta(t_k^o-t)\right] = -\int_{S_i} \vec{J}_c(\vec{r},t) \cdot d\vec{s}, \quad (3.23)$$

where we have used that $\Phi_i(\vec{r}_k[t]) = 0$ for those k-electrons entering or leaving the volume Ω through a surface different from S_i, while $\Phi_i(\vec{r}_k[t]) = 1$ for those k-electrons entering or leaving through S_i. This is just a consequence of the boundary conditions (3.13). We do also use $\delta(t-t_x) = \delta(\vec{r}-\vec{r}_n[t_x]) \cdot |\vec{v}_k[t_x]|$ to relate the temporal delta to the spatial delta in (3.23). Putting (3.23) and (3.21) together with the time derivative of the right hand side of (3.18) and reordering the terms, we obtain two sets of equivalent expressions to compute the total current $I_i(t)$ through the the surface S_i as [89],

$$I_i(t) = \Upsilon_i^c(t) + \Upsilon_i^d(t) = \Gamma_i^q(t) + \Gamma_i^e(t), \quad (3.24)$$

where the direct expressions for the total current $I_i(t)$ are [89],

$$\Upsilon_i^c(t) = \int_{S_i} \vec{J}_c(\vec{r},t)d\vec{s} \quad (3.25)$$

$$\Upsilon_i^d(t) = \int_{S_i} \epsilon(\vec{r}) \cdot \frac{d\vec{E}(\vec{r},t)}{dt} d\vec{s} \quad (3.26)$$

while the RSP expressions are [89],

$$\Gamma_i^q(t) = -\int_\Omega \vec{F}_i(\vec{r}) \cdot \vec{J}_c(\vec{r},t) \cdot dv \quad (3.27)$$

$$\Gamma_i^e(t) = \int_S \epsilon(\vec{r}) \cdot \vec{F}_i(\vec{r}) \cdot \frac{dV(\vec{r},t)}{dt} \cdot d\vec{s} \quad (3.28)$$

These expressions (3.27) and (3.28) are exactly the ones found by Pellegrini [80].

Finally, let us notice that the terms $\Gamma_i^q(t)$ and $\Gamma_i^e(t)$ cannot be interpreted as the conduction, $\Upsilon_i^c(t)$, and displacement, $\Upsilon_i^d(t)$, currents, respectively. For example, $\Gamma_i^q(t) \neq 0$ when the electron is not crossing the surface S_i, while $\Upsilon_i^c(t) = 0$. The term $\Gamma_i^q(t)$ includes itself the conduction and part of the displacement currents altogether. We call the first expression the volume expression of the RSP theorem, while the second expression the surface expression. See Appendix B for a discussion of the current continuity and the role of the boundary conditions (3.13).

3.5 Orthodox quantum version of the Ramo-Shockley-Pellegrini theorem

Hereafter, we present a quantum generalization of the classical theorem demonstrated in section 3.4. We will consider that the quantum system is described by a many-particle wave-function $\Psi(\vec{r}_1, ..., \vec{r}_N, t)$ solution of the time-dependent many-particle Schrödinger equation for Coulomb-interacting electrons. For simplicity, we assume spinless electrons.

We notice that the standard quantum mechanics does not provide information on individual experimental realization, but only on the probabilistic statistical results. In simple words, $|\Psi(\vec{r}_1, ..., \vec{r}_N, t)|^2$ provides the probability of finding particles in different positions, but it does not specify which are the position in one particular experiment. Thus, the extension of the RSP theorem into standard quantum mechanics has to be done in terms of ensemble of possible positions.

The scalar potential, $V(\vec{r})$ defined in expression (3.15) has to be interpreted as the value of the scalar potential at the position $\vec{r}$ and time t for a distribution of electrons given by $\vec{r}_1, ..., \vec{r}_N$. The probability of each position distributions is described by the (normalized) wave function $|\Psi(\vec{r}_1, ..., \vec{r}_N, t)|^2$ (where we obviously eliminate the time because we are not dealing with trajectories, but only positions). Hereafter, it will be useful to write explicitly the dependence of the scalar potential on all positions, i.e. $V(\vec{r}, \vec{r}_1, ..., \vec{r}_N)$. Thus, the mean "quantum" scalar potential $\overline{V(\vec{r}, t)}$ is,

$$\overline{V(\vec{r}, t)} = \int_{\Omega_\infty} dv_1 .... \int_{\Omega_\infty} dv_N |\Psi(\vec{r}_1, ..., \vec{r}_N, t)|^2 \cdot V(\vec{r}, \vec{r}_1, ..., \vec{r}_N), \tag{3.29}$$

where Ω_∞ means an infinite $3D$ space for volume-integration. Identically for the mean "quantum" electric field,

$$\overline{\vec{E}(\vec{r}, t)} = \int_{\Omega_\infty} dv_1 .... \int_{\Omega_\infty} dv_N |\Psi(\vec{r}_1, ..., \vec{r}_N, t)|^2 \cdot \vec{E}(\vec{r}, \vec{r}_1, ..., \vec{r}_N), \tag{3.30}$$

In addition, the left hand side of expressions (3.17) can be written as,

$$\int_{\Omega_\infty} dv_1 .. \int_{\Omega_\infty} dv_k .. \int_{\Omega_\infty} dv_N |\Psi(\vec{r}_1, ..., \vec{r}_N, t)|^2 \int_\Omega dv \cdot q \cdot \Phi_i(\vec{r}) \cdot \left[\sum_{k=1}^{N} \delta(\vec{r} - \vec{r}_k) \right]$$
$$= \sum_{k=1}^{N} \int_{\Omega_\infty} dv_1 .. \int_\Omega dv_k .. \int_{\Omega_\infty} dv_N |\Psi(\vec{r}_1, ..., \vec{r}_N, t)|^2 \cdot q \cdot \Phi_i(\vec{r}_k). \quad (3.31)$$

Notice the volume Ω for the integration of dv_k in the right hand side of (3.31), due to the restrictions of the delta function inside that volume Ω. The scalar functions $\overline{\Phi_i(\vec{r})}$ and its vector functions $\overline{\vec{F}_i(\vec{r})}$, are equivalent to its classical counterpart, i.e. $\overline{\Phi_i(\vec{r})} = \Phi_i(\vec{r})$ and $\overline{\vec{F}_i(\vec{r})} = \vec{F}_i(\vec{r})$, because they do not depend on the electron positions. Thus, we can rewrite the quantum ensemble/mean version of expression (3.17) as,

$$\sum_{k=1}^{N} \int_{\Omega_\infty} dv_1 .. \int_\Omega dv_k .. \int_{\Omega_\infty} dv_N |\Psi(\vec{r}_1, ..., \vec{r}_N, t)|^2 \cdot q \cdot \Phi_i(\vec{r}_k)$$
$$= - \int_S \epsilon(\vec{r}) \left[\overline{V(\vec{r}, t)} \cdot \vec{F}_i(\vec{r}) - \Phi_i(\vec{r}) \cdot \overline{\vec{E}(\vec{r}, t)} \right] \cdot d\vec{s}. \quad (3.32)$$

In order to do the time derivative of the left hand side of (3.32) we use the quantum local conservation law,

$$\frac{d|\Psi(\vec{r}_1, ..., \vec{r}_N, t)|^2}{dt} = - \sum_{h=1}^{N} \vec{\nabla}_{\vec{r}_h} \vec{J}_{\vec{r}_h}(\vec{r}_1, ..., \vec{r}_N, t), \quad (3.33)$$

where $\vec{J}_{\vec{r}_h}(\vec{r}_1, ..., \vec{r}_N, t)$ is the standard quantum current density associated to the $\vec{r}_h$ particle. Then, taking into account (3.33) and (3.11), we obtain for the time derivative of the left-hand side of (3.32),

$$- q \sum_{k=1}^{N} \sum_{h=1}^{N} \int_{\Omega_\infty} dv_1 .. \int_\Omega dv_k .. \int_{\Omega_\infty} dv_N \cdot \Phi_i(\vec{r}_k) \cdot \vec{\nabla}_{\vec{r}_h} \vec{J}_{\vec{r}_h}(\vec{r}_1, ..., \vec{r}_N, t) =$$
$$-q \sum_{k=1}^{N} \sum_{h=1}^{N} \int_{\Omega_\infty} dv_1 .. \int_\Omega dv_k .. \int_{\Omega_\infty} dv_N \cdot \vec{\nabla}_{\vec{r}_h} \left[\Phi_i(\vec{r}_k) \cdot \vec{J}_{\vec{r}_h}(\vec{r}_1, ..., \vec{r}_N, t) \right]$$
$$-q \sum_{k=1}^{N} \sum_{h=1}^{N} \int_{\Omega_\infty} dv_1 .. \int_\Omega dv_k .. \int_{\Omega_\infty} dv_N \cdot \vec{F}_i(\vec{r}_k) \cdot \vec{J}_{\vec{r}_h}(\vec{r}_1, ..., \vec{r}_N, t) \cdot \delta_{kh} \quad (3.34)$$

where δ_{kh} is the Kronecker delta, which appears because $\vec{\nabla}_{\vec{r}_h} \Phi_i(\vec{r}_k)$ is zero when $h \neq k$. Next, we evaluate the first integral of the right-hand side of (3.34) as,

$$-q\sum_{k=1}^{N}\sum_{h=1}^{N}\int_{\Omega_\infty}dv_1..\int_{\Omega}dv_k..\int_{\Omega_\infty}dv_N\cdot\vec{\nabla}_{\vec{r}_h}(\Phi_i(\vec{r}_k)\cdot\vec{J}_{\vec{r}_h}(\vec{r}_1,...,\vec{r}_N,t))=$$
$$-q\sum_{k=1}^{N}\int_{\Omega_\infty}dv_1..\int_{S}d\vec{s}_k..\int_{\Omega_\infty}dv_N\cdot\Phi_i(\vec{r}_k)\cdot\vec{J}_{\vec{r}_k}(\vec{r}_1,...,\vec{r}_N,t), \tag{3.35}$$

where we have used that any integral in the (infinite) volume Ω_∞ gives zero because it is equal to evaluating current density at the (infinite) surface S_∞. By using the boundary conditions (3.13) for $\Phi_i(\vec{r}_k)$ on the surface S (meaning $\Phi_i(\vec{r}_k)=0$ except for S_i), we can rewrite expression (3.35) as,

$$-q\sum_{k=1}^{N}\int_{\Omega_\infty}dv_1..\int_{S}d\vec{s}_k..\int_{\Omega_\infty}dv_N\cdot\Phi_i(\vec{r}_k)\cdot\vec{J}_{\vec{r}_k}(\vec{r}_1,...,\vec{r}_N,t)$$
$$=-\int_{S_i}d\vec{s}\cdot\overline{\vec{J}_c(\vec{r},t)}, \tag{3.36}$$

where the mean (many-particle) quantum current density $\overline{\vec{J}_c(\vec{r},t)}$ is defined as,

$$\overline{\vec{J}_c(\vec{r},t)}=\sum_{k=1}^{N}\left[\int_{\Omega_\infty}dv_1..\int_{\Omega_\infty}d\vec{v}_{k-1}\int_{\Omega_\infty}d\vec{v}_{k+1}\int_{\Omega_\infty}dv_N\cdot\vec{J}_{\vec{r}_k}(\vec{r}_1,...,\vec{r}_N,t)\right]_{\vec{r}_k=\vec{r}} \tag{3.37}$$

Next, we evaluate the second integral of the right-hand side of (3.34) as,

$$-\sum_{k=1}^{N}\int_{\Omega_\infty}dv_1..\int_{\Omega}d\vec{v}_k..\int_{\Omega_\infty}dv_N\cdot\vec{F}_i(\vec{r}_k)\cdot\vec{J}_{\vec{r}_k}(\vec{r}_1,...,\vec{r}_N,t)$$
$$=-\int_{\Omega}dv\cdot\vec{F}_i(\vec{r})\cdot\overline{\vec{J}_c(\vec{r},t)} \tag{3.38}$$

where again, we use the definition (3.37). The final quantum version of the RSP theorem can be written as [89],

$$\overline{I_i(t)}=\overline{\Upsilon_i^c(t)}+\overline{\Upsilon_i^d(t)}=\overline{\Gamma_i^q(t)}+\overline{\Gamma_i^e(t)}, \tag{3.39}$$

where the direct expressions for the total current $\overline{I_i(t)}$ are [89],

$$\overline{\Upsilon_i^c(t)}=\int_{S_i}\overline{\vec{J}_c(\vec{r},t)}d\vec{s}, \tag{3.40}$$

$$\overline{\Upsilon_i^d(t)}=\int_{S_i}\epsilon(\vec{r})\cdot\frac{d\overline{\vec{E}(\vec{r},t)}}{dt}d\vec{s}, \tag{3.41}$$

while the RSP expressions are [89],

$$\overline{\Gamma_i^q(t)} = -\int_\Omega \vec{F}_i(\vec{r}) \cdot \overline{\vec{J}_c(\vec{r},t)} \cdot dv, \tag{3.42}$$

$$\overline{\Gamma_i^e(t)} = \int_S \epsilon(\vec{r}) \cdot \vec{F}_i(\vec{r}) \cdot \frac{d\overline{V(\vec{r},t)}}{dt} \cdot d\vec{s}. \tag{3.43}$$

We obtain again, as in classical version , the volume term (3.42) and the surface term (3.43). Expressions (3.39)-(3.43) are the just the quantum averaged version of expression (3.24)-(3.28). The important point for the present chapter is that the quantum and classical versions of the total current share the same dependence on the function $\vec{F}_i(\vec{r})$.

3.6 Bohmian quantum version of the Ramo-Shockley-Pellegrini theorem

Here, we want to reproduce the previous quantum expressions with Bohmian trajectories. From a computational point of view, the most relevant properties of Bohmian trajectories is the fact that an appropriate ensemble of Bohmian trajectories does exactly reproduce the probability presence at any time. Such property is mathematically described with the following identity [90],

$$|\Psi(\vec{r}_1,...,\vec{r}_N,t)|^2 = \lim_{M\to\infty} \frac{1}{M} \sum_{j=1}^{M} \prod_{k=1}^{N} \delta(\vec{r}_k - \vec{r}_k^{\,j}[t]), \tag{3.44}$$

where $\{\vec{r}_1^{\,j}[t]....\vec{r}_N^{\,j}[t]\}$ is a many-particle Bohmian trajectory whose initial position are $\{\vec{r}_1^{\,j}[0]....\vec{r}_N^{\,j}[0]\}$. In order to ensure that expression (3.44) is valid one has to select $\{\vec{r}_1^{\,j}[0]....\vec{r}_N^{\,j}[0]\}$ according to the initial wave-packet probability distribution $|\Psi(\vec{r}_1,...,\vec{r}_N,0)|^2$. This last condition is called "quantum equilibrium hypothesis "[90], as we have showed in the second chapter. The super-index $j = 1,...,M$ accounts for the $M \to \infty$ number of different Bohmian trajectories that we have to consider to reproduce the standard quantum statistical results.

According to (3.44), we can rewrite (3.29) as,

$$\overline{V(\vec{r},t)} = \lim_{M\to\infty} \frac{1}{M} \sum_{j=1}^{M} \cdot V(\vec{r},\vec{r}_1^{\,j}[t],...,\vec{r}_N^{\,j}[t]), \tag{3.45}$$

and (3.30) as,

$$\overline{\vec{E}(\vec{r},t)} = \lim_{M\to\infty} \frac{1}{M} \sum_{j=1}^{M} \cdot \vec{E}(\vec{r},\vec{r}_1^{\,j}[t],...,\vec{r}_N^{\,j}[t]), \tag{3.46}$$

Identically, the right hand side of expression (3.31) gives,

$$\sum_{k=1}^{N}\int_{\Omega_\infty} dv_1..\int_{\Omega} dv_k..\int_{\Omega_\infty} dv_N|\Psi(\vec{r}_1,...,\vec{r}_N,t)|^2\cdot q\cdot\Phi_i(\vec{r}_k)$$
$$=\lim_{M\to\infty}\frac{1}{M}\sum_{j=1}^{M}\sum_{k=1}^{N} q\cdot\Phi_i(\vec{r}_k^{\,j}[t])\Theta(t-t_k^i)\Theta(t_k^o-t), \tag{3.47}$$

where we include $\Theta(t-t_k^i)\Theta(t_k^o-t)$ to ensure that only $\vec{r}_k[t]\in\Omega$ are considered. Now, we have to compute the time-derivative of expression (3.47). It can be done following the same steps done in section 3.4 from expressions (3.18) till (3.24) for classical trajectories. Conceptually, we have changed a classical trajectory by a quantum trajectory, but the mathematical procedure is identical. Finally, we have to include a sum over all possible Bohmian trajectories (the quantum ensemble). Thus, the direct current is $\overline{I_i(t)}=\overline{\Upsilon_i^c(t)}+\overline{\Upsilon_i^d(t)}$, with [89],

$$\overline{\Upsilon_i^c(t)}=\lim_{M\to\infty}\frac{1}{M}\sum_{j=1}^{M}\int_{S_i}\vec{J}_c(\vec{r},r_1^j[t],...,\vec{r}_N^{\,j}[t])\cdot d\vec{s}, \tag{3.48}$$

$$\overline{\Upsilon_i^d(t)}=\lim_{M\to\infty}\frac{1}{M}\sum_{j=1}^{M}\int_{S_i}\epsilon(\vec{r})\cdot\frac{d\vec{E}(\vec{r},r_1^j[t],...,\vec{r}_N^{\,j}[t])}{dt}\cdot d\vec{s}, \tag{3.49}$$

while the RSP expressions $\overline{I_i(t)}=\overline{\Gamma_i^q(t)}+\overline{\Gamma_i^e(t)}$ are [89],

$$\overline{\Gamma_i^q(t)}=-\lim_{M\to\infty}\frac{1}{M}\sum_{j=1}^{M}\int_{\Omega}\vec{F}_i(\vec{r}_k^{\,j})\cdot\vec{J}_c(\vec{r},r_1^j[t],...,\vec{r}_N^{\,j}[t])\cdot dv, \tag{3.50}$$

$$\overline{\Gamma_i^e(t)}=\lim_{M\to\infty}\frac{1}{M}\sum_{j=1}^{M}\int_{S}\epsilon(\vec{r})\cdot\vec{F}_i(\vec{r})\cdot\frac{dV(\vec{r},r_1^j[t],...,\vec{r}_N^{\,j}[t])}{dt}\cdot d\vec{s}. \tag{3.51}$$

Again, the volume expression (3.50) and the surface expression (3.51). It is quite simple to realize that, as expected, expressions (3.48)-(3.51) and (3.40)-(3.43) are identical. We have used a Bohmian definition of the quantum current [similar to the the classical expression (3.22)] as,

$$\vec{J}_c(\vec{r},\vec{r}_1^{\,j}[t],...,\vec{r}_N^{\,j}[t])=\sum_{k=1}^{N} q\cdot\vec{v}_k(\vec{r}_1^{\,j}[t],...,\vec{r}_N^{\,j}[t])\delta(\vec{r}-\vec{r}_k^{\,j}[t]), \tag{3.52}$$

where $\vec{v}_k(\vec{r}_1^{\,j}[t],...,\vec{r}_N^{\,j}[t])$ is the Bohmian velocity of the k-particle defined as,

$$\vec{v}_k(\vec{r}_1^{\,j}[t],...,\vec{r}_N^{\,j}[t])=\frac{\vec{J}_{\vec{r}_k}(\vec{r}_1^{\,j}[t],...,\vec{r}_N^{\,j}[t],t)}{|\Psi(\vec{r}_1^{\,j}[t],...,\vec{r}_N^{\,j}[t],t)|^2}, \tag{3.53}$$

where $J_{\vec{r}_k}(\vec{r}_1,...,\vec{r}_N,t)$ is the standard quantum current defined in (3.33). As expected, we straightforwardly realize that the mean (many-particle) quantum current density $\overline{\vec{J}_c(\vec{r},t)}$ defined in (3.37) is related to (3.52) through,

$$\overline{\vec{J}_c(\vec{r},t)} = \lim_{M\to\infty} \frac{1}{M} \sum_{j=1}^{M} \vec{J}_c(\vec{r}, r_1^j[t],..., \vec{r}_N^j[t]) \tag{3.54}$$

3.7 Instantaneous current and the noise

As we mentioned in the previous sections, the classical expression of the RSP theorem provides the instantaneous total (conduction plus displacement) current measured by the ammeters. On the contrary, the quantum version provides only an ensemble description. Strictly speaking, either the Bohmian version (3.50)-(3.51) or the orthodox quantum version (3.50)-(3.51) are computed by repeating the same experiment, defined through the same many-particle wave function, many times. For example, the Bohmian expressions are written as a sum over $M \to \infty$ selection of Bohmian trajectories. Each many-particle trajectory represents a different experiment associated to the exactly the same system. The quantum ensemble results check all quantum probabilities hidden in the many-particle wave function or many-particle Bohmian trajectories.

At this point, it seem mandatory to clarify whether this Bohmian trajectories can be useful to compute the fluctuations of the current, what we call the noise. Classically, the noise is always related to the autocorrelation expression,

$$R(\tau) = \int_{-\infty}^{+\infty} I(t+\tau)I(t)dt \tag{3.55}$$

From the last expression we see that the instantaneous current $I(t)$ is needed to compute the autocorrelation. The experimentally accessible power spectral density of the fluctuations is constructed by Fourier transforming (3.55). At this point, one can wounder weather we can use the Bohmian trajectories to compute the noise. The answer is yes. A similar discussion as the one done in the previous section ensures that the Bohmian trajectories provides a good description of the quantum ensemble value of the quantum noise. In simple words, by construction, any quantum observable that can be computed with the many-particle wave function can be exactly reproduced with the Bohmian trajectories.

At this point, a clarification is mandatory. The fact that we have demonstrated that we can compute the quantum ensemble value of the total currents and fluctuations from an ensemble of Bohmian trajectories, see expressions (3.50)-(3.51), does not certify the *reality* of these trajectories, but only that they are good *mathemathical* tools to compute total current and the correlations. These Bohmian trajectories cannot be measured in any experiment. Therefore, whether or not one wants to assume that these trajectories are real is just a subjective decision, without implications in its practical ability to provide accurate computations. In any case, getting intuition about the individual behavior of these trajectories helps us to understand the results of the ensemble of trajectories (i.e. the wave function).

Finally, let us mention that expression (3.55) implies two different measurements of the current at time t and $t+\tau$. In quantum mechanics, the interaction between the measure-

ment apparatus and the systems has to be considered explicitly. During the numerical results presented in next chapter we will assume that the current is measured through weak measurements that get information of the system with a very small perturbation of the system [91]. Ensemble Bohmian-like velocities of photons have been measured with this type of measurement [92]. In any case, these topics which are being developed by other members of the research group of Dr. Oriols is far from the scope of this thesis.

3.8 On the implementation of Ramo-Shockley-Pellegrini theorem

In the remain of this chapter, we discuss the numerical problems on the practical implementation of the expressions RSP theorem. The problems are directly related to the fact that when we select a spatial and a temporal grid, a time step Δt and a spatial step Δx has to be defined. Then, temporal and spatial derivatives are approximated by finite differences , with its pertinent numerical error.

During this chapter we mentioned two different methods to compute the total time dependent current, which involves four expressions. We will discuss the numerical solutions in the computation of each of them. They are the direct computation of the displacement current given by expression (3.1) and conduction (particle) current given by (3.2). Alternatively, we will discuss the computation of the currents from RSP expressions (3.27) and (3.28) or its Bohmian equivalents (3.42) and (3.43). We discuss explicitly the difficulties of each one of these terms:

3.8.1 The conduction and displacement current

By looking at expressions (3.2), we realize that the definition of Δt directly implies that the amount of conduction current that we compute each time an electron crosses a surface is inversely proportional to Δt. Thus, we get a arbitrary value. In principle, one can argue that this arbitrary value will be canceled by the discontinuity of the displacement current that we know it appears when the electron crosses the surface (we have shown explicitly that the total current is a continuous function of time). However, the discontinuities in the displacement current depends on Δx and the electron velocity v_x. Therefore, it is not easy at all to synchronize the spatial and temporal steps to ensure the desired continuity of the total current seen in section 3.2.1. This particular problem is not directly present in the implementation of the RSP theorem, where the conduction current is intrinsically added with part of the displacement current in the volume term (3.27). Other important problems appear in the computation of the displacement current (similar to the ones discussed in Sec. 3.8.3).

In any case, in the BITLLES simulator we will use the expressions of the current computed from the volume and surface expressions of the RSP theorem, therefore, we will not further discuss the numerical problems of the direct implementation. Unfortunately, other problems appear. Finally, we emphasize that the implementation of the RSP expressions in BITLLES simulator is exactly identical for Bohmian trajectories or for classical ones.

3.8.2 The volume term of the RSP theorem

In the computation of the volume term of the RSP total current, expression (3.27) or (3.42) , we need the value of the irrotational function $\vec{F}(\vec{r})$ along the path of the trajectory. Because of the spatial grid, $\vec{F}(\vec{r})$ keeps a constant value in each mesh, of length Δx, during the time interval $\Delta x/v_x$, that an electron with velocity v_x needs to cross it. Then, a spurious discontinuity appears in the computation of the currents when the electron changes the spatial mesh. The simplest solution of selecting a time simulation step Δt equal or larger than $\Delta x/v_x$ implies a loss of accuracy in the time-dependence of the simulations.

In order to solve the mentioned problem of the discontinuities of the irrotational function $\vec{F}(\vec{r})$ along the trajectory of the electron because of the temporal and spatial grids, we derive here an alternative definition of $\vec{F}(\vec{r})$ in which we provide a linear representation of this function inside the mesh depending on the electron position. Then, the irrotational function $\vec{F}(\vec{r})$ will change inside each mess. For simplicity, let us discuss only the x component of the irrotational function. The x components of the irrotational function $\vec{F}(\vec{r})$ is defined as:

$$F_c(l,m,n) = Ax + B, \tag{3.56}$$

The subindex c means the x directions. The vector function in the other directions can be understood looking at the development done below and using $c = y$, $c = z$. The terms l,m and n corresponds to the 3D grid points where of our spatial simulating box. Therefore, for example, a particle with positions $x(t)$, $y(y)$ and $z(t)$ which corresponds to a mesh point $l = 4$, $m = 5$ and $n = 3$, will have associated a x component of $\vec{F}(\vec{r})$ equal to $F_x(4,5,3) = Ax(t)+B$. The constants A and B are determined by the following new boundary conditions,

$$F_c^{new}(l_{min},m,n) = F_c(l_{min},m,n) - (\frac{F_c(l_{min}+1,m,n) - F_c(l_{min},m,n)}{2}), \tag{3.57}$$

where $F_c^{new}(l_{min},m,n)$ is the new component of $\vec{F}(\vec{r})$ in the $c-$direction at the first mesh.

The values $F_c(l_{min},m,n)$ and $F_c(l_{min}+1,m,n)$ are the old components of $\vec{F}(\vec{r})$ in the $c-$direction , respectively, at the first and the second mesh. A schematic representation to linearize this function is presented in Fig. 3.6. The boundary conditions at the last mesh is written,

$$F_c^{new}(l_{max},m,n) = F_c(l_{max}-1,m,n) + (\frac{F_c(l_{max}-1,m,n) - F_c(l_{max}-2,m,n)}{2}), \tag{3.58}$$

where $F_c^{new}(l_{max},m,n)$ is the new component of $\vec{F}(\vec{r})$ in the $c-$direction at the last mesh. The values $F_c(l_{max}-1,m,n)$ and $F_c(l_{max}-2,m,n)$ are the old components of $\vec{F}(\vec{r})$ in the $c-$direction at the last mesh and its previous one, respectively. We recall that the component of the irrotational function $\vec{F}(\vec{r})$, for instance in $x-$direction in terms of $\phi(\vec{r})$ is written as,

$$F_c(i,m,n) = -(\frac{\phi_c(i+1,m,n) - \phi_c(i,m,n)}{\Delta c}), \tag{3.59}$$

where $\phi_c(i,m,n)$ and $\phi_c(i+1,m,n)$ are the values of the "potential" [75] at the nodes i and $i+1$, respectively. The constants A and B are determined by the expression of $\vec{F}(\vec{r})$,

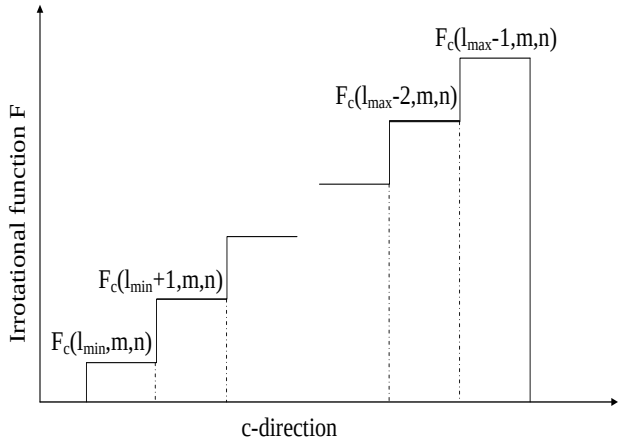

Figure 3.6: *Schematic representation for linearizing the irrotational function showing the discontinuity of that function between two mesh and its constant value along the mesh. This representation is for the $x-$direction*

(3.56), and two condition values (3.57) and (3.58), we have then two equations with two unknowns. This approximation presents a good tool to avoid , firstly keeping the value of the irrotational function $\vec{F}(\vec{r})$ in the same mesh with a constant value and secondly the discontinuity appearing when an electron displaces from one mesh to another. We recap this improvement in the Fig. (3.7) showing a comparison between the current $\Gamma^q(t)$ with and without linearizing of the irrotational function $\vec{F}(\vec{r})$.

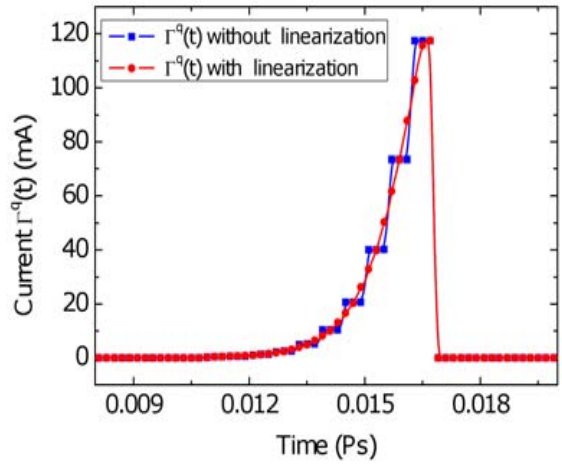

Figure 3.7: *A comparison between the current $\Gamma^q(t)$ with and without linearizing irrotational function $\vec{F}(\vec{r})$ for a transistor FET with the geometry $L_x \cdot L_y \cdot L_z = 8 \cdot 2.5 \cdot 2.5\ nm^3$ on the surface S_1.*

In the next paragraph we develop a technical solution for the currents (3.28).

3.8.3 The surface term of the RSP theorem

The problems of the surface term (3.28) are quite similar to the problems that we would get if we computed the displacement current directly in our simulation box with a spatial and temporal grid. During the all time that the an electron remains inside a spatial cell, the distribution of the charge density inside the grid remains constant (we assume the charge distributed uniformly in the cell). Therefore, the potential profile and electric field, which are related to the charge through the Poisson equation, remain invariant with time. Then, the displacement current is equal to zero, and only a large discontinuity appears on these current when the electron changes the spatial cell (see Appendix Fig. B.1).

One possible solution was the selection of (non-unitary) Gaussian distribution of the charge along the different nodes of the simulation box. The electron is assumed to have associated a Gaussian distribution of charge, whose central position is located at the electron position $x(t)$, $y(t)$ and $z(t)$ and spatial dispersion is arbitrarily selected. We have prove this assignment of the charge in order to obtain a smooth charge density as a function of time instead of a discontinuous one. The basic idea was that when an electron is inside a mesh, its electric charge spreads in a large number of meshes of the devices instead of being punctual, and the distribution of charge between the nodes changes continuously. Then, the electric filed and the potential profile changes continuously too. In order to avid discontinuities we have to select a spatial dispersion of the Gaussian that implies several (4,5,..) nodes. We have arbitrarily changes the "local" distribution of the charge by and "spurious" non-local distribution. This is conceptually wrong for classical electrons and also for Bohmian ones. Another problem was that the arbitrary spatial dispersion of the Gaussian charge distribution affects drastically the results.

The solution to the discontinuity problems of the numerical evaluation of the surface term of the total current, has been developing a new strategy to write the time derivative of the potential and of the electric field directly from the Coulomb law (assuming a uniform dielectric constant along the simulating box).

In order to explain how to derive this alternative solution, we consider two types of mathematically equivalents ways of solving the Poisson equation for a system of electrons as represented in figure 3.8. The electrons inside the box simulation feel the same boundary conditions. In figure 3.8.a the electrons out of the box simulation impose the boundary conditions to those inside interacting with them, while those inside the box in figure 3.8.b feel the boundary conditions fixed by an external field.

Let us now discuss mathematically this equivalence in a region. The potential evaluated at a point r inside the box is defined as $V(r, r_1(t), r_2(t), \ldots, r_N(t); r_{N+1}(t), \ldots, r_M(t))$, where N is the number of the electrons which are inside the simulation box and the number $(M-N)$ is those outside the box of figure 3.8.a. The $(M-N)$ electrons play the role of the external bias, thus we can write the potential at the position r inside the box as,

$$V(r, r_1(t), r_2(t), \ldots, r_{i-1}(t), ri(t), r_{i+1}(t), \ldots, r_N(t), t), \tag{3.60}$$

where we have substituted the dependence of all the terms $(r_{N+1}(t), \ldots, r_M(t))$ by t. We can consider the effect of the $(M-N)$ outside electrons on the N inside electrons as a change of the boundary conditions versus the time t. Expressions (3.60) will be the one we will use to evaluate the current in (3.28). The deal with those currents is similar, thus we study

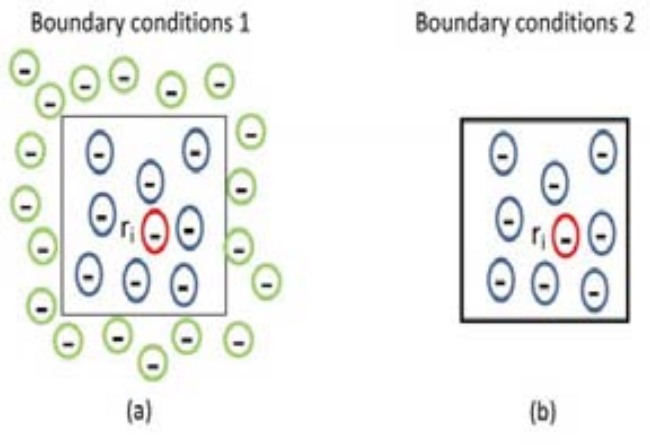

Figure 3.8: *The electron inside the simulation box feel the same boundary conditions, but with different representation. In (a) the boundaries are considered as a consequence of the reaction of the interactions inside the box with those outside of it. In the representation (b), they are presented by the values imposed on the electric field (Neumann) or the potential (Dirichlet) on the surfaces.*

only one of them for instance (3.28). The time derivative of the potential (3.60) when all electrons inside the box moves, $i = 1, ..., N$, reads,

$$\frac{dV(r, r_1(t), r_2(t), \ldots, r_{i-1}(t), r_i(t), r_{i+1}(t), \ldots, r_N(t), t)}{dt} = \frac{\partial V}{\partial t} + \sum_{i=1}^{N} \frac{\partial V}{\partial r_i} \frac{dr_i}{dt}, \tag{3.61}$$

where $v_i = \frac{dr_i}{dt}$ is the velocity of the $i-$electron and $\frac{\partial V}{\partial t}$ presents the external boundary conditions i.e. the effect of the electrons outside the box. Now to evaluate (3.61), we need to compute $\frac{\partial V}{\partial r_i}$. For this goal we express the potential with the Coulombic form for the moving $i-$electron ,

$$\begin{aligned} V(r, r_1(t), r_2(t), \ldots, r_{i-1}(t), r_i(t), r_{i+1}(t), \ldots, r_N(t), t) = & \frac{1}{4\pi\epsilon} \frac{q_1}{||r - r_1(t)||} \\ & + \frac{1}{4\pi\epsilon} \frac{q_2}{||r - r_2(t)||} + \ldots + \frac{1}{4\pi\epsilon} \frac{q_i}{||r - r_i(t)||} \\ & + \ldots + \frac{1}{4\pi\epsilon} \frac{q_N}{||r - r_N(t)||}. \end{aligned} \tag{3.62}$$

From the last equation (3.62) we find,

$$\frac{\partial V}{\partial r_i} = \frac{\partial (\frac{1}{4\pi\epsilon} \frac{q_i}{||r - r_i(t)||})}{\partial r_i} = \pm \frac{1}{4\pi\epsilon} \frac{q_i}{||r - r_i(t)||^2} \tag{3.63}$$

Many terms have been canceled because of their independence on r_i. Using (3.63) the time derivative of the potential (3.61) can be rewritten as:

$$\frac{dV(r,r_1(t),r_2(t),\ldots,r_{i-1}(t),r_i(t),r_{i+1}(t),\ldots,r_N(t),t)}{dt} = \frac{\partial V}{\partial t} \pm \sum_{i=1}^{N} \frac{1}{4\pi\epsilon} \frac{q_i v_i}{||r - r_i(t)||^2} \tag{3.64}$$

In using this procedure, the main limitation is that the Coulomb expressions are only valid for a uniform dielectric constant. No further approximation is present. Such solution is computationally acceptable when the number of electrons is limited to few hundreds, which is our scenario of interest in the 3D Poisson solver of the BITLLES. The great advantage is that most of the temporal derivatives are done analytically without problems associated to the grid.

The practically implemented version of the expression (3.28) in BITLLES simulator, where the data of the current is collected at each time step, Δt, is the following. We are not directly interested in the term (3.61), but on its time averaged value along Δt. Therefore, we have:

$$\frac{1}{\Delta t}\int_t^{t+\Delta t}(\frac{\partial V}{\partial t} + \sum_{i=1}^{N}\frac{\partial V}{\partial r_i}\frac{dr_i}{dt}) = \sum_{i=1}^{N}\frac{q}{4\pi\epsilon}(\frac{1}{\|r - r_i(t_i)\|} - \frac{1}{\|r - r_i(t_i - \Delta t)\|})\frac{1}{\Delta t} + \frac{(V'(t_i) - V(t_i - \Delta t))}{\Delta t} \tag{3.65}$$

where $r_i(t_i)$, $r_i(t_i - \Delta t)$ are the positions of electrons at the times t_i and $t_i - \Delta t$. The term $V(t_i - \Delta t)$ is the voltages at the times $t_i - \Delta t$. The term $V'(t_i)$ is the voltage at time t_i when only the boundary conditions are changed, but the electrons positions remains equal to the previous ones $r_i(t_i - \Delta t)$. In the Fig. 3.9 we have presented the implemented version of the displacement current (3.1).

From the current presented in Fig. 3.9, we see that it is continuous except when the electron cross the surface where we compute the current. In the annex (B.1) we show different ways we tried to reach this result.

3.9 Summary

In this chapter we have derived classical and quantum versions of the RSP theorem that allows us the practical the computation of classical and quantum total currents in nanoelectronic devices. In the quantum side, we have demonstrated that the Orthodox or Bohmian version are totally equivalent. The RSP expressions for classical or Bohmian particles have been implemented into the BITLLES simulator ,Appendix C, in order to discuss the high frequency behavior of nanoscale electron devices. The practical difficulties of its implementation are discussed. Numerical examples using these expressions applied to nanoscale devices will be discussed in next chapter.

Finally, let us emphasize how important is the computation of the current in the simulation of electron devices. Such devices, understood as a system of interacting electrons, are subjected to external conditions of the potential at the boundary fixed by a (DC, AC

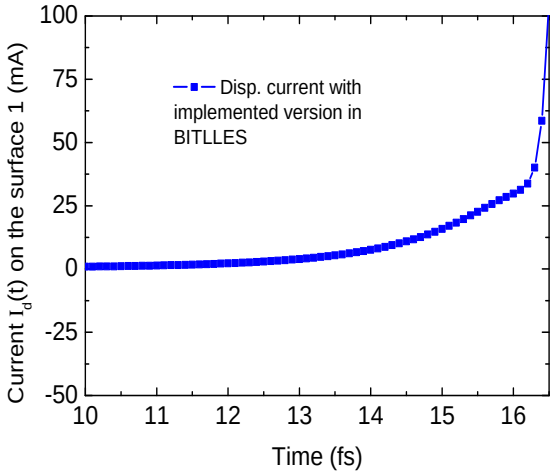

Figure 3.9: *Displacement current (3.1) on the surface S_1 for a transistor FET with the geometry $L_x \cdot L_y \cdot L_z = 8 \cdot 2.5 \cdot 2.5\ nm^3$ on the surface S_1.*

or transient batteries). Depending on these external potentials a different flux of electrons is generated. Such motion of electrons is the responsible of the total (conduction plus displacement) current measured in a external ammeter. Simulating the behavior of the device is just getting the correct relationship between the *a priori* fixed value of the voltage at the battery and the *a priori* unknown value of the current at the ammeter. This final reflection justify why is so important to we get an accurate calculation of the total current.

Chapter 4

High-frequency results for nanotransistors

4.1 Introduction

In the previous chapter, we develop and implement the tools for the computation of the total current in nanometric devices. The BITLLES simulator, in general, and the implementation of the Ramo-Shockley-Pellegrini theorem, in particular, are valid either for classical or quantum simulations. Therefore, we will mix classical and quantum simulations of noise, AC and transients. Most of our practical conclusions in this chapter are independent on whether we use classical or quantum (Bohmian) trajectories.

- **Noise** We study the power spectral density when nanometric devices are DC biases. Then, we study how the intrinsic noise in digital applications grows when small dimensions are considered.
- **AC and Transients** We study the effect of the FET geometries in the total current. We use this result to propose an original way of optimizing the cut-off frequency of nanoscale devices.

We start this chapter with some preliminary discussions on the relation between measured and computed total currents and on the effect of the geometry on the temporal behavior of nanoscale devices.

4.2 Preliminary discussions:

We can certainly compute different parameters in order to characterize and study nanoelectronic devices. However, all the results we will get are basically determined by the time-dependent behavior of the total current. Let us start by discussing the relation between the computed current (in the simulation box) and the measured current (in an ammeter situated far from the simulation box).

4.2.1 Discussion on the measured and computed current

In the study of any electron device, we do only take into account the active region. However, the real experimental system included many other parts, such as cables, batteries, ammeters, etc. which are not simulated explicitly. Therefore is mandatory to differentiate between the current computed on the surface $S1$ of trhe simulation bos $i_\Omega^{S1}(t)$ and the current measured measured by the drain ammeter $i_D(t)$ of Fig. 4.1. The same happens for $i_\Omega^{S4}(t)$ and the current $i_S(t)$ measured at the source. When dealing with DC current is trivially true that both current are identical. However, for time-dependent current, the situation is far from so simple. We will use the Ramo-Shockley-Pellegrini theorem (RSP) discussed in the previous chapter to discuss this issue in detail.

According to the RSP theorem, when using the volume Ω in the 2-terminal device drawn in Fig. 4.1(a), the displacement currents present on the surfaces S_2, S_3, S_5 and S_6 are finally collected by the drain or source cables. The lines of the electric field $\vec{E}(\vec{r},t)$ leaving these surfaces end on the drain or source cables, even without crossing $S1$ or $S4$. Therefore, clearly, $i_D(t) \neq i_\Omega^{S1}(t)$ and $i_S(t) \neq i_\Omega^{S4}(t)$. This results can be understood in a very simple way. The total current measured in $S1$ is different from the current measured in $S4$ because it is the current measured on the six surfaces that is zero $S1 = -S2 - S3 - S4 - S5 - S6$, not $S1 = -S4$. On the contrary, the current in the two ammeters has to be equal, at any time, because we are dealing with a two-terminal device.

Therefore, in a two terminal device, if we want to use the RSP theorem to compute the total current we need a volume Ω with surfaces $S1$ and $S4$ so large that all electric lines drawn in Fig. 4.1(a) cross such surfaces. Then, the other surfaces are so far from the active region that the displacement current crossing such surfaces is almost negligible. Then, we arrive to a situation with $S1 = -S2 - S3 - S4 - S5 - S6 \approx -S4$. As we will discuss below such type of volumes Ω corresponds to a situation where $\vec{F}_4(\vec{r}) = 1/L_x\vec{x}$ and $\vec{F}_1(\vec{r}) = -1/L_x\vec{x}$ that gives the some current for both surfaces.

On the contrary, for the multi-gate Field Effect Transistors (FET) structure drawn in Fig. 4.1(b), any volume Ω that coincides with the channel volume provides equal computed and measured currents. The lines of the electric field $\vec{E}(\vec{r},t)$ leaving the lateral surfaces S_2, S_3, S_5 and S_6 are collected immediately at the metallic gates. None of them arrives at the drain or source cables. See Fig. 4.1(b). Therefore, for the Gate All Around (GAA) FETs, we have $i_D(t) = i_\Omega^{S1}(t)$ and $i_S(t) = i_\Omega^{S4}(t)$.

4.2.2 The dependence of $\vec{F}_i(\vec{r})$ on L_x, L_y and L_z

Once we have clarified the relation between the simulated and the measured current, we want to explain how the geometry of the electron device and its electrostatic boundary conditions determine the behavior of the total current. Since we will use the RSP theorem discussed in the previous chapter, where the irrotational function $\vec{F}_i(\vec{r})$ plays a fundamental role, let us first discuss its dependence on the device geometry. In the introduction of the previous chapter, using a 2D *quick field* simulator, we have briefly discussed such dependence. Here, we enlarge such discussion by dealing with an analytical solution of equation, $\vec{\nabla}(\epsilon(\vec{r})\vec{F}_i(\vec{r})) = -\vec{\nabla}(\epsilon(\vec{r})\vec{\nabla}\Phi_i(\vec{r})) = 0$, when the particular boundary conditions,

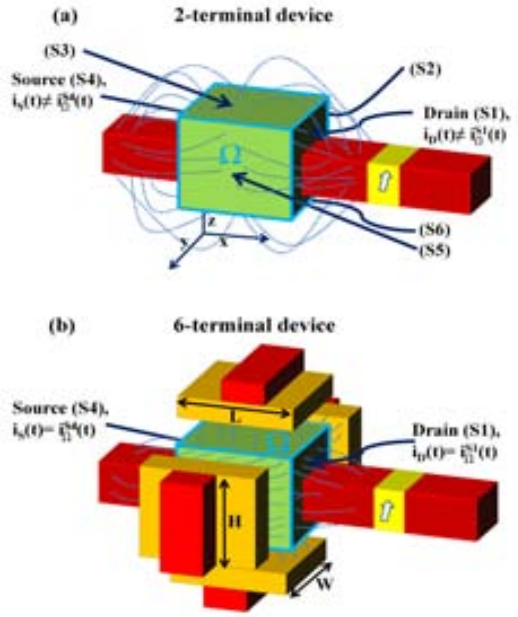

Figure 4.1: *(Color online) (a) Schematic representation of a 2-terminal device. When using the volume* Ω*, the current measured in the drain contact* $i_D(t)$ *is not equal to* $i_\Omega^{S1}(t)$ *because the lines of the electric field (dotted lines) on the other surfaces end finally in the drain contact without crossing* $S1$*. (b) A 6-terminal device satisfies* $i_D(t) = i_\Omega^{S1}(t)$ *for* Ω *equal to the channel volume because the lines of the electric field on the surfaces* S_2*,*S_3*,*S_5 *and* S_6 *are collected by 4 gates [93].*

$\Phi_i(\vec{r}) = 1; \vec{r} \in S_i$ and $\Phi_i(\vec{r}) = 0; \vec{r} \in S_{h\neq i}$, are used. We assume the particular volume Ω depicted in Fig. 4.2 with a homogenous dielectric constant. There are no difference between studying the current on the surface 1 or 4 , in the next we will carry on discussing the current on surface 1 instead of that on surface 4. Under such simple geometry, the solution for the scalar function $\phi_1(\vec{r})$ can be written as [94, 95]:

$$\phi_1(\vec{r}) = \frac{16}{\pi^2} \sum_{i=1,3,5...}^{\infty} \sum_{j=1,3,5...}^{\infty} \frac{\sinh\left(\pi\sqrt{(\frac{i}{L_y})^2 + (\frac{j}{L_z})^2} \cdot x\right)}{i \cdot j \cdot \sinh\left(\pi\sqrt{(\frac{i}{L_y})^2 + (\frac{j}{L_z})^2} \cdot L_x\right)} \cdot \sin(\frac{i\pi}{L_y} y) \cdot \sin(\frac{j\pi}{L_z} z), \tag{4.1}$$

with $\vec{r} = (x, y, z)$. First, let us discuss how (4.1) reproduces the boundary conditions of Laplace equation mentioned above. At the points $\vec{r} = (0, y, z)$, $\vec{r} = (x, 0, z)$ or $\vec{r} = (x, y, 0)$ we obtain $\phi_1(\vec{r}) = 0$. In order to compute $\phi_1(\vec{r})$ on the surface $\vec{r} = (L_x, y, z)$, we write a "square wave" defined as $f(y) = 1$ for $0 < y < L_y$ and $f(y) = -1$ for $L_y < y < 2 \cdot L_y$ as the following Fourier series:

$$f(y) = \frac{4}{\pi} \sum_{i=1,3,5..}^{\infty} \frac{1}{i} sin\left(\frac{i\pi y}{L_y}\right). \tag{4.2}$$

The same series can be used for the z variable and, as expected, we obtain $\phi_1(L_x, y, z) = f(y) \cdot f(z) = 1$ for $0 < y < L_y$ and $0 < z < L_z$.

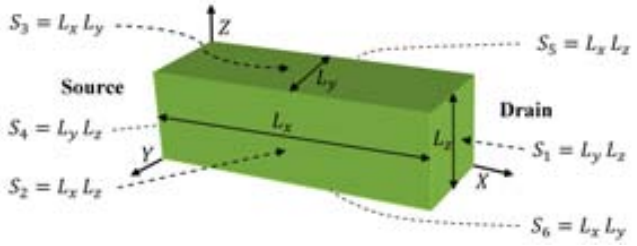

Figure 4.2: *Schematic representation of a two-terminal nano-resistor. We draw an arbitrary parallelepiped of dimensions $L_x.L_y.L_z$, whose volume Ω is limited by the closed surface $S = \{S_1, S_2, ..., S_6\}$.*

In addition, because of this particular boundary conditions, ($\phi_1(\vec{r}) = 1$ when $\vec{r} \in S_1$ and $\phi_1(\vec{r}) = 0$ when $\vec{r} \in S_{h\neq 1}$), the role of the lateral variables, y and z, is identical and interchangeable, but radically different from x. As a consequence, the shape of $\phi_1(\vec{r})$ does not depend on the exact magnitudes of L_x, L_y and L_z, but only on the proportionality among them. In particular two limit different shapes of $\phi_1(\vec{r})$ can be expected when $L_x \ll L_y, L_z$ or $L_x \gg L_y, L_z$.

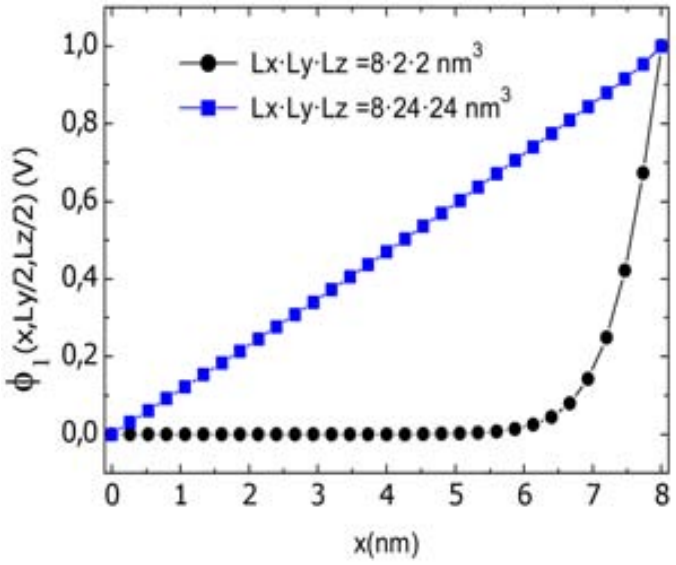

Figure 4.3: Representation of $\phi_1(\vec{r})$ along the points $\vec{r} = (x, L_y/2, L_z/2)$ for two particular geometry.

When $L_x \ll L_y, L_z$, we can use the approximation $sinh(\xi) \approx \xi$ when $\xi \to 0$. Then, expression (4.1) can be written as [76]:

$$\phi_1(\vec{r}) \approx \frac{x}{L_x} f(y) \cdot f(z) \approx \frac{x}{L_x}, \tag{4.3}$$

where we have used again (4.2). This is the shape seen in the line with squares in Fig. 4.3. Thus, a good approximation for the function $\vec{F_1}(\vec{r})$ along $\vec{r} = (x, L_y/2, L_z/2)$ for $0 \leq x \leq L_x$ is:

$$\vec{F_1}(\vec{r}) \cdot \vec{x} = F_{x1} \approx -\frac{1}{L_x}. \tag{4.4}$$

This is exactly the geometry discussed by Ramo and Shockley in the vacuum tube , it is the same result found in Fig. 3.4 in the chapter 3.

When $L_x \gg L_y, L_z$, we can make the approximation $sinh(\xi) = exp(\xi)/2$ when $\xi \to \infty$ in (4.1). For simplicity, due to the presence of $1/(i \cdot j)$ in (4.1), we take just the first terms ($i = 1$ and $j = 1$) to write $\phi_1(\vec{r})$ at $\vec{r} = (x, L_y/2, L_z/2)$ as [76]:

$$\phi_1(\vec{r}) \approx \ exp\left(\pi\sqrt{(\frac{1}{L_y})^2 + (\frac{1}{L_z})^2} \cdot (x - L_x)\right). \tag{4.5}$$

This is a quiet good approximation of what we have plotted in Fig. 4.3 for $\phi_1(\vec{r})$ when $L_x \gg L_y, L_z$ (solid circle). The shape of $\phi_1(\vec{r})$ in the x direction can be roughly approximated by an exponential function [96] starting at zero and arriving at the unity. Thus a reasonable approximation for $\vec{F_1}(\vec{r})$ along $\vec{r} = (x, L_y/2, L_z/2)$ for $0 \leq x \leq L_x$ is:

$$\vec{F_1}(\vec{r}) \cdot \vec{x} = F_{x1} \approx -\alpha_x \cdot exp\left(\alpha_x(x - L_x)\right). \tag{4.6}$$

being α_x defined from (4.5) and it is equal $(\sqrt{\frac{1}{L_y})^2 + (\frac{1}{L_z})^2}$. This result corresponds to the exponential shape of the magnitude of the arrows in Fig. 4, chapter 3. Expression (4.6) is valid under the condition $1/\alpha_x \ll L_x$. In summary, the shape of $\vec{F_1}(\vec{r})$ depends drastically on the relation between L_x and L_y,L_z.

4.2.3 The time dependent current behavior depending on device geometry

After discussing how the device geometry determines the shape of $\vec{F_i}(\vec{r})$, let us discuss directly the dependence on the geometry and electrostatic boundary conditions on the total current. We consider now an electron traversing the volume of the active region with a constant velocity $\vec{v} = (v_x, 0, 0)$ in the transport direction, from source to drain (this correspond to the ballistic transport in 1D quantum wire transistors considered in this work). According to the RSP theorem, this electron generates a current pulse on S_1. In our simplified scenario, the electron transit time can be defined as $\tau = L_x/v_x$. For the analytical arguments developed in this work showing the dependence of $I_1(t)$ on the geometry, we can assume that $I_1(t) \approx \Gamma_1^q(t)$. When $L_x \ll L_y, L_z$, we can use (4.4) to obtain:

$$I_1(t) \approx \Gamma_1^q(t) \approx \frac{|q|v_x}{L_x} \cdot \Theta(t - 0)\Theta(\tau - t). \tag{4.7}$$

As expected, the time-integration of this current is equal to the electron charge $\int_0^\tau \Gamma_1^q(t)dt = qv_x/L_x\tau = q$. It is easy to show that this is true for any well-defined function $\vec{F_i}(\vec{r})$.

On the contrary, when $L_x \gg L_y, L_z$, using (4.6), the current can be approximated by:

$$I_1(t) \approx \Gamma_1^q(t) \approx |q|\alpha \cdot e^{\alpha(t-\tau)} \cdot \Theta(t-0)\Theta(\tau - t). \tag{4.8}$$

We have defined $\alpha = v_x\alpha_x$ and used $x = v_x t$, meaning $L_x = v_x\tau$. The previous condition for the validity of (4.6), i.e. $1/\alpha_x \ll L_x$, is now rewritten as $1/\alpha \ll \tau$. Again, the time integration of (4.8) gives $\int_0^\tau \Gamma_1^q(t)dt = q \cdot (1 - e^{-\alpha\tau}) \approx q$ when $1 \ll \alpha\tau$. The important lesson that we have to learn from expressions (4.7) and (4.8) is that the temporal width of the current pulse $\Gamma_1^q(t)$ is related (through the electron velocity v_x) to the maximum spatial distance between the electron and the surface so that the electric field is still non-negligible on $I_1(t)$. See Fig. 4.4 for a computation of the current pulse without approximations confirming the transition from a square to an exponential pulse current.

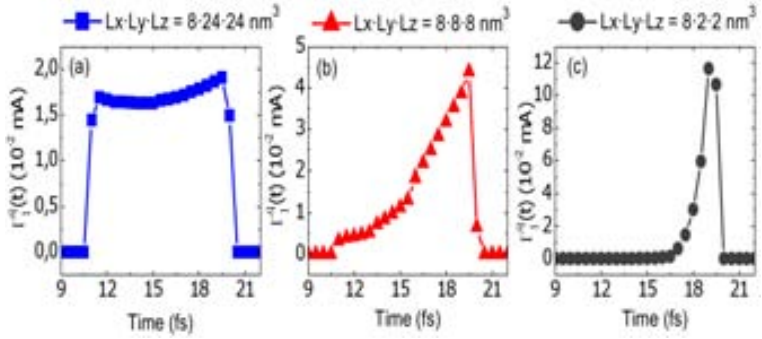

Figure 4.4: Time dependent current $I_1(t)$ for one electron traversing a gate-all-around transistor when three different geometries are considered.

At this point, before going to numerical classical and quantum simulations of real nanometric devices, it is important to emphasize again that for a two terminal device we have to use $\vec{F}_1(\vec{r})\cdot\vec{x} = -\frac{1}{L_x}$ and $\vec{F}_4(\vec{r}) = \frac{1}{L_x}$. For multi-gate devices, however, the richness of different types of functions $\vec{F}_i(\vec{r})$ can be used to improve high-frequency device performances.

4.3 High-frequency Noise

Studying noise is considered a complementary tools to characterize and model the electronic devices. Engineers want to study it to try to avoid its pernicious effect on device performance, while physicists look for it in order to show new physics hidden in the time-averaged results of the DC measurements. We study which are the consequences on the noise of the dependence of the total currents on the device geometry.

4.3.1 Power spectral densities in DC simulation

Via a simple example we analytically study the power spectral densities (PSD) in DC regime then we do the same work but using the BITLLES (with Monte Carlo solutions of the Boltzmann equation) to verify our conclusion.

4.3.1.1 Analytical result:

Now, we consider the noise spectrum for the two different device geometries mentioned above. Consequently, we have to define two volumes, $\Omega = 100\ nm \cdot L_y \cdot L_z$ and $\Omega^* = 100\ nm \cdot L_y^* \cdot L_z^*$, with identical length $L_x = 100\ nm$ but different lateral areas. Then, in order to compute the $PSD(\omega)$ of $I_1(t)$ in both volumes, we have to compute the autocorrelation function, $R(\Delta t)$:

$$R(\Delta t) = lim_{T\to\infty}\frac{1}{T}\int_{-T}^{T} I_1(t)I_1(t+\Delta t)dt, \tag{4.9}$$

and then Fourier transform such autocorrelation function.

We assume that all electrons are injected, from source to drain, with the same energy. The electrons are injected at an effective rate ν, meaning that the number of injected electrons during a time interval T is $T\nu$. We assume that electrons are injected, at a low rate, without correlation between their initial times t_k^i and t_g^i. This means that there is no correlation for the currents associated to different electrons. Thus, we obtain $R(\Delta t) = 0$ when $\Delta t > \tau$. Then, the autocorrelation function for $0 \leq \Delta t \leq \tau$ can be rewritten as:

$$R_1(\Delta t) = q^2\nu {v_x}^2 \int_{\Delta t}^{\tau} F_{x1}(v_x t)F_{x1}(v_x t + v_x\Delta t)dt, \tag{4.10}$$

where we have used that $x = v_x t$. Now, we consider the two geometries of the volume Ω mentioned above. We fix $v_x = 10^5 m/s$, giving $\tau = L_x/v_x = 1ps$.

First, for the geometry $L_x = 100\ nm \ll L_y, L_z$, we take the current (4.7) represented in Fig. 4.4(a). Then, the Fourier transform of the autocorrelation (4.10) gives [76]:

$$PSD_1(\omega) = 2q^2\nu\frac{sin^2(\omega\tau/2)}{(\omega\tau/2)^2}. \tag{4.11}$$

We have known that $sin^2(\xi)/\xi^2 \to 1$ when $\xi \to 0$. Thus, we obtain $PSD_1(0) = 2q^2\nu$. On the contrary, $PSD_1(\omega \to \infty) = 0$. The frequency where the PSD(f) drops down is $\omega_c = 2\pi f_c = 2\pi/\tau$.

Second, for the geometry $L_x = 100\ nm \gg L_y^*, L_z^*$, we take the current (4.8) represented in Fig. 4.4(c). Then, the Fourier transform of the autocorrelation (4.10) gives [76]:

$$PSD_1'(\omega) = 2q^2\nu'\frac{1}{1+(\omega/\alpha)^2}. \tag{4.12}$$

We have known that $PSD_1'(0) = 2q^2\nu'$ and that $PSD_1'(\omega \to \infty) = 0$. The frequency where the PSD(f) drops down is $\omega_c' = \alpha$. To avoid unnecessary discussions, we assume that there is no electron confinement in the lateral directions (see Ref.[97] for a discussion of confinement in the injection rates), so that the injection rate is roughly proportional to the S_1 or S_1^*. Thus, we can expect that the injection rate in the first case is much higher than in the second case $\nu \gg \nu^*$. This consideration on ν and ν^* does only affect the DC current of the two geometries. On the contrary, we are interested in the time dependent current

that is represented in Fig. 4.4, which do also depend on S_1 and S_1^*. In Fig. 4.5, we have represented the PSDs(f) corresponding to expressions (4.11) and (4.12) for the geometries $L_x = 100\ nm \ll L_y, L_z$(solid square) and $L_x = 100\ nm \gg L_y^*, L_z^*$ (solid triangle) , respectively. Certainly, the frequencies where the PSD(f) drops down of both geometries become different, $\omega_c^* \gg \omega_c$.

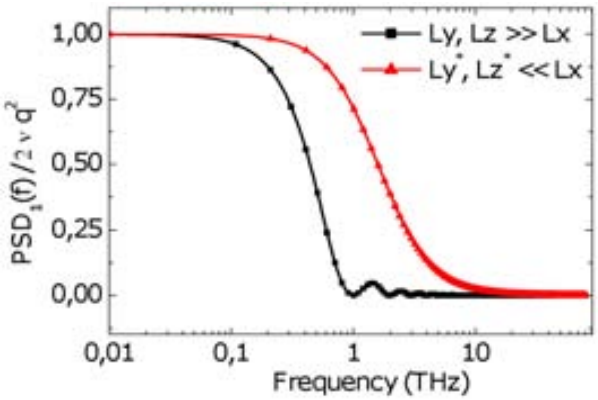

Figure 4.5: Power spectral densities $PSD_1(f)$ and $PSD_1'(\omega)$ (in units of $2q^2\nu$) , respectively, for the currents $I_1(t)$ expressions(4.7) and (4.8) for non-correlated transmitted electrons, moving with constant velocity $v_x = 10^5 m/s$, inside two different geometries. In particular, we consider a fixed value $L_x = 100\ nm$ giving a transit time $\tau = L_x/v_x = 1ps$.

At this point, it can be interesting to understand without the RSP theorem the differences in the frequencies (i.e. $\omega_c^* \gg \omega_c$) when two different lateral surfaces $S_1 \gg S_1^*$ are considered. Let us consider one electron situated so far away from the surface S_1^* that the contribution of this electron to the displacement current on the small surface S_1^* is negligible. However, this electron have a non-negligible influence on the displacement current on S_1. The reason is not that the electron has changed the magnitude of the electric field that it generates, but that $S_1 \gg S_1^*$. Thus, we have to take into account many more small "local" contributions to the displacement current [98] of this electron on S_1 than in the smaller surface S_1^*. Thus, the temporal width of the pulse on $I_1(t)$ on S_1 is larger than on the current $I_1^*(t)$ of the smaller surface S_1^*.

4.3.1.2 Simulation result:

In order to confirm previous results, we have carried out this simulation using the BITLLES simulator presented in the previous chapter. In the C , we present the interface of this simulator Fig. C.1 and current voltage charcteristic of GAA transistor with the geometry $L_x \cdot L_y \cdot L_z = 8 \cdot 12 \cdot 12\ nm^3$, see Fig. C.2. The noise spectrum of a gate-all-around Silicon nanowire (which is a typical multigate structure avoiding short-channel effects with a low-dimensional channel to reach higher mobilities) has been simulated.
In this simulation, we consider a gate-all-around Silicon nanowire depicted in Fig. 4.6.

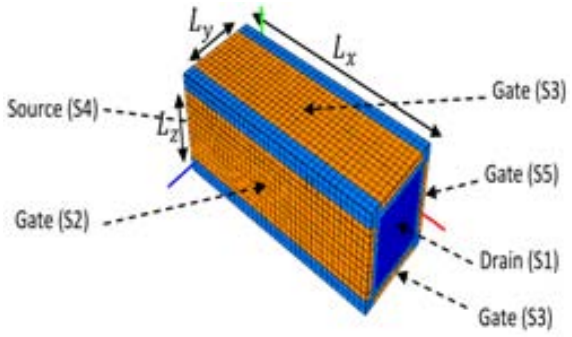

Figure 4.6: *Schematic representation of a gate-all-around transistor. The channel dimensions are L_x, L_y and L_z and it is limited by the closed surface $S = \{S_1, ..., S_6\}$. Transport takes place from source to drain. This transistor is designed by The BITLLES simulator*

We assume the transport along the (100) channel orientation (we use an electron effective mass equal to 0.19 times the electron free mass). An uniform relative permittivity equal to 11.75 in the whole volume Ω is considered. We consider two particular device geometries.

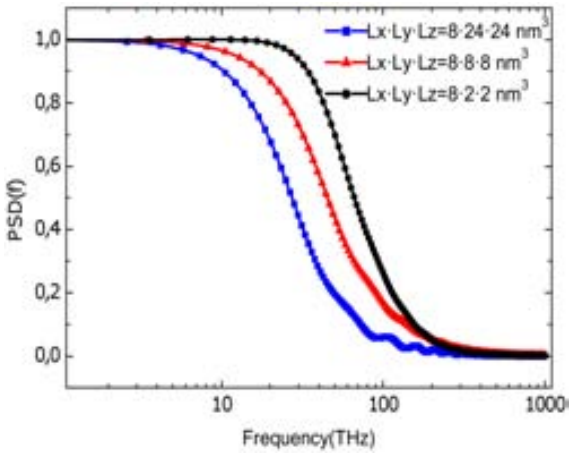

Figure 4.7: *Normalized $PSD(f)$ of non-correlated transmitted electrons. Three different geometries, with same longitudinal dimension (Lx) and different section area (L_y, L_z), are compared using Monte Carlo simulation (BITLLES) for gate-all-around Silicon nanowire [99].*

In Fig. 4.7, the numerical PSDs for three different geometries ($Lx \cdot Ly \cdot Lz = 8 \cdot 24 \cdot 24\ nm^3$), ($Lx \cdot Ly \cdot Lz = 8 \cdot 8 \cdot 8\ nm^3$) and ($Lx \cdot Ly \cdot Lz = 8 \cdot 2 \cdot 2\ nm^3$) are reported confirming the simpler analytical results. We emphasize again that this conclusions are valid for gate-all-around transistors with ballistic transport.

4.3.2 Intrinsic noise in digital applications

We move now towards another topic on noise. Here, we will explicitly consider two-terminal devices which imply that the total current generated by an electron of velocity v_x is $I(t) =$

$q\ v_x/L_x$. From this results, one can anticipate that the shape of the current pulse originated by one electron are modified when $L_x \to 0$. In particular, we know that the electron transit time is roughly equal to L_X/v_x. We notice that, obviously, the current multiplied by the electron transit time is $q\ v_x/L_x; L_x/v_x = q$. The current pulse is the responsible of transmitting an electron of charge q from left to right. Therefore, in the limit of $L_x \to 0$ studied in this section, we have pulse with a very large current during a very short transit time. This situation repersents a large noise in the current, which can be roughly understood as the difference between the instantaneous value and the average value. Let us notice that the average value is not modify by L_x, but it depends on the injection rate (i.e. on the doping or Fermi level).

A quantitative analysis of the THz noise in practical applications needs to recognize that a device is a part of a very large circuit. The rest of the circuit works as a low-pass filter so that only those current fluctuations with frequencies smaller than the cut-off frequency become relevant when analyzing the high frequency noise. The cut-off frequency depends on each particular application. In general, most applications are designed to work as fast as possible, being the inverse of the transit time, $1/\tau$, the ultimate intrinsic frequency limitation. In this regard, these ultra-small electronic devices are expected to work at or beyond THz frequencies.

In general, the high-frequency noise is discussed from the power spectral density of the current fluctuations, as we have done. Alternatively, in this paragraph, we discuss the frequency dependence of the THz noise in terms of the probability distribution function, $P(I_T, t)$, defined as the probability of finding the *time-averaging* current I_T at time t_o:

$$I_T(t) = \frac{1}{T}\int_{t-T/2}^{t+T/2} I(t')dt'. \tag{4.13}$$

In particular, the DC value is defined as $\mu(t) = I_{T\to\infty}(t)$. Clearly, as we increase T, the fluctuations of $I_T(t)$ around $\mu(t)$ decrease. Expression (4.13) can be interpreted as the result of passing the *intrinsic* current $I(t)$ through a low-pass filter whose transfer function is $sinc(wT/2)$. See Fig. 4.8 for the schematic description on how to construct the histogram $P(I_T, t)$. We assume many (infinite) different currents associated to identical samples. Each current is filtered through (4.13). Then, at each time t, we can construct the histogram $P(I_T, t)$. As seen in Figs. 4.8(a) and (b), different $T-$averaging provides different histograms. As indicated in Figs. 4.8(a) and (c), a small averaging time $T1$ can imply a non-negligible probability of logical errors when the output voltage $V_{1'}$ is misunderstood as $V_{0'}$. A larger averaging time $T2$ (see Fig. 4.8(d)) avoids these logical errors, but reduces the maximum operating frequency of the logical gate.

The computation of $P(I_T, t)$ instead of the power spectral density has several practical advantages. On one hand, it allows a direct estimation of digital errors expected from the circuit as the area of the tails of the histograms of Fig. 4.8 when the output voltages are related to the current, for example, through a load resistance R (as seen in Figs. 4.8(c) and (d)). On the other hand, $P(I_T, t)$ is the common language used in quantum mechanical descriptions of noise with full counting statistics [100]. For example, the asymmetry of the current histogram of Fig. 4.8(a), i.e. the skewness, has been predicted and measured [100]. Finally, it allows a quantification of the overall high-frequency noise (beyond $1/f$ and g-

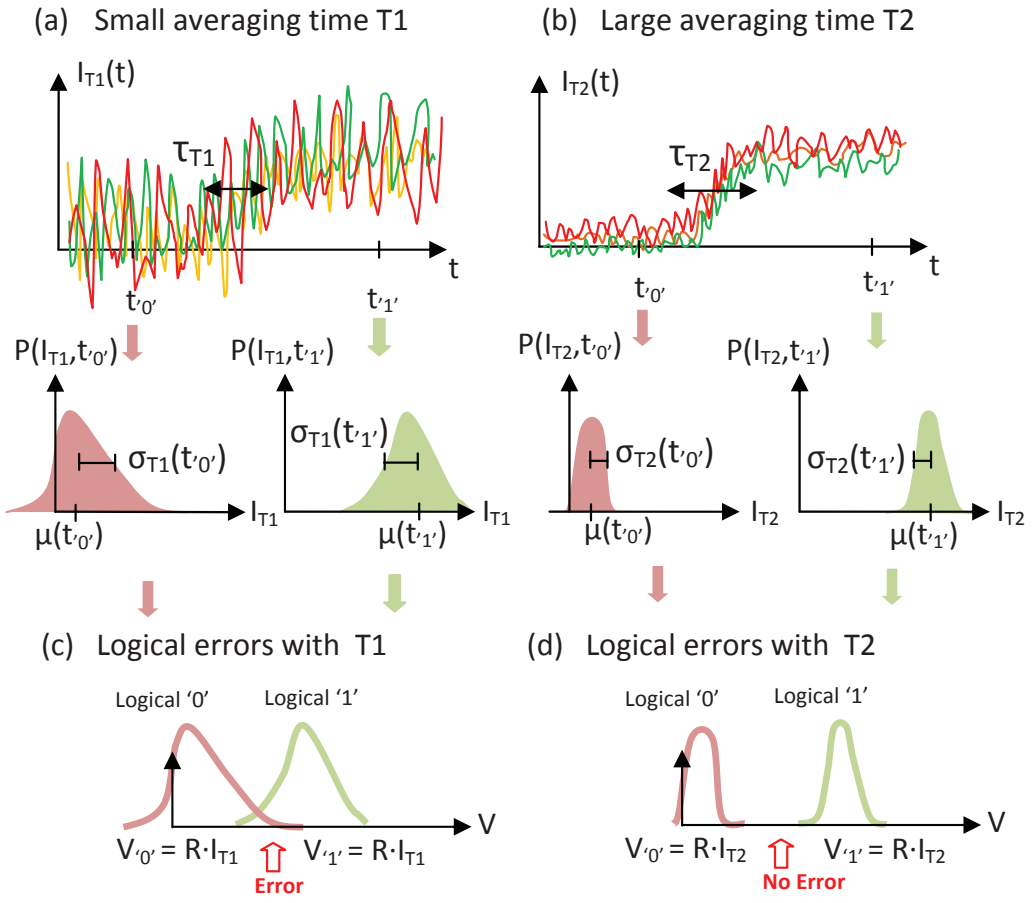

Figure 4.8: Schematic representation on the construction of the histogram $P(I_T, t)$ at different times t from a small $T1$ (a) and large $T2$ (b) ensemble of T-averaging currents. Logical error probability due to the noise after $T1-$averaging (c) and $T2-$averaging (d) using a resistor R that relates current and voltage fluctuations [101].

r noise) in just one parameter. The standard deviation $\sigma_T(t)$ of the distribution $P(I_T, t)$ provides such information:

$$\sigma_T(t) = \sqrt{\int_{-\infty}^{\infty} (I_T(t) - \mu(t))^2 \; P(I_T, t) dI_T} \tag{4.14}$$

In this framework, we will use this parameter $\sigma_T(t)$ to evaluate the noise. Its evolution for different averaging times T can be related to a different cut-off frequencies through $\omega = 2\pi/T$.

4.3.2.1 Numerical results for the standard deviation σ_T after T-averaging:

In Fig. 4.9 we plot the distribution $P(I_T, t)$ for transistor $L_x \cdot L_y \cdot L_z = 8 \cdot 24 \cdot 24 \; nm^3$ for several values of the averaging time T. As observed, a longer T leads to narrower distributions. Fig. 4.10 reports the values $\sigma_T(t)$ discussed in (4.14) for two different lengths . The smaller

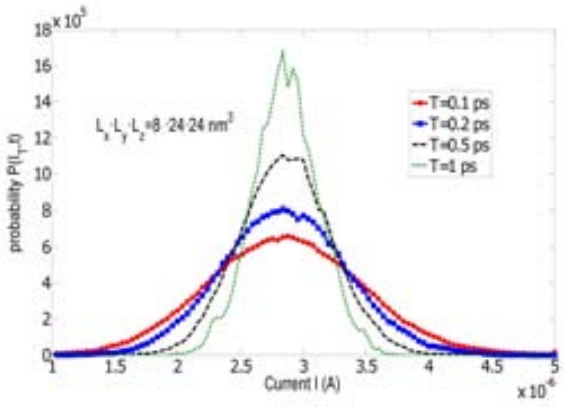

Figure 4.9: Computation of $P(I_T, t)$ for transistor $L_x \cdot L_y \cdot L_z = 8 \cdot 24 \cdot 24\ nm^3$ and for different values of T.

length implies larger fluctuations and higher noise. Roughly speaking, the noise remains independent of T when $T < \tau$, while it decreases nearly lineal with τ when $T > \tau$.

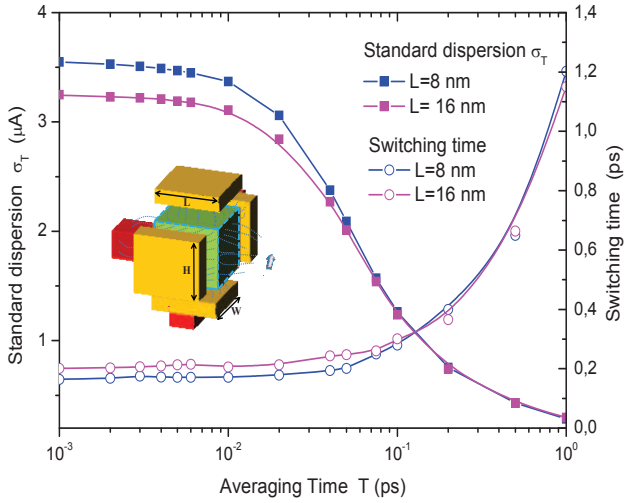

Figure 4.10: Effective switching time (right) and standard deviation σ_T (left) as a function of the averaging time T. (Inset) All around gate ballistic transistor with identical lateral dimensions H=W=24 nm and different length L are considered [101].

4.3.2.2 Numerical results for the *effective* transit time τ_T after T-averaging:

As we increase the averaging time T in Fig. 4.10, the noise drastically drops. Unfortunately, a large averaging time T will also degrade the transient behavior of the device. The result presented in Fig. 4.10 is for two different all around gate ballistic transistor with $L = 8\ nm$ and $L = 16\ nm$ (see inset in Fig. 4.10). In both devices, the lateral area is $24 \times 24\ nm^2$. In our Monte Carlo simulation, BITLLES simulator, the voltage changes from 0 V till 0.5 V

implying a transient current $I(t)$, as schematically seen in Fig. 4.8.

We plot the switching time elapsed to change from the current I_{OFF} till I_{ON} in Fig. 4.10. Initially, for small T, the switching time gives its *intrinsic* constant value, which is related to the delay time τ. However, after a larger $T-$averaging, the current $I_T(t)$ has degraded its dynamic response because of the time-integral (filtering) of expression (4.13). One can easily conclude that the *effective* switching time is roughly given by $\tau_T \approx \frac{L}{v_x} + T$. In Fig. 4.10, we see the expected degradation of the dynamic properties of that transistor because of the T-averaging. For large T, we have $\tau_T \approx T$.

We conclude from Fig. 4.10, that the smaller devices (short L_x) become noisier than the larger ones. Therefore, such small devices will require that a large $T-$averaging to reduce the noise. According to our results, such $T-$averaging is so severe, the advantages of the small transit time are not profitable. In this regard, it seems that the constant reduction of the dimensions of electron devices will find an unbreakable red-wall in the noise behavior.

4.4 Transient and AC simulation of nanoscale FETs

The last topic studied in this chapter will be devoted to the AC behavior of emerging nanoscale devices. In particular, we will discuss the cut-off frequency of gate-all-around devices. Therefore, the AC study needs the consideration of AC sources in the gate of the FET transistors. We start with a discussion on the relation between the transit time and the cut-off frequency, which will become crucial on our results.

4.4.1 On the transit time

It is generally believed that the electron transit time is the ultimate responsible for high-frequency limitations of electronic devices. Ramo [73] and Shockley [72], in the 30's, were the pioneers in determining how the electron transit time, τ, limits the high-frequency performance of electronic devices. They showed that an electron moving with velocity $\vec{v} = \{v_x, 0, 0\}$ between two (infinite) metallic plates separated by a distance L generates a current peak on one of the plates equal to $i(t) = -q \cdot v_x/L$ during $0 < t < \tau$, being q the (unsigned) electron charge. The time-integral of the current during $\tau = L/v_x$ gives the expected transmitted charge $-q$. The physical origin of this current peak is the electric field generated by the electron on the plates (that implies a displacement current there).

For FETs, the role of the transit time in their high-frequency performance is clearly manifested in the cut-off frequency, f_T, defined as the frequency at which the magnitude of the small signal current gain $h_{21}(f)$ rolls of to unity i.e., $|h_{21}(f_T)| = 1$. Such frequency can be simply approximated as $f_T \approx g_m/(2\pi C_d)$ where $g_m = \partial I_{DS}/\partial V_{GS}$ is the small-signal FET transconductance in saturation bias and C_d the dielectric capacitance [102]. After a simple calculation, it can be seen that $f_T \approx 1/(2\pi\tau)$ pointing out again the electron transit time as the ultimate limiting factor [102], without any influence from the lateral dimensions.

The preferred strategies to decrease the transit time of FETs have been (i) reducing L via scaling or (ii) increasing v_x via changing channel materials. Scaling down the length implies that most ultra-small FETs must be designed with double-gate, tri-gate and even (GAA)

structures to enhance the electrostatic gate control on the current [103]. According to ITRS 2012 [1] GAA and SOI (Substrate on Insulator) structures have been chosen as candidates for electrostatic control, see Fig. 4.11.

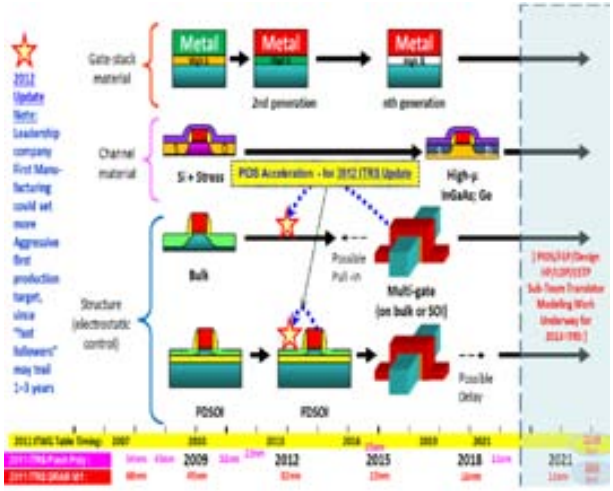

Figure 4.11: *Different solutions for increase carriers mobility looking for or improving materials and also for electrostatic control through GAA or SOI [1].*

There is a consensus in the scientific community that the scaling of these multi-gate ultra-small FETs are approaching its limits, and it is necessary to look for different strategies [1]. Increasing the electron velocity with the use of high-electron-mobility FETs, based on III-V materials such as GaAs and InP, have been also a successful alternative to reduce the transit time [104]. Identically, Graphene channels are expected to provide higher velocities [105].

Alternatively, in this work, we show through a careful analysis of the displacement current generated by a moving electron that, for some particular emerging FETs the limiting high frequency factor is an effective transit time, which can be much smaller than τ. For such particular FET, the high-frequency performance can be improved without neither length scaling nor using materials with higher electron mobility.

4.4.2 The effect of the FET geometry on the total current of a free electron

Previously we have studied the dependance of the current traversing the electron devices by means of the Ramo-Shockley-Pelligrini. This time we carry out this study using the definitions of the total current (particle plus replacement currents). For this end, first, we consider an electron with a trajectory $\vec{r}[t] = \{v_x \cdot t, 0, 0\}$, with $v_x = 10^5$ m/s, moving in free space inside the volume $\Omega = L \times W \times H$, limited by a closed surface $S = \{S1, S2, .., S6\}$, plotted in the inset of Fig. 4.12. The electron generates a time-dependent electric field $\vec{E}(\vec{r}, t)$ on the surface $S1$. Such electric field, together with the particle current density, $\vec{J}(\vec{r}, t)$, are the responsible for the total current on $S1$:

$$i_{\Omega}^{S1}(t) = \int_{S1} \vec{J}(\vec{r}, t) \cdot d\vec{s} + \int_{S1} \epsilon(\vec{r}) \frac{\partial \vec{E}(\vec{r}, t)}{\partial t} \cdot d\vec{s}, \tag{4.15}$$

with $\epsilon(\vec{r})$ the inhomogeneous electric permittivity. In a real system, as the transistors discussed afterwards, the surface S1 must be a material (a metal) whose electrons interact with the one considered in Fig. 4.12. The value of $i_\Omega^{S1}(t)$ plotted in Fig. 4.12 show the dependence of the temporal pulse of the current on the lateral area $W \times H$ for a fixed length $L = 8$ nm. A unique trajectory, meaning a unique electron transit time $\tau = L/v_x$, is used in all previous computations. We conclude from Fig. 4.12 that the shape of the current pulse is strongly dependent on the lateral surface $W \times H$. For the structure $8 \times 24 \times 24\ nm^3$ we recover the old result of Ramo [73] and Shockley [72].

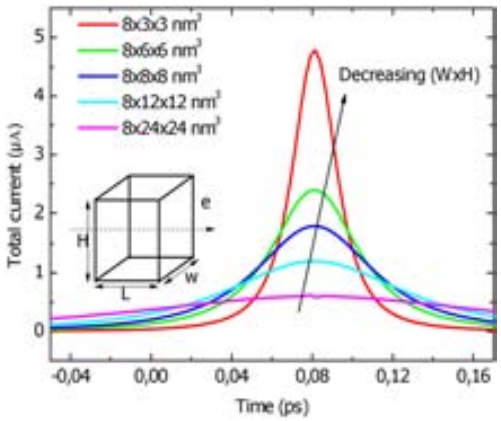

Figure 4.12: *(Color online) Total current on S1 (right side of the box) for an electron traversing the volume $\Omega = L \times W \times H$ of the inset. A fixed length $L = 8$ nm and several lateral $W \times H$ areas of the box are considered [93].*

Let us emphasize that the continuity of the current presented in Fig. 4.12 is due to had into account the two components current (conduction and displacement), this is because of the discontinuity appeared in the particle current when the electron traverses the interested surface is compensated by counterpart appeared in the displacement current. In Fig. 4.13 we have presented the electric flux in surface S_1, which its time derivative presents the displacement current. In that figure we clearly see the discontinuity at the moment the electron traverses the surface S_1.

4.4.3 The effect of the FET geometry on $\vec{F}_i(\vec{r})$

Before explaining this conclusion , going back to the Ramo-Shockley-Pelligrini theorem we present the irrotationnel function in 2D , for instance on the surface S_1, $\vec{F}_\Omega^{S1}(\vec{r})$. For two different geometries this functions have been presented in Fig. 4.14, from it we realize that a moving electron will have an influence on $\Gamma_\Omega^{S1}(t)$ (the first term in the Ramo-Shockley-Pelligrini current) only during the time when it is close to drain surface. In the rest of positions inside the channel, we get $\vec{F}_\Omega^{S1}(\vec{r}) \approx 0$. Thus, the transit time τ is no longer a relevant parameter to determine the temporal width of the $i_D(t)$ pulse. From (4.6), we can consider an effective device length L_α, which is smaller than L because $L \ll W, H$. Such effective device length, provides an "effective" transit time $L_\alpha/v_x < \tau$.

The main conclusion on the electron devices performance concerning AC regime is based on the fundamental difference between the current pulses obtained from either expression

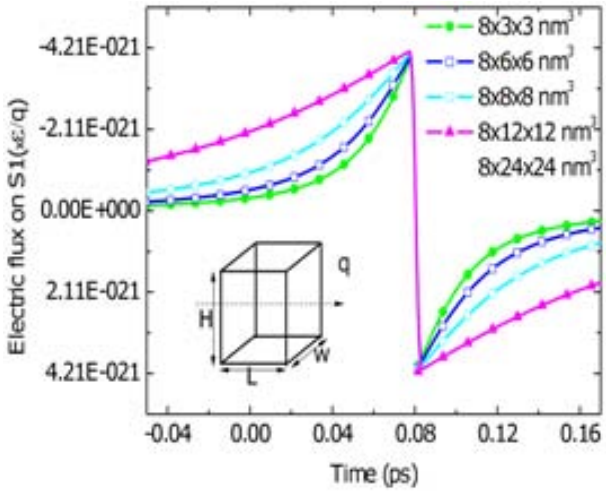

Figure 4.13: *Electric flux on S_1 (right side of the box) for an electron traversing the box of the inset. Different geometries with a fixed length of $L = 8nm$ and several lateral areas are considered [106].*

(4.4) or (4.6). However, when predicting the currents, we have assumed that electrons do not move in the lateral directions z and y. An electron with a zig-zag trajectory would produce a quite arbitrary current pulse. In this regard, the physical origin of the effective length L_α discussed in our work is different from the ones considered in the literature for larger devices [107, 108]. It can be straightforwardly demonstrated [109] that quantum (Bohmian) trajectories associated to a FET with confinement on the lateral surfaces single subband have zero velocities in the lateral directions when only one energy subband is available $E(k_x, n_y, n_z) = \hbar^2 k_x^2/(2m_h^*) + E_q$, with the confinement energy given by $E_q = \hbar^2\pi^2/m_l^*(n_y^2/W^2 + n_z^2/H^2)$. Then, the previous predictions of the current from (4.4) and (4.6) become very accurate. This is the reason why our conclusion is, strictly speaking, only valid for quantum wires (QWs). In particular, for transport through the (100) direction on Si channels, the presence of only one significant subbands is reasonable for lateral dimensions below $W, H \leq 12$ nm ($E_q \approx 0.14eV$ for $n_y = 2$ and $n_z = 1$ for $W = H = 12\ nm$).

4.4.4 Small signal equivalent circuit scheme for FET

To study gate-all-around transistor Fig. 4.6 in small signal regime , we consider its equivalent quadripole. In that regime , the gate-all-around transistor (quadripole) can be presented as it is shown in Fig.4.15. The elements C_{gs} and C_{gd} are in the respective source-gate and drain-drain capacitances , r_0 is the output resistance and g_m is the transconductance. From Fig. 4.15 , the admittance capacitance can be written,

$$\begin{aligned} I_1 &= Y_{1,1}V_1 + Y_{1,2}V_2, \\ I_2 &= Y_{2,1}V_1 + Y_{2,2}V_2, \end{aligned} \tag{4.16}$$

and the gain current reads,

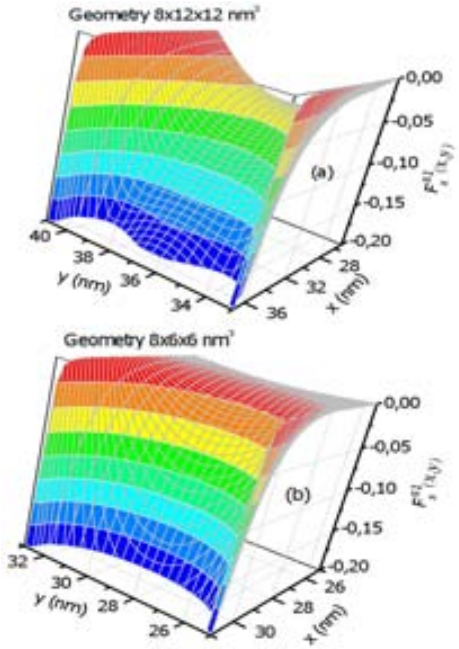

Figure 4.14: *(Color online) The unit-less irrotational function* $F_x^{S_1}(x,y) = \vec{F}_\Omega^{S_1}(x,y,H/2)\cdot\vec{x}$ *for the two geometries [93].*

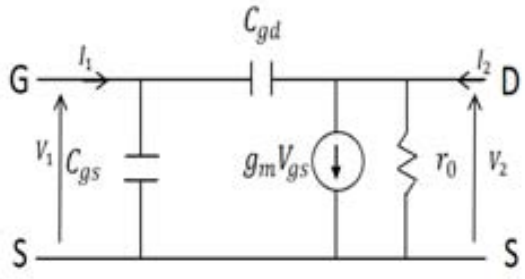

Figure 4.15: *Equivalent circuit schema for gate-all-around transistor in small signal regime.*

$$h_{21} = \frac{I_2}{I_1}|_{V_2=0} \tag{4.17}$$

The modified equivalent circuit schema to compute that current gain is presented in Fig.4.16. From that figure and using a small algebraic operation we found,

$$h_{21} \approx \frac{g_m}{\omega(C_{gs}+C_{gd})} \tag{4.18}$$

The cut-off frequency f_T is the frequency where the current gain small signal is approximatively equal to unity, i.e.

$$h_{21}(f_T) = \frac{g_m}{\omega(C_{gs}+C_{gd})} = 1 \tag{4.19}$$

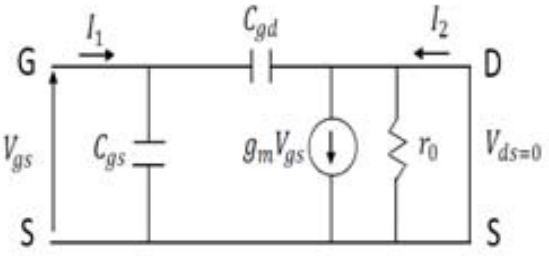

Figure 4.16: *Equivalent circuit schema for gate-all-around transistor in small signal regime used to compute the gain current.*

Thus the cut-off frequency reads,

$$f_T = \frac{g_m}{2\pi(C_{gs} + C_{gd})}. \tag{4.20}$$

The cut-off frequency in versus the transit time is also defined,

$$f_T = \frac{1}{2\pi\tau}. \tag{4.21}$$

4.4.5 Numerical simulation of the cut-off frequency from transient simulations

Now, we provide numerical support to the previous conclusions through a time-dependent simulation of electron transport through a GAA QW FET, using the small signal equivalent schema presented before. We can define the gate current as $i_G(t) = i_\Omega^{S2}(t) + i_\Omega^{S3}(t) + i_\Omega^{S5}(t) + i_\Omega^{S6}(t)$ satisfying $i_D(t) + i_S(t) + i_G(t) = 0$, at any time, because we know that $\sum_{i=1}^{6} i_\Omega^{Si}(t) = 0$. The six currents $i_\Omega^{Si}(t)$ are computed from expressions of Ramo-Shockley-Pelligrini current with the vector function $\vec{F}_\Omega^{Si}(\vec{r})$ obtained from the 3D numerical solution Laplace equation (i.e. the definition of the irrotationnal functions) , with a spatial grid of 0.5 nm in the x direction and 1 nm in the others. In all structures we consider a Si intrinsic channel (whose volume is Ω) and a 1 nm thick oxide layer. The Coulomb interaction among electrons in the channel, and between them and those in the drain, source and gate metallic contacts is obtained through a 3D solution of the Poisson equation with the appropriate Dirichlet or Neumann conditions [110]. In particular, we go beyond the standard mean-field approximation treating Coulomb interaction among electrons, by computing a particular 3D Poisson equation for each electron [111]. Time-dependent Monte Carlo simulations are done through the BITLLES simulator [112] where all the previous features can be included. For simplicity, semi-classical trajectories, with energy confinement in lateral directions, are used. Our conclusions do not depend on the differences between classical or quantum trajectories [109, 113].

We compute the transient current $i_D(t)$, $i_S(t)$ and $i_G(t)$ when the drain-source contacts have a fixed DC bias, $V_{DS} = 0.5$ V, and a step voltage of 0.5 V is applied to the gate for two different GAA FET geometries. The first structure A has $L = 8\ nm$, $W_A = 12\ nm$ and

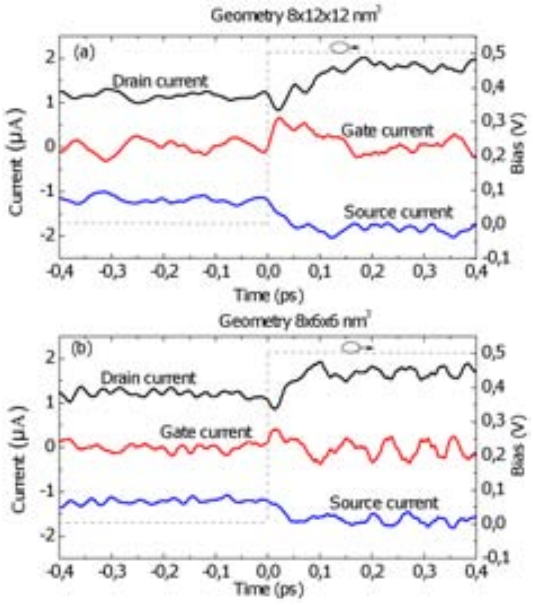

Figure 4.17: *(Color online) Total (displacement plus conduction) transients currents computed in the drain (solid black line), source (solid blue line) and gate (solid red line) ammeter of the structures A and B for the GAA QW FET of Fig. 4.1 when a step voltage from (grey dashed line) is applied on the gates, while the drain source voltage is fixed to* 0.5 *V. The sum of the three currents, in each structure, is equal to zero.*

$H_A = 12\ nm$ and the second one B has $L = 8\ nm$, $W_B = 6\ nm$ and $H_B = 6\ nm$. The first observation of the result plotted in Fig. 4.17(a) and (b) is that $i_D(t) + i_S(t) + i_G(t) = 0$. This confirms the correctness of our numerical RSP algorithm [114]. The gate current has a similar behavior in both structures. In addition, the perturbation on $i_D(t)$ of B finished earlier than that of A, meaning that the current in structure B reaches its DC value before the current in A. The differences between these currents can be perfectly understood from our discussion on expression (4.4) and (4.6) for GAA QW FETs. In the A structure, all electrons inside the simulating box affect the drain and source transients currents, while in the structure B only those electrons close to the drain affect $i_D(t)$ and those close to the source affect $i_S(t)$. This difference is due to the shape of the irrotational function $\vec{F}_{\Omega}^{Si}(\vec{r})$. For structure A, $\vec{F}_{\Omega}^{Si}(\vec{r})$ is non-zero along the whole device length of Fig. 4.14(a), while for structure B, $\vec{F}_{\Omega}^{Si}(\vec{r})$ is equal to zero in a large part of the length of Fig. 4.14(b). These differences are directly translated into differences between the high-frequency behavior of A and B FETs.

With the aim to see the effect of the cross section area on the transit time using the Bohmian trajectory, we have considered four different geometries with the same longitudinal length and different lateral sections. The structures are four GAA transistors with $L_x = 8\ nm$, a $0.5V$ had applied to produce the change current from state I_{off} to I_{on}. The result are presented in Fig. 4.18. It is clear from that figure that the time the current in the structure with section lateral $L_y \cdot L_z = 24 \cdot 24nm^2$ needs to change from the state I_{off} to I_{on} one is greater than those for the others while it is needed more verification to say the difference

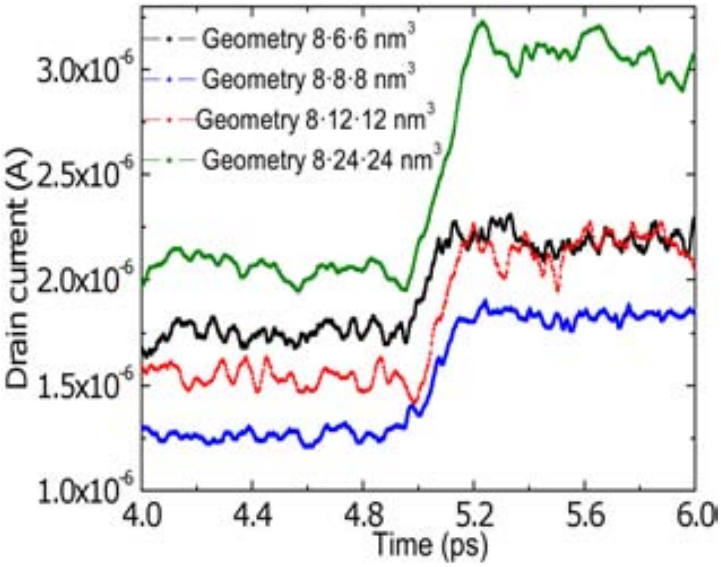

Figure 4.18: *A comparison of the time needs a transistor to shift from the state I_{off} to I_{on} for four different geometries is presented .*

between others.

We consider the conventional small-signal admittance parameter model for a three-terminal FET as drawn in Fig. 4.19, with $i_1(t) = i_G(t) - i_G^{DC}(t)$ and $i_2(t) = i_D(t) - i_D^{DC}(t)$, being $i_G^{DC}(t)$ and $i_D^{DC}(t)$ the DC value before the voltage step. We repeat several times the transient simulations in order to avoid fluctuations while focusing only on the deterministic admittance parameters (without noise sources). A Fourier transform [115] of $i_1(t)$ and $i_2(t)$ directly provides the small-signal admittance parameters $Y_{2,1}(f)$ and $Y_{1,1}(f)$. The intrinsic cut-off frequency, f_T, can be computed then as $|h_{2,1}(f_T)| = |Y_{2,1}(f_T)/Y_{1,1}(f_T)| = 1$. To see clearly the effect of the cross section area, we have presented the intrinsic cut off frequencies in Fig. 4.19 for the geometries considered in Fig. 4.12. We notice that for the same longitudinal length L, the cut off frequency increases from $f_T = 0.62\,THz$ to $f_T = 10.20\,THz$ when the later area is scaled down, as seen in Fig. 4.19. These results confirm that the geometry of the GAA QW FETs (for a fixed L) has a relevant role in their high-frequency behavior.

At this point it is important to clarify whether or not this THz intrinsic cut-off frequencies are expected to be reached soon. In fact, the cutoff frequency predicted by ITRS 2012 [1] is tending toward these frequencies in the next future, see table 4.1. We are somehow studying the electronic devices that are epxected to be on the market in 10 years [1].

Year of production	2011	2012	2013	2014	2015	2016	2017	2018
Extended Planar Bulk	347	396	445	512	578	669	756	-
UTB FD	-	-	477	545	614	704	790	889
Multigate	-	-	-	-	620	710	795	890

Table 4.1: Cutoff frequency (GHz) for different technology evolution according to ITRS 2011.

In order to confirm the role of the current pulse on the results, we present the correlations

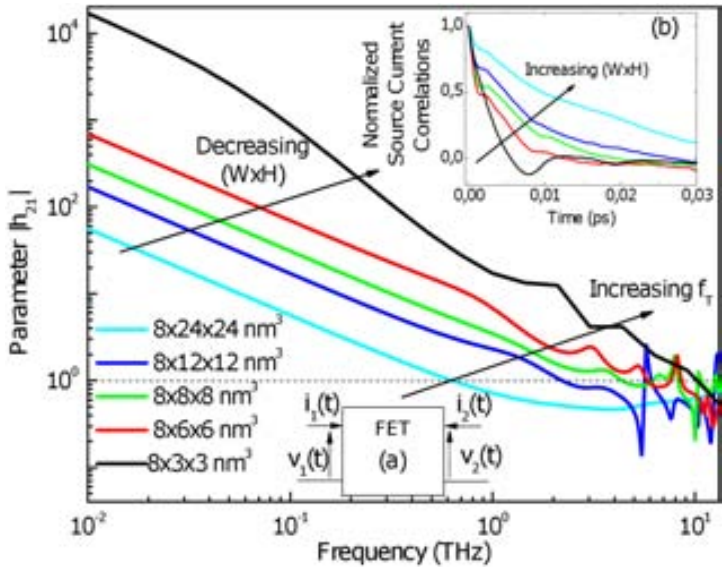

Figure 4.19: *(Color online) h_{21} parameters as a function of frequency for the structures considered in Fig. 4.12. (a) Two-port (admittance) small-signal circuit. (b) Source current autocorrelation with DC bias. The FET with larger lateral area does not satisfy the single band quantum wire requirement, but it is included to show the tendency of the results.*

of the source current with DC bias for previous FETs. The results in the Fig. 4.19(b) clearly show that the larger the lateral area is, the wider the current temporal pulse.

In conclusion, we have presented an original strategy to improve the device high-frequency performance without increasing the device length, but only playing with the lateral surfaces. For such study, we have computed the hybrid parameters (h_{ij}) in order to predict the cutoff frequency. However, the simulation tool developed here allows us to compute the scattering parameters (S_{ij}), which are very common in high-frequency measurement, from our BITLLES simulator. For a relation between hybrid parameters (h_{ij}) and scattering parameters (S_{ij}), see Ref. [116]. We are interested into these parameters (S_{ij}) because of their advantages at very high frequency. For instance using the hybrid or admittance parameters at those frequencies is impracticable because it is difficult to do a short circuit appearing radiation which alters the signal. While using the parameters (S_{ij}) do not need to do that short circuit and the matching is done easily. We emphasize that the BITLLES simulator is able to compute classical, but also quantum scattering parameters, where, for example, tunneling high-frequency phenomenology becomes relevant.

4.5 Summary

In this chapter, we have use of understanding of quantum and classical currents in terms of the RSP theorem, in order to make some predictions of the high-frequency behavior of nanoelectronic devices. We have shown that the pulse of the total current generated by one electron has temporal width that is drastically depending on the lateral area of the devices. The pulse becomes narrow when we decrease that lateral area. This property has a

strong effect on the power spectral density of the noise on DC transport. When the lateral area is small the pulse is narrow and the mentioned spectrum riches higher frequencies. We also discuss the noise in FETs for digital applications. For such scenarios, focused on two-terminal devices, we conclude that the reduction of the channel lenght implies an increment of the noise. The degradation is severe enough to be able to questioning the utility of further scaling down electron devices. Finally, based on the previous results, we have discover a new strategy to improve the cutoff frequency f_T of nanoscale FETs without neither scaling it nor using a another materials. The importance of playing with multi-gate (i.e. multi-terminal) structures that provide a richer high-frequency phenomenology is manifested along the whole chapter.

Chapter 5

Conclusions

The progress of our actual society is somehow ultimately linked to the progress of electronics. Such progress demands that each generation of new devices is faster and smaller than the previous one. The scientific community has done an important effort to provide reliable simulations tools for studying the DC behavior of state-of-the-art nanoscale devices. Some of the common classical and quantum simulation techniques are mentioned in the **first chapter**. However, a similar effort for the the quantum simulation of the AC performance of such nanoscale and TeraHertz devices is still missing. For micrometric dimensions or scenarios where the particle-like nature of electrons mainly determine the performance of the device, a Monte Carlo solution of the Boltzmann equation has been developed and it can be successfully used to study DC transport. On the other hand, there are scenarios where both the wave-like and the particle-like nature of electrons, become relevant. An example of such scenarios are the study of AC transport and noise in quantum devices. For these type of scenarios, the **second chapter** is dedicated to explain how Bohmian mechanics can be a very useful tool to study/understand/characterize them. We have also discussed how the measurement of the current is done in Bohmian mechanics without considering wave function collapse. Finally, we have discussed why it can be useful, from a computational point of view, to study many-particle quantum system in terms of conditional (Bohmian) wave-functions.

In the **third chapter** we have derived classical and quantum versions of the Ramo-Shockley-Pellegrini theorem that allows the computation of the total (conduction plus displacement) currents. In the quantum side, we have demonstrated that the Orthodox or Bohmian version are totally equivalent. The Ramo-Shockley-Pellegrini expressions for classical or Bohmian particles have been implemented in the BITLLES simulator. The practical difficulties of its implementation are discussed. The role of displacement current to obtain a continuous current at any time have been theoretically shown.

In the **fourth chapter**, we have shown that the temporal width of the current pulse genrated by an electron is drastically depending on the lateral area of the multi-gate electron devices, and it becomes narrow when we decrease that area. This property has a strong effect on the AC and noise behavior . In addition, we have presented an original strategy for improving the cutoff frequency f_T of multi-gate ballistic devices without neither scaling

it nor using a another materials.

We can sum up the conclusions of this thesis:

1. Extension of the Ramo-Shockley-Pellegrini theorem to the quantum Bohmian version and its discussion in terms of quantum (Bohmian) trajectories.

2. Practical implementation of the expressions of the Ramo-Shockley-Pellegrini theorem for the total (displacement and conduction) current into the BITLLES simulator for classical and quantum simulations.

3. Demonstration that the time dependent current of gate-all-around transistors drastically depends on the device geometry. This predictions have been confirmed by numerical Monte Carlo results on quantum wire gate-all-around.

4. Demonstration that the (properly averaged) high-frequency noise of two-terminal ballistic system increases when device dimensions are reduced.

5. Study of the effect of the cross section area of the multi-gate device geometry on the temporal width of the current pulse. It is shown that the smaller lateral section area provides the higher cut off frequency and the higher noise.

Finally, let us emphasize that the development of quantum electron transport models for electron devices are quite recent. Most simulators are developed for modeling/ understanding DC transport only and there are still many gaps to fill and some urgency in doing it. Among them, there are very few quantum simulators that are able to study AC transport, transients and fluctuations of the current (noise). This thesis is a step in the direction of proving a reliable dynamic quantum simulator to the industry and the scientific community .

Chapter 6

Bibliography

Bibliography

[1] Technology Roadmap for Semiconductors, update 2012 and the versions anteriors, http://www.itrs.net/.

[2] J. E. Lilienfeld, *Method and apparatus for controlling electric current*, New York, 1926.

[3] W. F. Brinkman,D. E. Haggan, and W. W. Troutman, *A History of the Invention of the Transistor and Where It Will Lead Us*, IEEE Journal of Solid-Circuits, **32**(12), pp. 1858-1865, 1997.

[4] P. A. Markowich, C. A. Ringhofer, C. Schmeiser, *Semiconductor Equations*, Springer-Verlag, Wien Newyork, 1990.

[5] O. V. Roos, *A Formal Solution of Liouville's Equation*, Journal of Mathematical Physics **1**(2), 107-111, 1960.

[6] E. Scholl, *Theory Transport Properties of semiconductors Nanostructures* (first ed.) Chapman and Hall, London, 1998.

[7] X. Oriols, D. K. Ferry, *Quantum transport beyond DC*, J. Comput. Electron, **12**, 317330, 2013.

[8] K. Hess, Ed., *Monte Carlo Device simulations: Full Band Beyond*, Kluwer Academic Publishers, USA, 1991.

[9] K. Hess, *Advanced theory of semiconductor devices*, IEEE Press, Newyork, USA, 2000.

[10] D. Supriyo, *Quantum phenomena* , (Vol. VIII Modular series on solid state devices), R. F. Pirret and Gerold W.Neudeck, Eds., Adisson-Wesley Publishing Company, USA, 1989.

[11] M. Lundstrom, *Fondamentals of carriers Transport* , (Vols. X, Modular series on solids state Devices), G. W. Neudeck and Robert F. Pirret, Eds., USA: Addison-Wesley, 1990.

[12] Majorana, A. and R. M. Pidatella, *A Finite Difference Scheme Solving the Boltzmann-Poisson System for Semiconductor Devices* , Journal of computational Physica, **174**, 649-668, 2001.

[13] M. D. Ventra, *Electrical Transport nanoscale systems*, United Kingdom, University press Cambridge, 2008.

[14] http://www.research.ibm.com/DAMOCLES

[15] http://www.synopsys.com

[16] R. Stratton, *Diffusion of Hot and Cold Electrons in Semiconductor Barriers*, Physical Review, **126**, 2002-2014, 1962.

[17] K. Blotekjaer, *Transport Equations for Electrons inTwo-Valley Semiconductors*, IEEE Transactions on Electron Devices , ED. **17**, 38-47, 1970.

[18] H. K. Gummel, *A Self -Consistent Iterative Scheme for One-Dimensional Steady State Transistor Calculations*, IEEE Transactions on Electron Devices, 455-465, 1964.

[19] D. L. Scharfetter and H. Gummel, *Large-Signal Analysis of a Silicon Read Diode Oscillator Electron Devices*, **1** (ED. 16), 64-77, 1969.

[20] A. Forghieri, R. Guerrieri, P. Ciampolini, A. Gnudi, M. Rudan, G. Baccarani, *A New Discretization Strategy of the Semiconductor Equations Comprising Momentum and Energy Balance* , IEEE Transactions on Computer-Aided Design, **7**(2), 231-242, 1988.

[21] http://www.silvaco.com

[22] D. Supriyo, *Electronic Transport in Mesoscopic Systems*, (H. Ahmed, M. Pepper, and A. Broers, Eds.), United Kingdom, Cambridge Univrsity Press,1995.

[23] A. Alarcón , *Quantum many-particle electron transport in time-dependent systems with Bohmian trajectories*, PhD. Thesis, Universitat Autònoma de Barcelona, 2011.

[24] L. P. Kadanoff and Gordon Baym, *Quantum Statistical Mechanics: Green's Functions Methods in Equilibrium and Nonequilibrium Problems*, Perseus Books Publishing, L. L. C. 1962.

[25] G. Albareda, *Classical and quantum trajectory-based approaches to electron transport with full Coulomb correlation* PhD. Thesis, Universitat Autònoma de Barcelona, 2010.

[26] P. Carruthers and F. Zachariasen, *Quantum collision theory with phase-space distributions*, Reviews of Modern Physics, **55** (1), 1983.

[27] L. Shifren, C. Ringhofer, and D. K. Ferry, *A Wigner Function-Based Quantum Ensemble Monte Carlo Study of a Resonant Tunneling Diode*, IEEE Transactions on Electron Devices, **50** (3), 769-773, 2003.

[28] P. Schwaha, D. Querlioz, P. Dollfus, J. Saint-Martin, M. Nedjalkov, S. Selberherr, *Decoherence effects in the Wigner function formalism*, J. Comput Electron, 2013.

[29] E. Scholl, *Theory Transport Properties of semicondurs Nanostructures*, first ed., Chapman and Hall, London, 1998.

[30] M. Di Ventra, *Electrical transport in nanoscale systems*, Cambridge University Press, The Edinburgh Building, Cambridge CB2 8RU, UK, First edition, 2008.

[31] R. E. Collin , *Field theory of guided waves* , McGRAW WILL Book Company, 1960.

[32] http://cobweb.ecn.purdue.edu/gekco/nemo3D

[33] P. Hohenberg and W. Kohn, *Inhomogeneous electron gas*, Physisical Review, **136**, pp. B864, 1964.

[34] J. P. Dahl, *Introduction to the quantum world of atoms and molecules*, World Scientific Publishing Co. Pte. Ltd , 2001.

[35] W. Kohn and L. J. Sham, *Self-consistent equations including exchange and correlation effects*, Physical Review, 140 (4A), A1133, 1965.

[36] http://www.uam.es/departamentos/ciencias/fismateriac/siesta

[37] http://vonbiber.iet.unipi.it/Transiestatutorial/transiesta.html

[38] http://www.tddft.org/programs/octopus

[39] M. Planck, *On the Law of Distribution of Energy in the Normal Spectrum*, Annalen der Physik, **4**, 553, 1901.

[40] N. Bohr, *On the Constitution of Atoms and Molecules*, Philosophical Magazine, **26**, 1 , 1913.

[41] William A. Fedak and Jeffrey J. Prentis, *The 1925 Born and Jordan paper On quantum mechanics*, Am. J. Phys. **77** 2, 2009.

[42] Luke Bovard, *An Introduction to the Path Integral Approach to Quantum Mechanics*, Journal of Phys. **334** 4 0014 , 2009.

[43] A. Komech, *Quantum Mechanics: Genesis and Achievements*,Springer Science+Business Media Dordrecht, 2013.

[44] Jens P. Dahl, *Introduction to the quantum world of atoms and molecules*, World Scientific Publishing, 2001.

[45] E. Schrödinger, *An Undulatory Theory of the Mechanics of Atoms and Molecules*, Phys. Rev., **28**, 1049 , 1926.

[46] K. Wodkiewicz, *Nonlocal and local ghost fields in quantum correlations*,`http://arxiv.org/pdf/quant-ph/9502017v1.pdf`, 1995.

[47] M. Born, *The Tnterpetation of Quantum Mechanic*, reply to Erwin Schrodinger's article, ' Are There Quantum Jumps', 1952.

[48] F. A. Muller *The Equivalence Myth of Quantum Mechanics*, Stud. Hist. Phil. Mod. Phys. **28**, No. 2. pp. 219-241, 1997.

[49] David Bohm , *A Suggested Interpretation of the Quantum Theory in Terms of "Hidden" Variables. I*, Physical Review, **85** (2), 166, 1952.

[50] David Bohm , *A Suggested Interpretation of the Quantum Theory in Terms of "Hidden" Variables. II*, Physical Review, **85** (2), 166, 1952.

[51] Peter R. Holland, *The Quantum Theory of Motion: an account of the de Broglie-Bohm causal interpretation of quantum mechanics*, Cambridge University Press, pp. 18, 1993.

[52] Robert E. Wyatt, *Quantum Dynamics with Trajectories: Introduction to Quantum Hydrodynamics*,Springer, 2005.

[53] X.Oriols and J.Mompart, *Applied Bohmian Mechanics: From Nanoscale Systems to Cosmology*, **ISBN:** 978-981-4316-39-2, Pan Stanford Publishing, pp. 58, 2011.

[54] J. O. Taylor, *Connections with Bohmian mechanics*, PhD Thesis, Graduate School New Brunswick Rutgers, The State University of New Jersey, 2003.

[55] M. Atiqa, M. Karamianb, M. Golshanic, *A Quasi-Newtonian Approach to Bohmian Mechanics I: Quantum Potential*,Annales de la Fondation Louis de Broglie, **34** (1), 67, 2009.

[56] G.Albareda, D. Marian, A. Benali, S. Yaro,N. Zanghì, X. Oriols, *Time-resolved Electron Transport with Quantum Trajectories*, **12**(3), 405-419, 2013.

[57] T. B. Boykin , *An alternative view of the continuity equation in quantum mechanics*, Am. J. Phys. **68** (7), 2000.

[58] D. Dürr, S. Goldstein , and N. Zanghì , *Quantum Equilibrium and the Role of Operators as Observables in Quantum Theory*, J. Stat. Phys. **116**, 959, 2004.

[59] G. Albareda , D. Marian, A. Benali , A. Alarcón , S. Moises , X. Oriols, *Electron Devices Simulation with Bohmian Trajectories*, chapter book.

[60] D. Dürr, S. Goldstein , and N. Zanghì , *Quantum equilibrium and the origin of absolute uncertainty*, J. Stat. Phys. **67**, 843, 1992.

[61] Dürr D., Goldstein S., Tumulka R., and Zanghì N., On the Role of Density Matrices in Bohmian Mechanics. Found. Phys. **35**, 449 , 2005.

[62] X. Oriols, *Quantum trajectory approach to time dependent transport in mesoscopic systems with electron-electron interactions*, Phys. Rev. Lett.,**98**, 066803, 2007.

[63] J. Jackson, *Classical Electrodynamics*, John Wiley, New York, 1962.

[64] Robert E. Collin , *Field theory of guided waves*, McGRAW WILL Book Company,1960.

[65] M. Javid and P. M. Brown *Field Analysis and Electromagnetics*, McGraw-Hill Book Company Inc., New York, USA, 1963.

[66] A. Alarcón and X. Oriols, *Computation of quantum electron transport with local current conservation using quantum trajectories*, J. Stat. Mech. 2009 P01051, 2009.

[67] A. El Fatimy et al., *AlGaN/GaN high electron mobility transistors as a voltage-tunable room temperature terahertz sources*,J. Appl. Phys. **107**, 024504 (2010).

[68] M.Asada, S.Suzuki, N.Kishimoto,*Resonant Tunneling Diodes for Sub-Terahertz and Terahertz Oscillators*, Japanese Journal of Applied Physics **47**, 4375 (2008).

[69] N. Orihashi, S. Suzuki, and M. Asada,*One THz harmonic oscillation of resonant tunneling diodes*, Appl. Phys. Lett. **87**, 233501 (2005).

[70] P.J. Burke, *AC performance of nanoelectronics: towards a ballistic THz nanotube transistor* Solid-State Electronics, **48(10-11)**, 1981 (2004).

[71] N. L. Rangel, and J. M. Seminario, *Graphene Terahertz Generators for Molecular Circuits and Sensors*, J. Phys. Chem. A, **112 (51)**, 13699 (2008).

[72] W. Shockley, *Currents to conductors induced by a moving point charge*, Appl. Phys. **9**, (10), 635, (1938).

[73] S. Ramo, *Currents induced by electron motion*, Proceedings of the I. R. E. **27**, 584, 1939.

[74] It can be argued that there are discontinuities in the definition of $V(\vec{r})$ in the point $\vec{r} = \vec{r}_n[t]$. However, one can apply Green's identities to $V(\vec{r})$ by using a limiting approxing process $\vec{r} \to \vec{r}_n[t]$. See page 41 in Ref.[63]

[75] Consistently with expression (3.11) and equation (3.12), it is argued in the literature that $\phi_i(\vec{r})$ and $\vec{F}_i(\vec{r})$ are the scalar potential and electric field, respectively, when there is no electron charge inside the volume. However, we will avoid this definition because it can lead to misleading interpretations of the boundary conditions (3.13).

[76] A. Benali, F. L. Traversa., G. Albareda,A. Alarcn, M. Aghoutane and X. Oriols, *Effect of gate-all-around transistor geometry on the high-frequency noise: an analytical discussion*, Fluctuations and Noise Letters **11** 1241002, 2012.

[77] G. Cavalleri, E. Gatti, G. Fabri, V. Svetlo, *Extension of Ramo theorem as applied to induced charge in semiconductor detectors*, Nucl. Instrum. and methods. **92**, 137, 1971.

[78] T. Wessel Berg, *A General Reciprocity Theorem for Conducting Media*, Pyisica Scripta, **18**, 375, 1978.

[79] Hunsuk Kim et al., *An extended proof of the Ramo-Shockley-Pellegrini theorem*, Solid-State Electronics **34** (11), 1251, 1991.

[80] B.Pellegrini, *Electric charge motion, induced current, energy balance, and noise*, Physical Review B, **34** (8), 5921, 1986.

[81] P. D. Yoder, K. Grtner, and W. Fichtner, *A generalized Ramo Shockley theorem for classical to quantum transport at arbitrary frequencies*, J. Appl. Phys. **79**, 1951, 1996.

[82] C.Jacoboni and L. Reggiani,*Monte Carlo method for the simulation of electronic noise in semiconductors*, Rev.Mod. Phys.,**55**(3),645, 1983.

[83] T. Kuhn, L. Reggiani, L. Varani, and V. Mitin, *Monte Carlo method for the simulation of electronic noise in semiconductors*, Phys. Rev. B **42**, 5702, 1990.

[84] J. Lusakowski et al.*Voltage tuneable terahertz emission from a ballistic nanometer InGaAs/InAlAs transistor* Journal of Applied Physics, **97**, 064307, 2005.

[85] J.H. Davies, P. Hyldgaard, S. Hershfield, and J.W. Wilkins, *Classical theory of shot noise in resonant tunneling*, Phys. Rev. B **46**, 9620, 1992.

[86] N.Lambert, R.Aguado and T.Brandes, *Nonequilibrium entanglement and noise in coupled qubits*, Phys. Rev. B. **75**, 045340, 2007.

[87] X. Oriols, A. Alarcón, and E. Fernndez-Díaz, *Time-dependent quantum current for independent electrons driven under nonperiodic conditions*, Phys. Rev. B **71**, 245322, 2005.

[88] X. Oriols, *Quantum-Trajectory Approach to Time-Dependent Transport in Mesoscopic Systems with Electron-Electron Interactions*, Phys. Rev. Lett. **98**, 066803 (2007)

[89] G. Albareda, F. L. Traversa, A. Benali and X. Oriols, *Computation of quantum electrical currents through the Ramo-Shockley-Pellegrini-Pellegrini theorem with trajectories*, Fluctuation and Noise Letters, **11**, 1242008, 2012.

[90] P. R. Holland, *The Quantum Theory of Motion*, Cambridge University Press, Cambridge, U.K., 1993.

[91] A. G. Kofman., S. Ashhab, F. Nori, *Nonperturbative theory of weak pre- and post-selected measurements*, Physics Reports **520**, 43133, 2012.

[92] S. Kocsis, B. Braverman, S. Ravets, M. J. Stevens, R. P. Mirin, L. K. Shalm, and A. M. Steinberg , *Observing the Average Trajectories of Single Photons in a Two-Slit Interferometer*, Science **332**, 1170, 2011.

[93] A. Benali, F. L. Traversa, G. Albareda, M. Aghoutane, and X. Oriols, *Improving the intrinsic cut-off frequency of gate-all-around quantum-wire transistors without channel length scaling*, Appl. Phys. Lett. **102**, 173506 , 2013.

[94] J. Jackson, *Classical Electrodynamics*, John Wiley, New York, 1962.

[95] Nathan Ida, *Engineering Electromagnetics*, Springer-Verlag (2000).

[96] One can argue that a differential equation with a second-order spatial derivative can only produce linear or parabolic solutions. This is true for a 1D systems. However, for a 3D system, much more general solutions are possible because three slopes, in three spatial directions, are added.

[97] X. Oriols et al. *Solid-State Electronics* **51** 1287 (2007).

[98] The Gauss law says that the computation of the integral of the electric field on a surface, that includes an electron inside, is equal to q. This results is independent of the size of the surface. In particular, when the surface is very far away from the electron (so that the electric field on the surface is almost negligible), the integral still gives the value q because many very small contributions have to be added on such a large surface.

[99] A. Benali, F. L. Traversa, G. Albareda, M. Aghoutane and X.Oriols *Geometry engineering for the RF behavior of low-dimensional gate-all-around transistors*, Proceeding (IEEE) 15th International Workshop on Computational Electronics (IWCE), Madison, USA, 2012.

[100] Bomze Y. *et al.* Phys. Rev. Lett. **95**, 176601 (2005).

[101] X. Oriols, A. Benali, S. M. Yaro, G. Albareda, J. Mateos, T. González, *Accurate predictions of terahertz noise in ultra-small devices: A limiting factor for their practical application?*, Proceeding (IEEE) of 22nd International Conference on Noise and Fluctuations (ICNF), France, 2013.

[102] D.V.Morgan and M.J.Howes, *Microwave Solid State Devices and Applications* (Peter Peregrinus Ltd. , New York, 1980).

[103] I. Ferain,C. A. Colinge and J.-P. Colinge, Nature, **479**, 310 (2011).

[104] F.Schwierz, H.Wong, J.J.Liou, *Nanometerr CMOS* (Pan Stanford, 2010).

[105] F. Schwierz, Nature Nanotechnology, **5**, 487 (2010).

[106] A. Benali, F. L. Traversa, G. Albareda, M. Aghoutane and X.Oriols *Towards frequency performance improvement of emerging devices without length scaling*, Proceeding (IEEE) of Spanish Conference on Electron Devices (CDE), Valladolid, Spain, 2013.

[107] Y. R. Wu, M. Singh and J. Singh, IEEE Trans. on Electron Devices, **53(4)**, 588 (2006).

[108] R. Akis, J. S. Ayubi-Moak, N. Faralli, D. K. Ferry, S. M. Goodnick and M. Saraniti, IEEE Electron Device Letters, **29(4)**, 360 (2008).

[109] X.Oriols, Physical Review Letters **98** 066803, (2007).

[110] G. Albareda , H. Lopez , X. Cartoixà , J. Suñé and X. Oriols, Phys. Rev. B **82**, 085301 (2010).

[111] G. Albareda , J. Suñé and X. Oriols, Phys. Rev. B **79**, 075315 (2009).

[112] http://europe.uab.es/bitlles/

[113] G. Albareda, F.L.Traversa, A.Benali and X.Oriols, Fluctuation and Noise Letters **11(3)**, 1242008 (2012).

[114] A. Alarcón and X. Oriols, Journal of Statistical Mechanics: Theory and Experiment. **2009**, P01051 (2009).

[115] S.E.Laux, IEEE Trans. on Electron Devices **32**, 2028 (1985).

[116] D. A. Frickey, *Conversions Between S, 2, Y, h, ABCD, and T Parameters which are Valid for Complex Source and Load Impedances*, IEEE Transactions on Micrwave theory and techniques. **42**, NO 2. FEBRUARY 1994.

[117] J. S. Goo, H.T. Ahn, D. J. Ladwig and Z. Yu, *A Noise Optimization Technique for Integrated Low-Noise*, IEEE Journal of Solid-State Circuits , **37**(8), 994, 2002.

[118] D. C. Murry, A. G. Evans and J. C. Carter, *Shallow Defect Responsible for GR Noise in MOSEFT's*, IEEE transactions on Electron Devices, textbf38(2), 416, 1991.

[119] C. Jacoboni and P. Lugli , *The Monte Carlo method for semiconductor device simulation*, Springer, Wien , 1989.

[120] G. Albareda, J. Suñé, and X. Oriols *Many-particle Hamiltonian for open systems with full Coulomb interaction: Application to classical and quantum time-dependent simulations of nanoscale electron devices*, Phys. Rev. B, **79**, 075315, 2009.

[121] X. Oriols, E. Fernndez-Das, *Electron injection model for the particle simulation of 3D, 2D,and 1D nanoscale FETs*, J. Comput. Electron (2007), **6**, 2007.

Appendix A

Quasi-static approximation

In principle, the electric field $\vec{E}(\vec{r},t)$ present in expression (3.14) has to be defined from the scalar potential, $V(\vec{r},t)$, and also from a vector potential $\vec{A}(\vec{r},t)$ via:

$$\vec{E}(\vec{r},t) = -\nabla V(\vec{r},t) - \partial\vec{A}(\vec{r},t)/\partial t \tag{A.1}$$

Then, if we use (A.1) in the development of the Ramo-Shockley-Pellegrini, we will obtain an additional term in the Ramo-Shockley-Pellegrini expression of the current[66], $I_i(t) = \Gamma_i^q(t) + \Gamma_i^e(t) + \Gamma_m^e(t)$ with:

$$\Gamma_i^m(t) = \int_\Omega \epsilon(\vec{r}) \cdot \vec{F}_i(\vec{r}) \cdot \frac{\partial^2 \vec{A}(\vec{r},t)}{\partial t^2} d^3\vec{r} \tag{A.2}$$

This term, $\Gamma_i^m(t)$, where $\vec{A}(\vec{r},t)$ appears, can be neglected in most practical situations. In particular, the condition for neglecting $\Gamma_i^m(t)$ is that the device size, L, is much smaller than the minimum wavelength of the electromagnetic field $\lambda = c/f \gg L$, where c is the electromagnetic propagation speed and f is the signal oscillating frequency [66].

Appendix B

Conservation current with and without the RSP theorem

In this appendix we will demonstrate that the sum of the total current $I_i(t)$ over the six $i = 1.....6$ surfaces of the parallelepiped of Fig. 3.3 is zero. There are two possible demonstration. First, looking for the current conservation of the direct expression of $I_i(t)$ and, then, invoking the equality between the direct and Ramo-Shockley-Pellegrini expressions, see (3.24). Second, looking for current conservation directly inside the mathematical expressions of the Ramo-Shockley-Pellegrini theorem. Here, we will do both. The following "local" charge conservation law is a necessary requirement for any transport formalism,

$$\vec{\nabla}\vec{j_c}(\vec{r},t) + \frac{\partial\rho(\vec{r},t)}{\partial t} = 0. \tag{B.1}$$

The first term of Eq. (B.1) is the conduction current density and the second term is the temporal variations of electron charge density, $\rho(\vec{r},t)$ defined in the right hand side of Eq. (3.15), that can be related to the electric field, $\vec{E}(\vec{r},t)$, by using the Gauss equation. Then, we can rewrite Eq. (B.1) as,

$$\vec{\nabla}\vec{j_c}(\vec{r},t) + \vec{\nabla}\left[\varepsilon(\vec{r})\frac{\partial\vec{E}(\vec{r},t)}{\partial t}\right] = \vec{\nabla}\vec{j_T}(\vec{r},t) = 0. \tag{B.2}$$

where we have defined the total current density, $\vec{j_T}(\vec{r},t)$, as the sum of the conduction plus displacement current densities. From Eq. (B.2), we can use the divergence theorem to obtain the following identity for the total current,

$$\int_\Omega \vec{\nabla}\vec{j_T}(\vec{r},t)dv = \int_S \vec{j_T}(\vec{r},t)d\vec{s} = \sum_{i=1}^{6} I_i(t) = 0, \tag{B.3}$$

Finally, since we known that $I_i(t) = \Upsilon_i^c(t) + \Upsilon_i^d(t) = \Gamma_i^q(t) + \Gamma_i^e(t)$, see expression (3.24), we obtain from (B.3):

$$\sum_{i=1}^{6} [\Gamma_i^q(t) + \Gamma_i^e(t)] = 0, \tag{B.4}$$

Next, we want to reobtain the final result (B.4) directly from the expressions of the Ramo-Shockley-Pellegrini theorem.

From (3.27), we know that:

$$\sum_{i=1}^{6}\Gamma_i^q(t)=\sum_{i=1}^{6}\int_{\Omega}\vec{F}_i(\vec{r})\cdot\vec{J}_c(\vec{r},t)dv$$
$$=\int_{\Omega}\cdot\vec{J}_c(\vec{r},t)\left[\sum_{i=1}^{6}\vec{F}_i(\vec{r})\right]dv \tag{B.5}$$

Identically, from (3.28),

$$\sum_{i=1}^{6}\Gamma_i^q(t)=\sum_{i=1}^{6}\int_{S}\vec{F}_k(\vec{r})\cdot\epsilon(\vec{r})\cdot\frac{\partial V(\vec{r},t)}{\partial t}d\vec{S}$$
$$=\int_{S}\epsilon(\vec{r})\cdot\frac{\partial V(\vec{r},t)}{\partial t}\left[\sum_{i=1}^{6}\vec{F}_i(\vec{r})\right]d\vec{S} \tag{B.6}$$

In order to obtain the condition (B.4), we just have to show that $\sum_{i=1}^{6}\vec{F}_i(\vec{r})=0$. From the definition of $\vec{F}_i(\vec{r})$, we know that:

$$\sum_{i=1}^{6}\vec{F}_i(\vec{r})=-\sum_{i=1}^{6}\vec{\nabla}\phi_i(\vec{r})=-\vec{\nabla}\left[\sum_{i=1}^{6}\phi_i(\vec{r})\right] \tag{B.7}$$

Thus, the condition $\sum_{i=1}^{6}\vec{F}_i(\vec{r})=0$ can be translated into the new condition $\sum_{i=1}^{6}\phi_i(\vec{r})=cte$.

We define $\phi(\vec{r})=\sum_{i=1}^{6}\phi_i(\vec{r})$ as the potential function constructed as the sum of the solution of the previous six functions $\phi_i(\vec{r})$. By construction, according to (3.13), for each surface S_i, we have $\phi_i(\vec{r})=1$ for any $\vec{r}\in S_i$, while $\phi_i(\vec{r})=0$ for the other surfaces. In summary, $\phi(\vec{r})=1$ for any $\vec{r}\in S$. In addition, because of the superposition principle that applies to the equation (3.12), we know that $\phi(\vec{r})$ is also solution of the "Laplace" equation (3.12). According to the uniqueness theorem for the solution of the Poisson (Laplace) equation [74], we known $\phi(\vec{r})=1$. Therefore, as expected, the sum of the total current over the six surfaces is zero. In fact, we have demonstrated that $\sum_{i=1}^{6}\Gamma_i^q(t)=0$ and $\sum_{i=1}^{6}\Gamma_i^e(t)=0$. This demonstration confirms that $\Upsilon_i^c(t)\neq\Gamma_i^q(t)$ because $\sum_{i=1}^{6}\Upsilon_i^c(t)\neq 0$. In addition, we show that the boundary conditions (3.13) are mandatory to obtain $\phi(\vec{r})=1$.

Finally, we want to emphasize that we are discussing the current continuity in a 3D space, where $I_1(t)$ can be different from $I_4(t)$. The condition that these current have to fulfill is just $\sum_{i=1}^{6}I_i(t)=0$, not $I_1(t)=I_4(t)$. On the contrary, since the DC (average) current of the non-electrode surface will be zero, we do obtain the DC current through S_1 is equal to S_4 for a two-terminal 3D device.

B.1 Numerical problems on the currents (3.1) and (3.28)

In this annex we show the different ways we followed to improve the displacement current assigning the electric charge by two different methods. The displacement current (3.1) presented in Fig. B.1 is when the electric charge assigned to a mesh is equal free path time divided by simulation time step Δt , we call it standard.

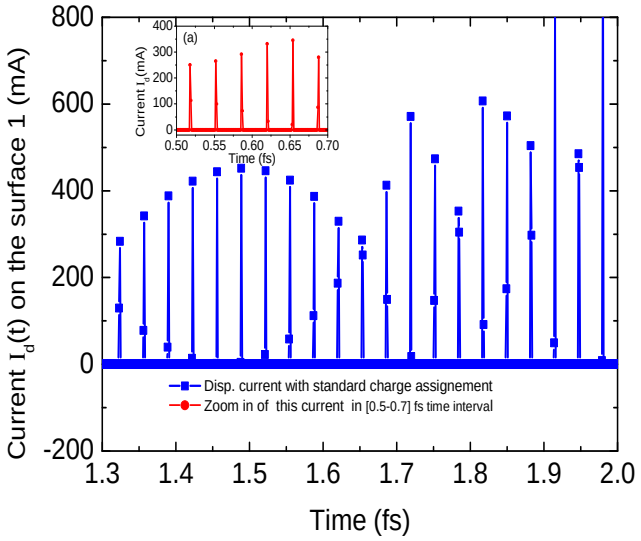

Figure B.1: *Displacement current (3.1) on the surface S_1 for a transistor using the (standard) assignment charge. The inset (a) is zoom in of $Id(t)$ in $[0.5-0.7]fs$ time interval.*

We conclude from that figure that current has two numerical problems : i) there is a discontinuity when the electron displaces from one mesh to another and ii) the current magnitude maintains at zero value .
To overcome the first dilemma we tried another charge assignment version whose the function weight is written [119],

$$\omega(r) = (1 - \frac{\|x - x(i)\|}{\Delta x})(1 - \frac{\|y - y(i)\|}{\Delta y})(1 - \frac{\|z - z(i)\|}{\Delta z}), \tag{B.8}$$

and whose displacement current is presented in Fig.B.2.
This presentation shows that the charge assignment equ. (B.8) allowed to avoid only the nullity of the current inside the meshes.

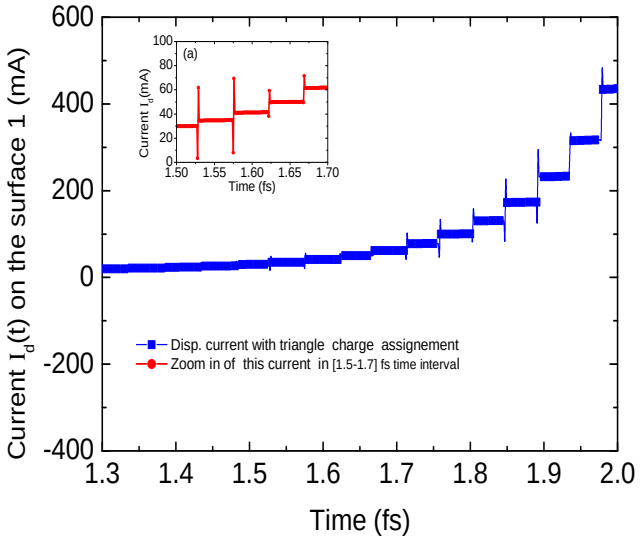

Figure B.2: *Displacement current (3.1) for a transistor on the surface S_1 using the assignment charge equ. (B.8) . The inset (a) is zoom in of $I^d(t)$ in $[1.5-1.7]fs$ time interval.*

Appendix C

The BITLLES simulator

Due to the expensiveness of the technologies used to fabricate and then to study the electron devices , it is necessary to do a prior study for these devices. For this reason it is very important to look for tools to do these preliminary works, there are *simulators* which can be considered as a virtual labs. In this chapter we present a simulator which is called *BITLLES*[1]. This tool is recently developed by Xavier Oriols and his co-workers in electronic department in Universitat Autònoma de Barcelona and it is dedicated to study and characterize time-dependent $3D$ electron transport in classical and quantum nanoelectronic devices. In this simulator and for classical transport, Monte Carlo technique for Boltzmann equation selfconsistently with Poisson equation are implemented to find classical trajectories. In the counterpart , for the quantum electronic devices, the quantum trajectories for Schrödinger's equation are determined by means of Monte Carlo technique too. Besides that , both mean field and field for each electron Poisson equation solutions are considered [120]. What is more, an electron injection model suitable for the semi-classical Monte Carlo simulation of nanoscale devices is included [121]. The Ramo-Shockley-Pelligrini theorem besides the Bohmian trajectories are taken into account considering their advantages.
This simulator gives access to time-resolved electron dynamics and then to provide any moment of currents. It have been shown the ability of the BITLLES simulator to predict DC, AC, noise, transients for electron devices,
By means of this recently developed simulator we can design nanoelectronic devices such as resonant diode tunneling (RTD) or transistors. And by its friendly interface it can easily edit the geometries or the properties of the materials, this interface in illustrated in Fig. C.1.
Via this simulator we carried out current voltage characteristic of GAA transistor.

[1]The acronym *BITLLES* (Bohmian Interacting Transport for non-equiLibrium eLEctronic Structures) is also the catalan name of the bowling pins, which are solid pieces of plastic or wood situated in a *periodic* structure (similar to a solid-state structure) waiting for a ball (an electron) to impinge on them. See the website http://europe.uab.es/bittles

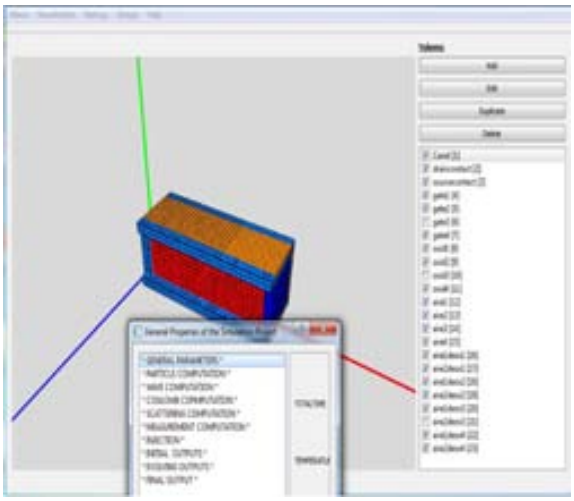

Figure C.1: *GAA transistor designed by BITLLES simulator.*

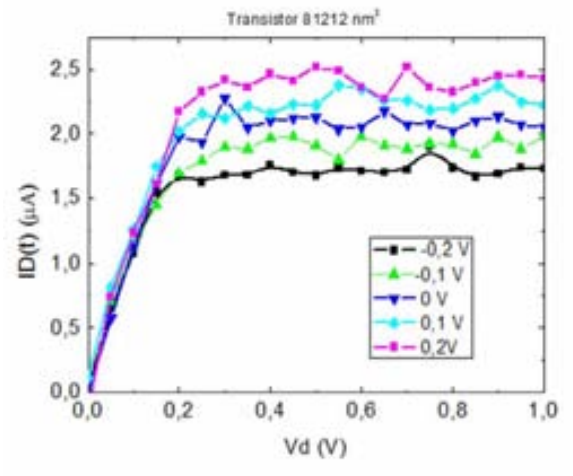

Figure C.2: *Current voltage characteristic for GAA transistor with the geometry* $L_x \cdot L_y \cdot L_z = 8 \cdot 12 \cdot 12\ nm^3$.

Appendix D

List of publications, Conferences/Workshops Attended

D.1 Chapters in books

1. G. Albareda , D. Marian, A. Benali, A. Alarcón , S. Moises , X. Oriols , *Electron Devices Simulation with Bohmian Trajectories*.
2. G. Albareda, F. L. Traversa, A. Benali, and X. Oriols, Book title : *Theory and Applications of Monte Carlo Simulations*, Chapter *Monte Carlo simulations beyond the mean field approximation: Application to Electron transport at the nanoscale*. Editorial: InTech Estimated Date of Publication: January 2011.

D.2 International publications

1. G.Albareda, A. Benali, X.Oriols, *Analytical solution of reservoirs and leads for static and dynamic self-consistent simulations of small electron devices*, J. Comput. Electron (submitted).
2. G.Albareda, D. Marian, A. Benali, S. Yaro, N. Zanghì, X.Oriols, *Time-resolved Electron Transport with Quantum Trajectories*, J. Comput. Electron (12), 405, July 2013.
3. A. Benali, F. L. Traversa, G. Albareda, M. Aghoutane, and X. Oriols, *Improving the intrinsic cut-off frequency of gate-all-around quantum-wire transistors without channel length scaling*, Appl. Phys. Lett. 102, 173506 , May 2013.
4. G. Albareda, F. L. Traversa, A. Benali and X. Oriols, *Computation of quantum electrical currents through the Ramo-Shockley-Pellegrini-Pellegrini theorem with trajectories*, Fluctuation and Noise Letters, 11, 1242008, September 2012.
5. A. Benali, F. L. Traversa., G. Albareda, A. Alarcón, M. Aghoutane and X. Oriols, *Effect of gate-all-around transistor geometry on the high-frequency noise: an analytical discussion*, Fluctuations and Noise Letters 11, 1241002, September 2012.

D.3 Conferences/Workshops Attended

1. X. Oriols, A. Benali, S. M. Yaro, G. Albareda, J. Mateos, T. González, *Accurate predictions of terahertz noise in ultra-small devices: A limiting factor for their practical application?*, of 22nd International Conference on Noise and Fluctuations (ICNF), France, 2013. (Oral presentation).
   -Proceeding of ICNF 2013, IEEE Xplore .
2. A. Benali, F. L. Traversa, G. Albareda, M. Aghoutane and X. Oriols, *Towards frequency performance improvement of emerging devices without length scaling*, Spanish Conference on Electron Devices (CDE), Valladolid, Spain, 2013. (Oral presentation).
   -Proceeding of CDE 2013, IEEE Xplore.
3. A. Benali, F. L. Traversa, G. Albareda, M. Aghoutane and X. Oriols, *Geometry engineering for the RF behavior of low-dimensional gate-all-around transistors*, 15th International Workshop on Computational Electronics (IWCE), 2012 , Madison , USA (poster Presentation).
   -Proceedings of IWCE 2012 , IEEE Xplore.
4. X. Oriols, F. L. Traversa, G. Albareda, A. Benali, A. Alarcón, S. M. Yaro, X. Cartoixà , *Multi-time measurement and displacement current in time-dependent quantum Transport*, IWCE 2012 , Madison , USA (Invited talk).
   -Proceedings of IWCE 2012 , IEEE Xplore.
5. A. Benali, F. L. Traversa, G. Albareda, M. Aghoutane and X. Oriols , *How does the geometry of nanoelectronic devices affect their high-frequency noise?* Unsolved Problems on Noise 2012, Kolkata, India (Invited talk).
6. G. Albareda, F. L. Traversa, A. Benali and X. Oriols, *High frequency quantum noise: the many-body and the continuous-measurement problems* , Unsolved Problems on Noise 2012 , Kolkata , India . (Oral presentation).
7. A. Benali, G. Albareda, F. L. Traversa, A. Alarcón X. Cartoixà and X. Oriols , *BITLLES: A quantum trajectory simulator with explicit Coulomb and exchange correlations among transport electrons for DC, AC, and noise applications*, BNC-b RESEARCH MEETING , July 2011 , Bellaterra, Spain.
8. G. Albareda, A. Alarcón, F. Traversa, A. Benali, A. Padrò, and X. Oriols, *BITLLES: a quantum-trajectory simulation tool for electron transport in large electronic structures*, HPC-NN2011 (High performance Computing), April 2011, Bilbao , Spain. (poster Presentation).
9. G. Albareda, A. Alarcón, F. Traversa, A. Benali and X. Oriols, *A quantum trajectory simulator for DC, AC, and noise with explicit Coulomb and exchange correlations among transport electrons*, Congress: NanoSpain 2011, NanoSudoe, (Spain, Portugal and France), April 2011, Bilbao ,Spain . (Collaboration in the abstract).
10. A. Benali, F. Traversa , G. Albareda, A. Alarcón, M. Aghoutane and X. Oriols, *On the relationship between the intrinsic cut-off frequency and the electron transit time in nanoscale devices*, 8 th Spanish Conference on Electron Devices (CDE)

2011, Palma de Mallorca , Spain. (poster Presentation).
-Proceeding of CDE 2011, IEEE Xplore.

11. A. Alarcón, A.Benali, A. Padrò, G.Albareda, F.L.Traversa and X. Oriols, *The BITLLES simulator for nanoscale devices*, International Workshop on Computational Electronics (IWCE), October 2010, Pisa , Italy. (poster Presentation).
12. A.Benali, G. Albareda, A. Alarcón, M. Aghoutane and X. Oriols, *High frequency modeling of classical and quantum nanoscale electron devices*, Trends in Nanotechnology , September 2009, Barcelona, Spain. (poster Presentation).
13. A. Alarcón, A. Benali, G. Albareda and X. Oriols, *On the computation of high frequency current in nanoelectronic ballistic devices*, 7 th Spanish Conference on Electron Devices (CDE) 2009, Santiago de Compostela , Spain,. Febrary 2009. (Oral presentation).
-Proceeding of CDE 2009, IEEE Xplore.

D.4 Invention

BITLLES simulator.

Developed by: X. Oriols , G. Albareda, F. Traversa, A. Alarcón, A. Padro, X. Cartoixà , A. Benali , S. Moises.
It is a simulator for modeling the classical and quantum nanoelectronbic devices. More details can be found in http://europe.uab.es/bitlles.

D.5 Awards

Best five poster of the CDE 2011 award,

obtained by the authors:

A. Benali, F. Traversa , G. Albareda, A. Alarcón, M. Aghoutane and X. Oriols,
for the work:

On the relationship between the intrinsic cut-off frequency and the electron transit time in nanoscale devices,

in 8 th Spanish Conference on Electron Devices (CDE) 2011, Palma de Mallorca , Spain.